An exact generalised function approach to frequency response analysis of beams and plane frames with the inclusion of viscoelastic damping

AN EXACT GENERALISED FUNCTION APPROACH TO FREQUENCY RESPONSE ANALYSIS OF BEAMS AND PLANE FRAMES WITH THE INCLUSION OF VISCOELASTIC DAMPING

Giuseppe Failla

Dipartimento di Ingegneria Civile, dell'Ambiente, dell'Energia e dei Materiali (DICEAM)

Università di Reggio Calabria, 89124 Reggio Calabria, Italy.

Tel.: +39-0965-1692221. Email: giuseppe.failla@unirc.it

ABSTRACT

This paper concerns the frequency response analysis of beams and plane frames with an arbitrary number of Kelvin-Voigt viscoelastic dampers. Typical external and internal dampers are considered, as grounded translational, tuned mass, rotational and axial dampers, for bending and axial vibrations, respectively. Using the theory of generalised functions within a 1D formulation of equations of motion, exact closed-form expressions are derived for beam dynamic Green's functions and frequency response functions under arbitrary polynomial load, for any number of dampers. For a plane frame, exact global frequency response matrix and load vector are built, with size depending only on the number of beam-to-column nodes, for any number of dampers and point/polynomial loads along the frame members. From the nodal displacement solution, the exact frequency response in all frame members is also obtained in closed analytical form. Numerical applications show many of the advantages of the proposed method.

Keywords: Dampers; Euler-Bernoulli theory; Beams; Frames; Kelvin-Voigt viscoelasticity; Dynamic Green's function; Frequency response function; Generalised functions; Discontinuities.

LIST OF ABBREVIATIONS

AD = axial damper
DGF = dynamic Green's function
DSM = dynamic stiffness matrix
EB = Euler-Bernoulli

FE = finite element
FEMA = Federal Emergency Management Agency
FRF = frequency response function
FRM = frequency response matrix
KV = Kelvin-Voigt
LV = load vector
MDOF = multi-degree-of-freedom
MIMO = multi-input-multi-output
RD = rotational damper
SDOF = single-degree-of-freedom
SIMO = single-input-multi-output
SISO = single-input-single-output
TD = translational damper
TM = Timoshenko
TMD = tuned mass damper

1. INTRODUCTION

Dampers are very important to control bending and axial vibrations in beams and frame structures [1-3]. Examples are grounded translational dampers (TDs), tuned mass dampers (TMDs), rotational dampers (RDs) and axial dampers (ADs). A typical constitutive model includes linear elasticity and viscous damping, corresponding to a Kelvin-Voigt (KV) model of viscoelasticity [4-11], consistent with Federal Emergency Management Agency (FEMA) code of practice [12]. Also in bolted or welded joints, where flexibility and damping arise due to imperfections or damage, KV RDs [13-14] or ADs [15] are often used.

Within a standard 1D formulation of the vibration problem, several studies have addressed the frequency response of beams with dampers. Frequency response analysis is of great interest as it provides the steady-state response to harmonically varying excitations, as those caused, for instance, by reciprocating or rotating machine parts including motors, fans or compressors. Frequency response data are used for control design, finite element (FE) model updating, system identification or damage detection (e.g., see ref. [16-18] and the cross references therein). In the context of frequency response analysis, particular attention has been focused on the computation of the dynamic Green's functions (DGFs), which provide the displacement/rotation and stress-

resultant responses to a harmonically varying unit point load at an arbitrary position on the beam, based on which the frequency response functions (FRFs) under harmonic distributed loads can be derived by spatial integration over the beam axis. In principle, the DGFs can be built by a classical approach where the steady-state response over every uniform beam segment between two consecutive dampers/point load locations is expressed in a typical trigonometric form with a number of unknown integration constants (4 for the bending problem and 2 for the axial problem), computed by enforcing the B.C. and a set of matching conditions between the responses over adjacent beam segments, at the locations of the dampers and harmonic point load. However, when using this approach the coefficient matrix associated with the equations to be solved has to be re-inverted for any forcing frequency of interest. Of course, it has to be updated whenever the dampers/point load locations change along the axis, and the size of the matrix will inevitably increase with the number of dampers, as expected. Therefore, as beams carrying multiple TDs, TMDs, RDs, ADs are encountered in many engineering applications [4-15], alternative methods to compute the DGFs and FRFs, which may overcome the inherent limitations of the classical approach, have been actively sought in several studies, for both bending and axial vibrations.

As for bending vibrations, the exact DGFs of Euler-Bernoulli (EB) and Timoshenko (TM) beams with KV TDs have been derived by Sorrentino et al. [19-21]. Following a transfer matrix approach in conjunction with an appropriate state-variable representation, the authors obtained the characteristic equation of the free vibration problem as a determinant of a 4×4 matrix regardless of the number of TDs, and, upon demonstrating orthogonality conditions for the eigenfunctions, they derived exact DGFs by the complex modal superposition method [19,21]. They also built a corresponding exact solution by direct integration method [20]. Exact DGFs by the complex modal superposition method have been obtained for TM beams with KV TDs and RDs by Hong and Kim [22], using the dynamic stiffness matrix (DSM) approach in conjunction with a Laplace transformation of the beam governing equations. In this case, clearly the DGFs are obtained by a matrix whose size increases with the number of dampers. For an EB simply-supported beam carrying a TMD subjected to a harmonic excitation, Tang et al. [23] derived exact DGFs using the

recurrence method. Several other authors have shown that approximate, but accurate DGFs of beams with dampers can be derived by a modal representation using the eigenfunctions of the bare beam, i.e. the beam without dampers. Examples may be found in the studies of Wu and Chen [24] for an EB beam with an arbitrary number of TMDs, Gürgöze and Erol [25] for an EB beam with an intermediate viscous TD, an intermediate fixed support and a tip mass. Gürgöze and Erol [26] later applied the method in ref. [25] to derive the DGFs of a cantilever with an end viscous damper and subjected to external distributed damping. Some further studies have been sought not only to obtain approximate DGFs, but also to ascertain approximate FRFs under distributed loads. For an EB beam with an arbitrary number of TDs and RDs, Failla [27] built approximate FRFs under arbitrary distributed loads, as superposition of modal FRFs. The modal FRFs have been derived based on appropriate orthogonality conditions for the complex eigenfunctions of the beam with dampers, using the theory of generalised functions to treat the discontinuities of the response variables at the dampers locations. The study in ref. [27] generalises an approach originally devised by Oliveto et al. [28] for EB beams with end viscous RDs.

In the context of frequency analysis of bending vibrations, it is worth noting that DGFs and FRFs have been sought for EB or TM beams including elastic supports, attached masses or spring-mass systems, but without damping. In particular, exact DGFs have been obtained by the classical approach [29-30] or by using the DGFs of the bare beam in conjunction with appropriate conditions at locations of supports/masses [31-33]. In all these cases, the number of equations to be solved increases with the number of supports/attachments [29-33]. Other exact DGFs have been proposed for EB beams including an arbitrary number of rotational joints modelling cracks [34] by inverting a 8×8 DSM built by a transfer matrix method. Finally, approximate DGFs have been built as modal superposition of eigenfunctions of the bare beam, for an EB model including a fixed support [35].

As for axial vibrations, the DGFs for a beam with an end viscous damper have been derived in a closed form by Hull [36]. Approximate DGFs and FRFs have been derived by Alati et al. [37] for a beam with an arbitrary number of either TDs/TMDs or ADs, as superposition of modal DGFs or

FRFs built upon solving the complex eigenvalue problem and utilizing orthogonality of the eigenfunctions. This approach mirrors the one proposed by Failla [27] for the bending problem.

Exact and efficient solutions for frequency response analysis are of great interest not only for single beams but also for frames, as many applications involve frames carrying multiple TMDs, RDs and ADs [4-11, 13-14]. The frequency response matrix (FRM) of frames with TMDs has been constructed by Guo and Chen [38] using the reverberation matrix approach in conjunction with generalised matrix inversion. The global DSM, from which the FRM can be derived by matrix inversion [16-18], has been obtained in ref. [11, 13-14] for frames with KV RDs at beam-to-column nodes modelling dissipating beam-to-column connections [11] or bolted/welded joints with imperfections or damage [13-14], and by Caddemi and Caliò [39-40] for frames with elastic rotational joints arbitrarily located along the frame members, using the theory of generalised functions. A recent approach has been devised by Caddemi et al. [41], where a TM beam element with an arbitrary number of deflection and rotation singularities is formulated based on the static shape functions, and corresponding stiffness and mass matrices are derived for a global FE dynamic analysis. The methodology as it appears can be generalised to frequency response analysis of frames with dampers. For the same purpose, a TM beam element with an arbitrary number of singularities in deflection/rotation and axial displacement, recently proposed by Donà et al. [42], can be evidently used.

Refs. [19-42] demonstrate considerable interest in deriving frequency response solutions for beams and frames with multiple dampers. Here, the purpose is to build exact solutions for the frequency response of EB beams and plane frames that include an arbitrary number of KV dampers. In particular, TDs/TMDs and RDs are considered for the bending problem, whereas TDs/TMDs and ADs for the axial problem. Using the theory of generalised functions to treat the discontinuities of the response variables at the dampers/point load locations [43-56], it is shown that simple manipulations provide exact closed-form expressions of the steady-state response to a harmonic point load and arbitrary polynomial load, with only 4 and 2 integration constants for the bending and axial problem respectively, regardless of the number of dampers. Exact closed-form

expressions are obtained for all response variables and serve two purposes. First, they provide the exact closed-form DGFs and FRFs for a single beam, upon enforcing the B.C. Secondly, they are used to derive a 6×6 DSM and 6×1 load vector (LV) of the beam, to build the exact global DSM and LV of a frame by a standard assembling procedure, and the corresponding exact FRM by inverting the global DSM. From the nodal displacement solution, exact FRFs in all frame members are then obtained, in a closed form, for all response variables. The proposed solutions involve relevant advantages over existing ones, as will be shown later.

The paper is organized in six Sections. Upon introducing the problem under study and basic notation in Section 2, DGFs and FRFs of a single beam are constructed in Section 3. Corresponding DSM and LV of the beam are derived in Section 4, FRM and LV of a plane frame are given in Section 5. Numerical results are presented in Section 6. Three Appendices are also included.

2. PROBLEM STATEMENT

Consider the EB beam in Figure 1, where x is the longitudinal axis, y is the transverse axis, L is the length, EI and EA are flexural and axial rigidities, m_0 is the mass per unit length; $v(x)$, $\theta(x)$ and $u(x)$ denote flexural deflection, bending rotation and axial displacement of the cross section; $S(x)$, $M(x)$ and $N(x)$ are shear force, bending moment and axial force (positive sign conventions are shown in Figure 1).

The beam carries an arbitrary number N of KV dampers at abscissas x_j's along the axis, $0 < x_1 < x_2 < \ldots < x_N < L$: external TDs and TMDs in y- (transverse) and x- (longitudinal) directions; internal RDs and ADs. For the j^{th} damper, the following parameters are used:

- TDs: $k_{G_j}^{(\cdot)}$ =stiffness; $c_{G_j}^{(\cdot)}$ =damping, with superscripts (u) for axial problem and (v) for bending problem.
- TMDs: $k_{M_j}^{(\cdot)}$ =stiffness; $c_{M_j}^{(\cdot)}$ =damping; $M_j^{(\cdot)}$ =mass, with superscripts (u) for axial problem and (v) for bending problem.
- RDs: $k_{\Delta\theta_j}$ = stiffness; $c_{\Delta\theta_j}$ = damping.
- ADs: $k_{\Delta u_j}$ = stiffness; $c_{\Delta u_j}$ = damping.

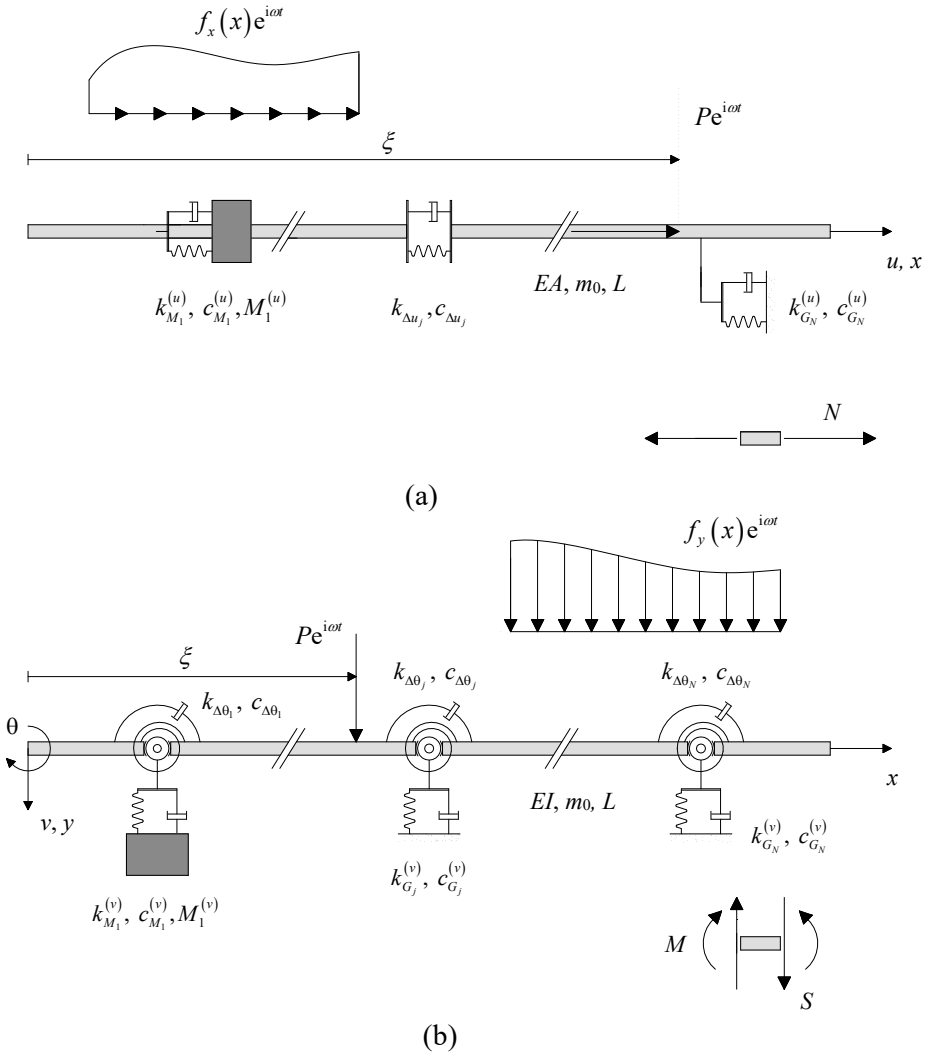

Figure 1. Beam with arbitrary number of KV dampers: (a) axial problem; (b) bending problem.

The beam equations of motion will be written within the standard 1D EB theory, under the following assumptions:

(a) bending and axial problems are uncoupled and treated separately (small displacements);

(b) y-direction TDs/TMDs and RDs occur simultaneously at any location x_j. This assumption is made only for the ease of formulation and, as shown in Appendix C, the derived solutions will apply, with trivial changes, also if only a TD/TMD or a RD occurs at a location x_j.

(c) x-direction TDs/TMDs and ADs cannot occur simultaneously at a location x_j. The case of TDs/TMDs and ADs occurring simultaneously should be treated following the approach devised in ref. [48,54] for the static response of beam with multiple singularities, and is left as a further development.

In this study, the beam in Figure 1 will be considered as a single beam and as a part of a plane frame with an arbitrary number of KV dampers, as shown in Figure 2.

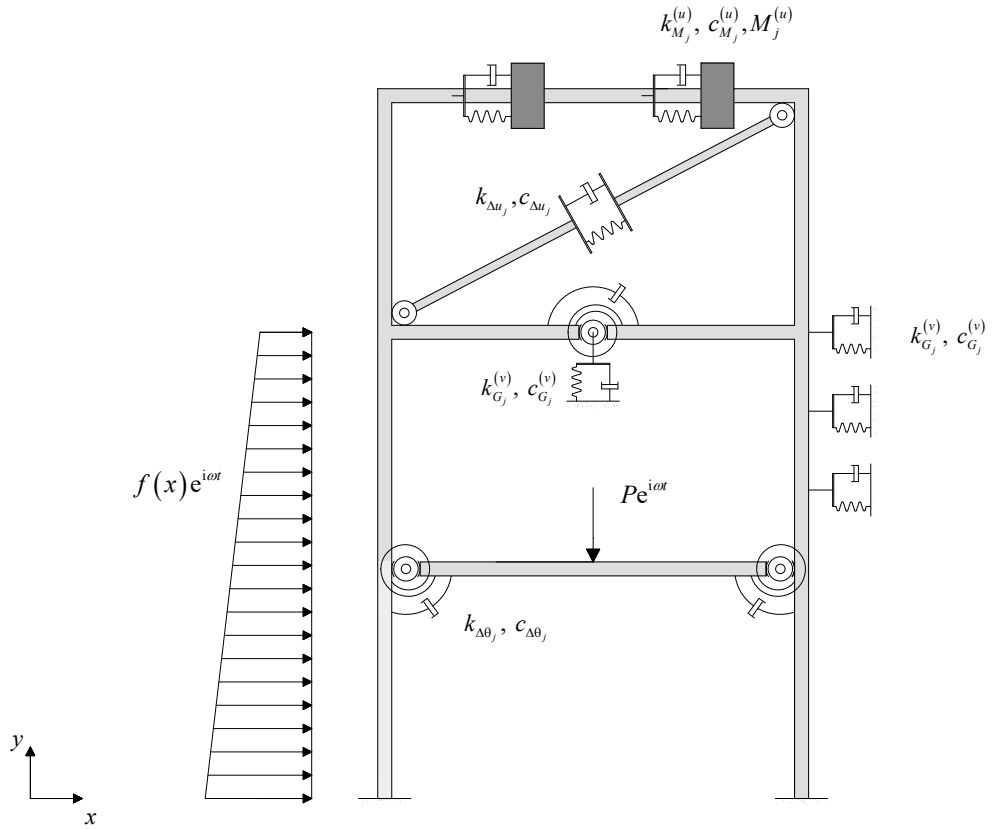

Figure 2. A plane frame with arbitrary number of KV dampers.

3. FREQUENCY RESPONSE OF BEAMS WITH DAMPERS

3.1. Dynamic Green's functions of beams with dampers

The first step is to derive the exact DGFs of the beam in Figure 1. For the ease of reading, axial and bending problems will be discussed separately.

3.1.1. Axial problem

Assume that the beam is loaded by an axial harmonically varying point load at $x=\xi$, denoted as $P\mathrm{e}^{\mathrm{i}\omega t}$; ω is the frequency and i is the imaginary unit. Using the theory of generalised functions and representing the steady-state axial displacement as $u=U(x,\xi,\omega)\mathrm{e}^{\mathrm{i}\omega t}$, the following steady-state motion equation is derived [37]:

$$EA\frac{\bar{\mathrm{d}}^2U\left(x,\xi\right)}{\mathrm{d}x^2}+\sum_{j=1}^{N}G_j^{(u)}\left(x\right)+P\delta\left(x-\xi\right)+m_0\omega^2U\left(x,\xi\right)=0 \tag{1}$$

where frequency dependence in $U\left(x,\xi,\omega\right)$ and $G_j^{(u)}\left(x\right)$ is omitted for brevity. In Eq.(1), symbol $\delta\left(x-\xi\right)$ denotes a Dirac's delta at $x=\xi$, and bar means generalised derivative; $G_j^{(u)}\left(x\right)$ is a generalised function given as

$$G_j^{(u)}\left(x\right)=R_j^{(u)}\delta\left(x-x_j\right)-EA\cdot\Delta U_j\delta^{(1)}\left(x-x_j\right) \tag{2}$$

where $\delta\left(x-x_j\right)$ and $\delta^{(n)}\left(x-x_j\right)$ denote a Dirac's delta and its formal n^{th} derivative at x_j. In Eq.(2), $R_j^{(u)}$ is the reaction of the j^{th} TD/TMD in x-direction, ΔU_j is the relative axial displacement between adjacent sections at the j^{th} AD, given as:

$$R_j^{(u)}=-\left[k_{Geq_j}^{(u)}\left(\omega\right)+k_{Meq_j}^{(u)}\left(\omega\right)\right]U\left(x_j,\xi\right)=-k_{T_j}^{(u)}\left(\omega\right)U\left(x_j,\xi\right) \tag{3a}$$

$$\Delta U_j=\left(k_{\Delta ueq_j}\left(\omega\right)\right)^{-1}N\left(x_j,\xi\right) \tag{3b}$$

for j=1,2,….N. Symbols $k_{Geq_j}^{(u)}\left(\omega\right)$, $k_{Meq_j}^{(u)}\left(\omega\right)$, $k_{\Delta ueq_j}\left(\omega\right)$ are frequency-dependent stiffness parameters

$$k_{Geq_j}^{(u)}\left(\omega\right)=k_{G_j}^{(u)}+\mathrm{i}\omega c_{G_j}^{(u)};\qquad k_{Meq_j}^{(u)}\left(\omega\right)=\frac{\left(k_{M_j}^{(u)}+\mathrm{i}\omega c_{M_j}^{(u)}\right)M_j^{(u)}\omega^2}{M_j^{(u)}\omega^2-\left(k_{M_j}^{(u)}+\mathrm{i}\omega c_{M_j}^{(u)}\right)} \tag{4a,b}$$

$$k_{\Delta ueq_j}\left(\omega\right)=k_{\Delta u_j}+\mathrm{i}\omega c_{\Delta u_j} \tag{5}$$

Eq.(4b) can be derived as explained in ref. [38,56] and shows that in the frequency domain TMDs can be treated as TDs, i.e. the (steady-state) reaction force of a TMD depends on the displacement of the attachment point only through a pertinent frequency-dependent term, involving stiffness/damping/mass of the TMD. Also, notice that a lumped mass along the beam can be modelled as TMD with $k_{M_j}^{(u)}=\infty$ in Eq.(4b).

Next, the steady-state function $U(x,\xi)$ in Eq.(1) is to be built. For this purpose, $U(x,\xi)$ is written in the following form, by applying the linear superposition principle:

$$U(x,\xi)=\mathbf{U}_{HM}(x)\mathbf{c}^{(u)}+\sum_{j=1}^{N}\mathbf{U}_{\Lambda}(x,x_j)\mathbf{\Lambda}_j^{(u)}+P\cdot U_P(x,\xi) \tag{6}$$

where $\mathbf{U}_{HM}(x)\mathbf{c}^{(u)}$ is the solution to the homogeneous equation associated with Eq.(1); $\mathbf{U}_{\Lambda}(x,x_j)\mathbf{\Lambda}_j^{(u)}$ are the particular integrals associated with reactions $R_j^{(u)}$ and relative axial displacements ΔU_j at x_j; $U_P(x,\xi)$ is the particular integral associated with the harmonic load [37]. That is,

$$\mathbf{U}_{HM}(x)=\left[\cos(\eta x)\quad \sin(\eta x)\right];\qquad \mathbf{c}^{(u)}=\left[c_1^{(u)}\quad c_2^{(u)}\right]^T \tag{7a,b}$$

$$\mathbf{U}_{\Lambda}(x,x_j)=\left[U_R(x,x_j)\quad U_{\Delta U}(x,x_j)\right];\qquad \mathbf{\Lambda}_j^{(u)}=\left[R_j^{(u)}\quad \Delta U_j\right]^T \tag{8a,b}$$

$$U_R(x,x_j)=-\rho\sin\left(\eta(x-x_j)\right)H(x-x_j) \tag{9a}$$

$$U_{\Delta U}(x,x_j)=\cos\left(\eta(x-x_j)\right)H(x-x_j) \tag{9b}$$

$$U_P(x,\xi)=-\rho\sin\left(\eta(x-\xi)\right)H(x-\xi) \tag{10}$$

where $\eta=EA^{-1/2}m_0^{1/2}\omega$, $\rho=EA^{1/2}m_0^{-1/2}\omega^{-1}$, while $H(x-x_j)$ denotes the unit-step function: $H(x-x_j)=0$ for $x<x_j$ and $H(x-x_j)=1$ for $x>x_j$. The analytical expression of the axial force $N(x,\xi)$, corresponding to Eq.(6) for $U(x,\xi)$, can be derived from the beam governing equations, and is given in Appendix A for brevity.

At this stage, vectors $\mathbf{\Lambda}_j^{(u)}$ in Eq.(6) are unknown. However, they can be expressed as linear functions of the integration constants $\mathbf{c}^{(u)}$ only, as follows. First, upon considering that $U(x,\xi)$ and $N(x,\xi)$ on the r.h.s. of Eqs.(3), when computed at $x=x_j$, involve only unknowns $\mathbf{\Lambda}_k^{(u)}$ for $k\le j$ (unit-step functions $H(x-x_k)$ in Eqs.(9) vanish for $x_k > x$, i.e. $H(x_j-x_k)=0$ for $k>j$), from Eqs.(3) the following expression can be derived for $\mathbf{\Lambda}_j^{(u)}$:

$$\boldsymbol{\Lambda}_j^{(u)} = \mathbf{h}^{(u)}\left(x_j\right)\mathbf{c}^{(u)} + \sum_{k=1}^{j-1}\mathbf{E}^{(u)}\left(x_j, x_k\right)\boldsymbol{\Lambda}_k^{(u)} + \mathbf{p}^{(u)}\left(x_j, \xi\right) \tag{11}$$

In Eq.(11), $\mathbf{h}^{(u)}$ and $\mathbf{E}^{(u)}$ are 2×2 matrices, $\mathbf{p}^{(u)}$ is a 2×1 vector, with elements $h_{il}^{(u)}$, $E_{il}^{(u)}$ and $p_i^{(u)}$ that depend on whether a *x*-direction TD/TMD or an internal AD occur at x_j and x_k (it has been assumed that TD/TMD and AD do not occur simultaneously at same location). In particular:

(a) if a *x*-direction TD/TMD occurs at x_j (i.e., $\Delta U_j = 0$):

$$\begin{aligned} h_{11}^{(u)}\left(x_j\right) &= -k_{T_j}^{(u)}\left(\omega\right)\cos\left(\eta x_j\right) \qquad h_{12}^{(u)}\left(x_j\right) = -k_{T_j}^{(u)}\left(\omega\right)\sin\left(\eta x_j\right) \\ h_{21}^{(u)} &= 0 \qquad\qquad\qquad\qquad\quad h_{22}^{(u)} = 0 \end{aligned} \tag{12a-d}$$

for $k_{T_j}^{(u)}\left(\omega\right) = k_{Geq_j}^{(u)}\left(\omega\right) + k_{Meq_j}^{(u)}\left(\omega\right)$ (see Eq.(3a)),

$$E_{11}^{(u)}\left(x_j, x_k\right) = \begin{cases} \rho k_{T_j}^{(u)}\left(\omega\right)\sin\left(\eta\left(x_j - x_k\right)\right) & \text{if a } x\text{-direction TD / TMD occurs at } x_k \\ 0 & \text{if an AD occurs at } x_k \end{cases} \tag{13a}$$

$$E_{12}^{(u)}\left(x_j, x_k\right) = \begin{cases} 0 & \text{if a } x\text{-direction TD/TMD occurs at } x_k \\ -k_{T_j}^{(u)}\left(\omega\right)\cos\left(\eta\left(x_j - x_k\right)\right) & \text{if an AD occurs at } x_k \end{cases} \tag{13b}$$

$$E_{21}^{(u)} = E_{22}^{(u)} = 0 \qquad \text{for any } k \tag{13c,d}$$

$$p_1^{(u)}\left(x_j, \xi\right) = P \cdot k_{T_j}^{(u)}\left(\omega\right)\rho\sin\left(\eta\left(x_j - \xi\right)\right)H\left(x_j - \xi\right); \qquad p_2^{(u)} = 0 \tag{14a,b}$$

(b) if an AD occurs at x_j (i.e., $R_j^{(u)} = 0$):

$$\begin{aligned} h_{11}^{(u)} &= 0 \qquad\qquad\qquad\qquad\quad h_{12}^{(u)} = 0 \\ h_{21}^{(u)}\left(x_j\right) &= -\mu_j^{(u)}\left(\omega\right)\sin\left(\eta x_j\right) \qquad h_{22}^{(u)}\left(x_j\right) = \mu_j^{(u)}\left(\omega\right)\cos\left(\eta x_j\right) \end{aligned} \tag{15a-d}$$

for $\mu_j^{(u)}\left(\omega\right) = EA^{1/2}m_0^{1/2}\omega\left(k_{\Delta ueq_j}\left(\omega\right)\right)^{-1}$,

$$E_{11}^{(u)}=E_{12}^{(u)}=0 \qquad \text{for any } k \tag{16a,b}$$

$$E_{21}^{(u)}\left(x_j,x_k\right)=\begin{cases}-\left(k_{\Delta ueq_j}\left(\omega\right)\right)^{-1}\cos\left(\eta\left(x_j-x_k\right)\right) & \text{if a } x\text{-direction TD / TMD occurs at } x_k\\ 0 & \text{if an AD occurs at } x_k\end{cases} \tag{16c}$$

$$E_{22}^{(u)}\left(x_j,x_k\right)=\begin{cases}0 & \text{if a } x\text{-direction TD/TMD occurs at } x_k\\ -\chi\left(k_{\Delta ueq_j}\left(\omega\right)\right)^{-1}\sin\left(\eta\left(x_j-x_k\right)\right) & \text{if an AD occurs at } x_k\end{cases} \tag{16d}$$

$$p_1^{(u)}=0; \qquad p_2^{(u)}\left(x_j,\xi\right)=-P\cdot\left(k_{\Delta ueq_j}\left(\omega\right)\right)^{-1}\cos\left(\eta\left(x_j-\xi\right)\right)H\left(x_j-\xi\right) \tag{17a,b}$$

In Eq.(16d), $\chi=EA^{1/2}m_0^{1/2}\omega$. Hence, it can readily be seen that, starting from Eq.(11) at $x=x_1$ to express $\mathbf{\Lambda}_1^{(u)}$ as $\mathbf{\Lambda}_1^{(u)}=\mathbf{h}^{(u)}\left(x_1\right)\mathbf{c}^{(u)}+\mathbf{p}^{(u)}\left(x_1,\xi\right)$, Eq.(11) can be used recursively to derive all unknowns $\mathbf{\Lambda}_j^{(u)}$ as linear functions of the integration constants $\mathbf{c}^{(u)}$. This provides the following final expressions for $U\left(x,\xi\right)$ in Eq.(6):

$$U\left(x,\xi\right)=\mathbf{U}\left(x\right)\mathbf{c}^{(u)}+\tilde{U}_P\left(x,\xi\right) \tag{18}$$

where $\mathbf{U}\left(x\right)$ and $\tilde{U}_P\left(x,\xi\right)$ are given as

$$\mathbf{U}\left(x\right)=\mathbf{U}_{HM}\left(x\right)+\sum_{j=1}^{N}\mathbf{U}_\Lambda\left(x,x_j\right)\mathbf{h}^{(u)}\left(x_j\right)+\sum_{j=2}^{N}\mathbf{U}_\Lambda\left(x,x_j\right)\left\{\sum_{(j,m)\in\Pi_2^{(j)}}\mathbf{E}^{(u)}\left(x_j,x_m\right)\mathbf{h}^{(u)}\left(x_m\right)+\right.$$
$$\left.\sum_{2<q\le j}\sum_{\underbrace{(j,m,n,\ldots,r,s)}_{q}\in\Pi_q^{(j)}}\mathbf{E}^{(u)}\left(x_j,x_m\right)\mathbf{E}^{(u)}\left(x_m,x_n\right)\cdots\mathbf{E}^{(u)}\left(x_r,x_s\right)\mathbf{h}^{(u)}\left(x_s\right)\right\} \tag{19}$$

$$\tilde{U}_P\left(x,\xi\right)=P\cdot U_P\left(x,\xi\right)+\sum_{j=1}^{N}\mathbf{U}_\Lambda\left(x,x_j\right)\mathbf{p}^{(u)}\left(x_j,\xi\right)+\sum_{j=2}^{N}\mathbf{U}_\Lambda\left(x,x_j\right)\left\{\sum_{(j,m)\in\Pi_2^{(j)}}\mathbf{E}^{(u)}\left(x_j,x_m\right)\mathbf{p}^{(u)}\left(x_m,\xi\right)+\right.$$
$$\left.\sum_{2<q\le j}\sum_{\underbrace{(j,m,n,\ldots,r,s)}_{q}\in\Pi_q^{(j)}}\mathbf{E}^{(u)}\left(x_j,x_m\right)\mathbf{E}^{(u)}\left(x_m,x_n\right)\cdots\mathbf{E}^{(u)}\left(x_r,x_s\right)\mathbf{p}^{(u)}\left(x_s,\xi\right)\right\} \tag{20}$$

In Eqs.(19)-(20), $\Pi_q^{(j)} = \{ \underbrace{(j,m,n,...r,s)}_{q} : j>m>n>...>r>s;\ m,n,...r,s = 1,2,...,(j-1) \}$ is the set including all possible q-ples of indexes $\underbrace{(j,m,n,...r,s)}_{q}$ such that $j>m>n>...>r>s$, being $2 \le q \le j$.

For instance, with N=4 damper locations the following sets shall be considered in Eqs.(19)-(20):

for j=2: $\Pi_2^{(2)} = \{(2,1)\}$

for j=3: $\Pi_2^{(3)} = \{(3,1),(3,2)\}$; $\Pi_3^{(3)} = \{(3,2,1)\}$

for j=4: $\Pi_2^{(4)} = \{(4,1),(4,2),(4,3)\}$; $\Pi_3^{(4)} = \{(4,3,2),(4,3,1),(4,2,1)\}$; $\Pi_4^{(4)} = \{(4,3,2,1)\}$

It is noticed that, while $\mathbf{U}(x)$ in Eq.(19) depends on the beam parameters through matrices $\mathbf{E}^{(u)}$ and $\mathbf{h}^{(u)}$, $\tilde{U}_P(x,\xi)$ in Eq.(20) depends on the beam parameters through matrices $\mathbf{E}^{(u)}$, and on the applied load P at x=ξ through the particular integral $U_P(x,\xi)$ and the load-dependent vector $\mathbf{p}^{(u)}$.

Next, using the beam governing equations, the axial force $N(x,\xi)$ can be obtained in the following form, with obvious meaning of the symbols:

$$N(x,\xi) = \mathbf{N}(x)\mathbf{c}^{(u)} + \tilde{N}_P(x,\xi) \tag{21}$$

For brevity, terms in Eq.(21) are given in Appendix A.

The integration constants $\mathbf{c}^{(u)}$ in Eqs.(18)-(21) depend on the B.C. of the beam. Enforcing the B.C. will lead to 2 equations, regardless of the number of dampers, with the general form

$$\mathbf{B}^{(u)}\mathbf{c}^{(u)} = \tilde{\mathbf{r}}^{(u)} \quad \rightarrow \quad \mathbf{c}^{(u)} = \left(\mathbf{B}^{(u)}\right)^{-1} \tilde{\mathbf{r}}^{(u)} \tag{22a,b}$$

where vectors $\tilde{\mathbf{r}}^{(u)}$ involve the load-dependent terms $\tilde{U}_P(x,\xi)$, $\tilde{N}_P(x,\xi)$ in Eqs.(18)-(21), computed at the beam ends. As matrix $\mathbf{B}^{(u)}$ can readily be inverted in a symbolic form (see Appendix B), from Eq.(22b) closed-form expressions can be derived for $\mathbf{c}^{(u)}$, to be replaced in Eqs.(18)-(21) to obtain

the exact closed-form DGFs of the beam with an arbitrary number of KV dampers, due to an axial harmonic point load (P = 1), with frequency ω, at arbitrary abscissa x=ξ.

Eqs.(22) can be used for both homogeneous and non-homogeneous B.C., the latter as due to end dampers. In this case, the B.C. can still be considered as homogeneous, while the end dampers are modelled as internal dampers located at $x_1 = 0^+$ and $x_N = L^-$. Examples can be found in ref. [54].

3.1.2. Bending problem

Exact DGFs can be derived for the bending problem based on the same concepts used for the axial problem. Let v=$V\left(x,\xi,\omega\right)\mathrm{e}^{\mathrm{i}\omega t}$ be the steady-state flexural deflection response to a transverse harmonically varying point load $P\,\mathrm{e}^{\mathrm{i}\omega t}$ at $x = \xi$. The steady-state motion equation is [28,56]:

$$EI\frac{\overline{\mathrm{d}}^4 V\left(x,\xi\right)}{\mathrm{d}x^4} - \sum_{j=1}^{N} G_j^{(v)}\left(x\right) - P\delta\left(x-\xi\right) - m_0\omega^2 V\left(x,\xi\right) = 0 \tag{23}$$

where $G_j^{(v)}\left(x\right)$ is a generalised function given as

$$G_j^{(v)}\left(x\right) = R_j^{(v)}\delta\left(x-x_j\right) + EI\cdot\Delta\Theta_j\delta^{(2)}\left(x-x_j\right) \tag{24}$$

In Eq.(24), $R_j^{(v)}$ is the reaction of the j^{th} TD/TMD in y-direction, $\Delta\Theta_j$ is the relative rotation between adjacent sections at the j^{th} RD, given as:

$$R_j^{(v)} = -\left[k_{Geq_j}^{(v)}\left(\omega\right) + k_{Meq_j}^{(v)}\left(\omega\right)\right]V\left(x_j,\xi\right) = -k_{T_j}^{(v)}\left(\omega\right)V\left(x_j,\xi\right) \tag{25a}$$

$$\Delta\Theta_j = -\left(k_{\Delta\theta eq_j}\left(\omega\right)\right)^{-1} M\left(x_j,\xi\right) \tag{25b}$$

for j=1,…N. For the TDs/TMDs, symbols $k_{Geq_j}^{(v)}\left(\omega\right)$, $k_{Meq_j}^{(v)}\left(\omega\right)$ mirror those in Eqs.(4), i.e. $k_{Geq_j}^{(v)}\left(\omega\right) = k_{G_j}^{(v)} + \mathrm{i}\omega c_{G_j}^{(v)}$, $k_{Meq_j}^{(v)}\left(\omega\right) = \left(k_{M_j}^{(v)} + \mathrm{i}\omega c_{M_j}^{(v)}\right)M_j^{(v)}\omega^2\left(M_j^{(v)}\omega^2 - \left(k_{M_j}^{(v)} + \mathrm{i}\omega c_{M_j}^{(v)}\right)\right)^{-1}$, for the RDs

$$k_{\Delta\theta eq_j}\left(\omega\right) = k_{\Delta\theta_j} + \mathrm{i}\omega c_{\Delta\theta_j} \tag{26}$$

By applying the linear superposition principle, $V(x,\xi)$ in Eq.(23) can be written as

$$V(x,\xi)=\mathbf{V}_{HM}(x)\mathbf{c}^{(v)}+\sum_{j=1}^{N}\mathbf{V}_{\Lambda}(x,x_j)\mathbf{\Lambda}_j^{(v)}+P\cdot V_P(x,\xi) \tag{27}$$

where $\mathbf{V}_{HM}(x)\mathbf{c}^{(v)}$ is the solution to the homogeneous equations associated with Eq.(23), i.e.

$$\mathbf{V}_{HM}(x)=\left[\mathrm{e}^{-\beta x}\quad \mathrm{e}^{\beta x}\quad \cos(\beta x)\quad \sin(\beta x)\right];\qquad \mathbf{c}^{(v)}=\left[c_1^{(v)}\quad c_2^{(v)}\quad c_3^{(v)}\quad c_4^{(v)}\right]^T \tag{28a,b}$$

for $\beta=EI^{-1/4}m_0^{1/4}\omega^{1/2}$; $\mathbf{V}_{\Lambda}(x,x_j)\mathbf{\Lambda}_j^{(v)}$ are the particular integrals associated with reactions $R_j^{(v)}$ and relative rotations $\Delta\Theta_j$ at x_j, while $V_P(x,\xi)$ is the particular integral associated with the load, that is:

$$\mathbf{V}_{\Lambda}(x,x_j)=\left[V_R(x,x_j)\quad V_{\Delta\Theta}(x,x_j)\right];\qquad \mathbf{\Lambda}_j^{(v)}=\left[R_j^{(v)}\quad \Delta\Theta_j\right]^T \tag{29a,b}$$

$$V_R(x,x_j)=\alpha\left[-\sin\left(\beta(x-x_j)\right)+\sinh\left(\beta(x-x_j)\right)\right]H(x-x_j) \tag{30a}$$

$$V_{\Delta\Theta}(x,x_j)=\gamma\left[\sin\left(\beta(x-x_j)\right)+\sinh\left(\beta(x-x_j)\right)\right]H(x-x_j) \tag{30b}$$

$$V_P(x,\xi)=\alpha\left[-\sin\left(\beta(x-\xi)\right)+\sinh\left(\beta(x-\xi)\right)\right]H(x-\xi) \tag{31}$$

where $\alpha=2^{-1}EI^{-1/4}m_0^{-3/4}\omega^{-3/2}$ and $\gamma=2^{-1}EI^{1/4}m_0^{-1/4}\omega^{-1/2}$. Eqs.(30) for $\mathbf{V}_{\Lambda}(x,x_j)$ are the exact particular integrals due to shear-force and rotation discontinuities, obtained by Wang and Xiao [56] by Laplace transforming the steady-state motion equations. Alternative exact particular integrals also exist [27], but are not used here as their analytical form is more involved. The analytical expressions of the bending moment $M(x,\xi)$ and the other response variables, corresponding to Eq.(27) for $V(x,\xi)$, are given in Appendix A for brevity.

Next, based on the observation that $V(x,\xi)$ and $M(x,\xi)$ on the r.h.s. of Eqs.(25), when computed at $x=x_j$, involve only unknowns $\mathbf{\Lambda}_k^{(v)}$ for $k\le j$ (again, in Eqs.(30) $H(x_j-x_k)=0$ for $k>j$), from Eqs.(25) the following expression can be derived for $\mathbf{\Lambda}_j^{(v)}$:

$$\mathbf{\Lambda}_j^{(v)} = \mathbf{h}^{(v)}\left(x_j\right)\mathbf{c}^{(v)} + \sum_{k=1}^{j-1}\mathbf{E}^{(v)}\left(x_j, x_k\right)\mathbf{\Lambda}_k^{(v)} + \mathbf{p}^{(v)}\left(x_j, \xi\right) \tag{32}$$

In Eq.(32), $\mathbf{h}^{(v)}$ is a 2×4 matrix with elements $h_{il}^{(v)}$:

$$\begin{aligned} &h_{11}^{(v)}\left(x_j\right) = -k_{T_j}^{(v)}(\omega)\mathrm{e}^{-\beta x_j} \quad h_{12}^{(v)}\left(x_j\right) = -k_{T_j}^{(v)}(\omega)\mathrm{e}^{\beta x_j} \quad h_{13}^{(v)}\left(x_j\right) = -k_{T_j}^{(v)}(\omega)\cos\left(\beta x_j\right) \quad h_{14}^{(v)}\left(x_j\right) = -k_{T_j}^{(v)}(\omega)\sin\left(\beta x_j\right) \\ &h_{21}^{(v)}\left(x_j\right) = \mu_j^{(v)}(\omega)\mathrm{e}^{-\beta x_j} \quad h_{22}^{(v)}\left(x_j\right) = \mu_j^{(v)}(\omega)\mathrm{e}^{\beta x_j} \quad h_{23}^{(v)}\left(x_j\right) = -\mu_j^{(v)}(\omega)\cos\left(\beta x_j\right) \quad h_{24}^{(v)}\left(x_j\right) = -\mu_j^{(v)}(\omega)\sin\left(\beta x_j\right) \end{aligned} \tag{33a,h}$$

for $\mu_j^{(v)}(\omega) = EI^{1/2}m_0^{1/2}\omega\left(k_{\Delta\theta eq_j}(\omega)\right)^{-1}$ and $k_{T_j}^{(v)}(\omega) = k_{Geq_j}^{(v)}(\omega) + k_{Meq_j}^{(v)}(\omega)$, see Eq.(25a). Symbol $\mathbf{E}^{(v)}$ denotes a 2×2 matrix with elements $E_{il}^{(v)}$:

$$E_{11}^{(v)}\left(x_j, x_k\right) = \alpha k_{T_j}^{(v)}(\omega)\left[\sin\left(\beta\left(x_j - x_k\right)\right) - \sinh\left(\beta\left(x_j - x_k\right)\right)\right] \tag{34a}$$

$$E_{12}^{(v)}\left(x_j, x_k\right) = -\gamma k_{T_j}^{(v)}(\omega)\left[\sin\left(\beta\left(x_j - x_k\right)\right) + \sinh\left(\beta\left(x_j - x_k\right)\right)\right] \tag{34b}$$

$$E_{21}^{(v)}\left(x_j, x_k\right) = \gamma\left(k_{\Delta\theta eq_j}(\omega)\right)^{-1}\left[\sin\left(\beta\left(x_j - x_k\right)\right) + \sinh\left(\beta\left(x_j - x_k\right)\right)\right] \tag{34c}$$

$$E_{22}^{(v)}\left(x_j, x_k\right) = \psi\left(k_{\Delta\theta eq_j}(\omega)\right)^{-1}\left[-\sin\left(\beta\left(x_j - x_k\right)\right) + \sinh\left(\beta\left(x_j - x_k\right)\right)\right] \tag{34d}$$

for $\psi = 2^{-1}EI^{3/4}m_0^{1/4}\omega^{1/2}$. Further, in Eq.(32) $\mathbf{p}^{(v)}$ is a 2×1 vector with components

$$p_1^{(v)}\left(x_j, \xi\right) = P\cdot\alpha k_{T_j}^{(v)}(\omega)H\left(x_j - \xi\right)\left[\sin\left(\beta\left(x_j - \xi\right)\right) - \sinh\left(\beta\left(x_j - \xi\right)\right)\right] \tag{35a}$$

$$p_2^{(v)}\left(x_j, \xi\right) = P\cdot\gamma\left(k_{\Delta\theta eq_j}(\omega)\right)^{-1}H\left(x_j - \xi\right)\left[\sin\left(\beta\left(x_j - \xi\right)\right) + \sinh\left(\beta\left(x_j - \xi\right)\right)\right] \tag{35b}$$

Hence, following the reasoning adopted for the axial problem in Section 3.1.1, the unknowns $\mathbf{\Lambda}_j^{(v)}$ can be all found as linear functions of the integration constants $\mathbf{c}^{(v)}$ starting from Eq.(32) at x=x_1, providing the following final expressions for $V\left(x, \xi\right)$ in Eq.(27):

$$V\left(x, \xi\right) = \mathbf{V}\left(x\right)\mathbf{c}^{(v)} + \tilde{V}_P\left(x, \xi\right) \tag{36}$$

In Eq.(36), $\mathbf{V}(x)$ and $\tilde{V}_P(x,\xi)$ are given as

$$\mathbf{V}(x)=\mathbf{V}_{HM}(x)+\sum_{j=1}^{N}\mathbf{V}_{\Lambda}(x,x_j)\mathbf{h}^{(v)}(x_j)+\sum_{j=2}^{N}\mathbf{V}_{\Lambda}(x,x_j)\left\{\sum_{(j,m)\in\Pi_2^{(j)}}\mathbf{E}^{(v)}(x_j,x_m)\mathbf{h}^{(v)}(x_m)+\right.$$
$$\left.\sum_{2<q\le j}\sum_{\underbrace{(j,m,n,\ldots,r,s)}_{q}\in\Pi_q^{(j)}}\mathbf{E}^{(v)}(x_j,x_m)\mathbf{E}^{(v)}(x_m,x_n)\cdots\mathbf{E}^{(v)}(x_r,x_s)\mathbf{h}^{(v)}(x_s)\right\} \tag{37}$$

$$\tilde{V}_P(x,\xi)=P\cdot V_P(x,\xi)+\sum_{j=1}^{N}\mathbf{V}_{\Lambda}(x,x_j)\mathbf{p}^{(v)}(x_j,\xi)+\sum_{j=2}^{N}\mathbf{V}_{\Lambda}(x,x_j)\left\{\sum_{(j,m)\in\Pi_2^{(j)}}\mathbf{E}^{(v)}(x_j,x_m)\mathbf{p}^{(v)}(x_m,\xi)+\right.$$
$$\left.\sum_{2<q\le j}\sum_{\underbrace{(j,m,n,\ldots,r,s)}_{q}\in\Pi_q^{(j)}}\mathbf{E}^{(v)}(x_j,x_m)\mathbf{E}^{(v)}(x_m,x_n)\cdots\mathbf{E}^{(v)}(x_r,x_s)\mathbf{p}^{(v)}(x_s,\xi)\right\} \tag{38}$$

where $\Pi_q^{(j)}$ for $2\le q\le j$ holds the same meaning as in Eqs.(19)-(20). Next, using the beam governing equations, the full set of response variables can readily be obtained by successive differentiation of Eq.(36) for $V(x,\xi)$. The following general expressions can be derived with obvious meaning of the symbols:

$$\Theta(x,\xi)=\boldsymbol{\Theta}(x)\mathbf{c}^{(v)}+\tilde{\Theta}_P(x,\xi) \tag{39a}$$

$$M(x,\xi)=\mathbf{M}(x)\mathbf{c}^{(v)}+\tilde{M}_P(x,\xi) \tag{39b}$$

$$S(x,\xi)=\mathbf{S}(x)\mathbf{c}^{(v)}+\tilde{S}_P(x,\xi) \tag{39c}$$

For brevity, terms in Eqs.(39) are given in Appendix A. Notice, however, that successive differentiations of Eq.(36) are particularly straightforward, because $\mathbf{V}(x)$ and $\tilde{V}_P(x,\xi)$ depend on the differentiation variable x only through $\mathbf{V}_{HM}(x)$, $\mathbf{V}_{\Lambda}(x,x_j)$ and $V_P(x,\xi)$.

At this stage, enforcing the B.C. will lead to 4 equations, regardless of the number of dampers, with the general form

$$\mathbf{B}^{(v)}\mathbf{c}^{(v)}=\tilde{\mathbf{r}}^{(v)} \quad \rightarrow \quad \mathbf{c}^{(v)}=\left(\mathbf{B}^{(v)}\right)^{-1}\tilde{\mathbf{r}}^{(v)} \tag{40a,b}$$

where vector $\tilde{\mathbf{r}}^{(u)}$ involves the load-dependent terms $\tilde{V}_P(x,\xi)$, $\tilde{\Theta}_P(x,\xi)$ in Eqs.(36)-(39), computed at the beam ends. Due to the limited size (4×4), matrix $\mathbf{B}^{(v)}$ can be inverted in a symbolic form, as shown in Appendix B. Therefore, from Eq.(40b) closed-form expressions can be derived for $\mathbf{c}^{(v)}$, to be replaced in Eqs.(36)-(39) to obtain the exact closed-form DGFs of the beam with an arbitrary number of KV dampers, due to a transverse harmonic point load (P = 1), with frequency ω, at arbitrary abscissa x=ξ. Eqs.(40) can be used for both homogeneous and non-homogeneous B.C., the latter as due to end dampers [54].

Exact DGFs (36)-(39) have been derived based on the assumption that TDs/TMDs and RDs occur simultaneously at every location x_j. For cases in which either a TD/TMD or a RD occurs at a location x_j, modifications are straightforward, as shown in Appendix C.

3.2. Frequency response functions of beams with dampers

Eqs.(18)-(21) and Eqs.(36)-(39) for the DGFs can be used to construct exact closed-form expressions of the FRFs under harmonic distributed loads $f_x(x)\mathrm{e}^{\mathrm{i}\omega t}$ (axial) and $f_y(x)\mathrm{e}^{\mathrm{i}\omega t}$ (transverse). The only changes in Eqs.(18)-(21), Eqs.(36)-(39) affect the load-dependent terms, as detailed next.

Consider harmonic loads $f_x(x)\mathrm{e}^{\mathrm{i}\omega t}$ and $f_y(x)\mathrm{e}^{\mathrm{i}\omega t}$ distributed over an interval [a,b], with $0 \le a$ and $b \le L$. The FRFs can be derived from Eqs.(18)-(21) and Eqs.(36)-(39) as follows:

$$U(x)=\mathbf{U}(x)\mathbf{c}^{(u)}+\tilde{U}_f(x); \qquad \tilde{U}_f(x)=\int_a^b \tilde{U}_P(x,\xi)f_x(\xi)d\xi \tag{41a}$$

$$N(x)=\mathbf{N}(x)\mathbf{c}^{(u)}+\tilde{N}_f(x); \qquad \tilde{N}_f(x)=\int_a^b \tilde{N}_P(x,\xi)f_x(\xi)d\xi \tag{41b}$$

$$V(x)=\mathbf{V}(x)\mathbf{c}^{(v)}+\tilde{V}_f(x); \qquad \tilde{V}_f(x)=\int_a^b \tilde{V}_P(x,\xi)f_y(\xi)d\xi \tag{42a}$$

$$\Theta(x)=\mathbf{\Theta}(x)\mathbf{c}^{(v)}+\tilde{\Theta}_f(x); \qquad \tilde{\Theta}_f(x)=\int_a^b \tilde{\Theta}_P(x,\xi)f_y(\xi)d\xi \tag{42b}$$

$$M(x)=\mathbf{M}(x)\mathbf{c}^{(v)}+\tilde{M}_f(x);\qquad \tilde{M}_f(x)=\int_a^b \tilde{M}_P(x,\xi)f_y(\xi)d\xi \tag{42c}$$

$$S(x)=\mathbf{S}(x)\mathbf{c}^{(v)}+\tilde{S}_f(x);\qquad \tilde{S}_f(x)=\int_a^b \tilde{S}_P(x,\xi)f_y(\xi)d\xi \tag{42d}$$

In view of the analytical expressions of $\tilde{U}_P(x,\xi)$ and $\tilde{N}_P(x,\xi)$, $\tilde{V}_P(x,\xi)$, $\tilde{\Theta}_P(x,\xi)$, $\tilde{M}_P(x,\xi)$ and $\tilde{S}_P(x,\xi)$, (see Eq.(20), Eq.(38) and Appendix A), it can be stated that every integral in Eqs.(41)-(42) can be reverted to the general form $\int_a^b g(\xi)H(x-\xi)d\xi$, with $g(\xi)$ given by the product of the loading functions and certain trigonometric functions. For instance, in view of Eq.(38) for $\tilde{V}_P(x,\xi)$, computing $\tilde{V}_f(x)$ in Eq.(42a) involves, among others, the integral

$$\int_a^b V_P(x,\xi)f_y(\xi)d\xi=\int_a^b g(\xi)H(x-\xi)d\xi,\qquad g(\xi)=f_y(\xi)\alpha\left[-\sin(\beta(x-\xi))+\sinh(\beta(x-\xi))\right] \tag{43a,b}$$

Using the theory of generalised functions [54], integrals $\int_a^b g(\xi)H(x-\xi)d\xi$ can be computed as:

$$\begin{aligned}\int_a^b g(\xi)H(x-\xi)d\xi&=\left\{H(x-\xi)\left[g^{[1]}(\xi)-g^{[1]}(x)\right]\right\}_a^b=\\&=H(x-b)\left[g^{[1]}(b)-g^{[1]}(x)\right]-H(x-a)\left[g^{[1]}(a)-g^{[1]}(x)\right]\end{aligned} \tag{44}$$

where $g^{[1]}$ denotes the first-order primitive function of $g(\xi)$. It is noticed that, for polynomial loads $f_x(\xi)$ and $f_y(\xi)$ generally encountered in engineering applications, the first-order primitive $g^{[1]}$ can be obtained in a closed form by any symbolic package [57]. This means that, upon enforcing the B.C. and deriving closed-form expressions of $\mathbf{c}^{(u)}$ and $\mathbf{c}^{(v)}$ from equations given in the same form as Eqs.(22) and Eqs.(40), respectively, Eqs.(41)-(42) provide the exact closed-form expressions of the FRFs under polynomial loads, for all the response variables.

3.3. Remarks on the proposed solutions for beams with dampers

The derived exact DGFs and FRFs inherently fulfil all required conditions at the dampers and point load locations (i.e. shear force and rotation discontinuities, axial force and axial displacement

discontinuities, as well as continuities of the other response variables). The analytical form is easy to implement in any symbolic package, and can readily be computed for any forcing frequency ω, dampers parameters (location, stiffness, damping), position of the point and distributed loads, regardless of the number of dampers and positions of the dampers relative to the loads. For these reasons, the derived DGFs and FRFs lend themselves for those applications, as sensitivity or optimization analyses, where a considerable number of solutions are to be built for changing parameters of dampers and/or loads. Advantages over the classical exact approach (see Introduction) are considerable, as in the latter the coefficient matrix associated with the equations to be solved has to be re-inverted for any forcing frequency of interest, and updated whenever dampers/load positions change; also, the size inevitably increases with the number of dampers.

Being exact solutions, the derived DGFs and FRFs may represent a benchmark for a standard FE solution with two-node beam elements. In addition, notice that, in a FE solution, a mesh node shall be inserted where a damper or a point load is applied, and re-meshing may be required whenever dampers/loads change position. Also, FE solutions require re-computing the FRM, in general by matrix inversion of the DSM involving mass, damping and stiffness matrices, as forcing frequency ω, beam/dampers parameters and loads change, while the derived DGFs and FRFs are analytical and can quickly be evaluated for any forcing frequency ω, beam/dampers parameters and loads.

Free vibration analysis can be pursued using Eq.(22a) and Eq.(40a). Representing the eigenvalues as $\lambda = \mathrm{i}\omega$ in all terms of $\mathbf{B}^{(u)}$ and $\mathbf{B}^{(v)}$ on the l.h.s. of Eq.(22a) and Eq.(40a), and setting equal to zero the load-dependent terms on the r.h.s., i.e. $\tilde{\mathbf{r}}^{(u)} = 0$ and $\tilde{\mathbf{r}}^{(v)} = 0$, the characteristic equation can be built as determinant of $\mathbf{B}^{(u)}$ and $\mathbf{B}^{(v)}$ for axial and bending problems, respectively:

$$\det \mathbf{B}^{(u)}(\lambda) = 0; \qquad \det \mathbf{B}^{(v)}(\lambda) = 0 \tag{45a,b}$$

The size of $\mathbf{B}^{(u)}$ and $\mathbf{B}^{(v)}$ is 2×2 and 4×4, respectively, for any number of dampers. The eigenfunctions can readily be derived from Eqs.(41)-(42) with zero load-dependent terms (i.e.

$\tilde{U}_f(x)=0$, $\tilde{N}_f(x)=0$, $\tilde{V}_f(x)=0,\ldots)$, $\mathbf{c}^{(v)}$ and $\mathbf{c}^{(u)}$ obtained as non-trivial solutions of Eq.(22a) and Eq.(40a), where $\tilde{\mathbf{r}}^{(u)}=0$ and $\tilde{\mathbf{r}}^{(v)}=0$ on the r.h.s., while λ is replaced by the computed eigenvalues on the l.h.s. Analogous results have been obtained by the author in ref. [27, 37], in ref. [27] by using alternative expressions for the generalised integrals due to shear-force and rotation discontinuities. Advantages over existing methods are discussed in ref. [27, 37], and are not repeated for brevity.

As for further applications and developments, the derived DGFs and FRFs can readily be generalised to beams on elastic Winkler foundation [58].

4. EXACT DYNAMIC STIFFNESS MATRIX AND LOAD VECTOR OF BEAMS WITH DAMPERS

Eqs.(18)-(21) and Eqs.(36)-(39) for the DGFs, as well as Eqs.(41)-(42) for the FRFs, lead to further important results.

Refer to the beam ends in Figure 1 as "nodes" with 3 degrees of freedom each and consider, for generality, the case of arbitrary polynomial loads. Using Eqs.(41a)-(42a)-(42b) to build the vector of nodal displacements/rotations $\mathbf{u}=\left[u_1 \quad v_1 \quad \theta_1 \quad u_2 \quad v_2 \quad \theta_2\right]^T$, with $u_1=U(0)$, $v_1=V(0)$, $\theta_1=\Theta(0)$, $u_2=U(L)$, $v_2=V(L)$, $\theta_2=\Theta(L)$, Eqs.(41b)-(42c)-(42d) to build the vector of nodal forces/moments $\mathbf{f}=\left[H_1 \quad T_1 \quad C_1 \quad H_2 \quad T_2 \quad C_2\right]$, with $H_1=-N(0)$, $T_1=-S(0)$, $C_1=M(0)$, $H_2=N(L)$, $T_2=S(L)$, $C_2=-M(L)$ (positive sign conventions for the nodal forces/moments agree with those for the nodal displacements/rotations) the following expressions can be written:

$$\mathbf{u}=\mathbf{\Gamma c}+\tilde{\mathbf{u}}_f \ ; \qquad \mathbf{f}=\mathbf{\Xi c}+\tilde{\mathbf{f}}_f \tag{46a,b}$$

with $\tilde{\mathbf{u}}_f=\left[\tilde{U}_f(0) \quad \tilde{V}_f(0) \quad \tilde{\Theta}_f(0) \quad \tilde{U}_f(L) \quad \tilde{V}_f(L) \quad \tilde{\Theta}_f(L)\right]^T$, $\tilde{\mathbf{f}}_f=\left[-\tilde{N}_f(0) \quad -\tilde{S}_f(0) \quad \tilde{M}_f(0) \quad \tilde{N}_f(L) \quad \tilde{S}_f(L) \quad -\tilde{M}_f(L)\right]^T$, $\mathbf{c}=\left[c_1^{(u)} \quad c_2^{(u)} \quad c_1^{(v)} \quad c_2^{(v)} \quad c_3^{(v)} \quad c_4^{(v)}\right]^T$, while $\mathbf{\Gamma}$ and $\mathbf{\Xi}$ are

$$\boldsymbol{\Gamma}=\begin{bmatrix} U_{11}(0) & U_{12}(0) & 0 & 0 & 0 & 0 \\ 0 & 0 & V_{11}(0) & V_{12}(0) & V_{13}(0) & V_{14}(0) \\ 0 & 0 & \Theta_{11}(0) & \Theta_{12}(0) & \Theta_{13}(0) & \Theta_{14}(0) \\ U_{11}(L) & U_{12}(L) & 0 & 0 & 0 & 0 \\ 0 & 0 & V_{11}(L) & V_{12}(L) & V_{13}(L) & V_{14}(L) \\ 0 & 0 & \Theta_{11}(L) & \Theta_{12}(L) & \Theta_{13}(L) & \Theta_{14}(L) \end{bmatrix} \tag{47}$$

$$\boldsymbol{\Xi}=\begin{bmatrix} -N_{11}(0) & -N_{12}(0) & 0 & 0 & 0 & 0 \\ 0 & 0 & -S_{11}(0) & -S_{12}(0) & -S_{13}(0) & -S_{14}(0) \\ 0 & 0 & M_{11}(0) & M_{12}(0) & M_{13}(0) & M_{14}(0) \\ N_{11}(L) & N_{12}(L) & 0 & 0 & 0 & 0 \\ 0 & 0 & S_{11}(L) & S_{12}(L) & S_{13}(L) & S_{14}(L) \\ 0 & 0 & -M_{11}(L) & -M_{12}(L) & -M_{13}(L) & -M_{14}(L) \end{bmatrix} \tag{48}$$

In Eqs.(47)-(48), $U_{ij}(\cdot)$, $V_{ij}(\cdot)$, $\Theta_{ij}(\cdot)$, $N_{ij}(\cdot)$, $M_{ij}(\cdot)$ and $S_{ij}(\cdot)$ denote the (i,j) element of the corresponding matrices $\mathbf{U}(x),\mathbf{V}(x),\boldsymbol{\Theta}(x),\mathbf{N}(x),\mathbf{M}(x)$ and $\mathbf{S}(x)$ in Eqs.(41)-(42). Based on Eqs.(46) the following nodal matrix relation can be derived

$$\mathbf{f}=\boldsymbol{\Xi}\boldsymbol{\Gamma}^{-1}\left(\mathbf{u}-\tilde{\mathbf{u}}_f\right)+\tilde{\mathbf{f}}_f=\mathbf{D}(\omega)\mathbf{u}+\tilde{\mathbf{q}}(\omega) \tag{49}$$

$$\mathbf{D}(\omega)=\boldsymbol{\Xi}\boldsymbol{\Gamma}^{-1};\qquad \tilde{\mathbf{q}}(\omega)=-\boldsymbol{\Xi}\boldsymbol{\Gamma}^{-1}\tilde{\mathbf{u}}_f+\tilde{\mathbf{f}}_f \tag{50a,b}$$

In Eqs.(49)-(50), $\mathbf{D}(\omega)$ and $\tilde{\mathbf{q}}(\omega)$ are the exact 6×6 DSM and the exact 6×1 LV of the two-node beam element with an arbitrary number of KV dampers, shown in Figure 1. Respective sizes of $\mathbf{D}(\omega)$ and $\tilde{\mathbf{q}}(\omega)$ are 6×6 and 6×1 regardless of the number of dampers.

Matrix $\mathbf{D}(\omega)$ in Eq.(50a) is available in a closed form, because the inverse matrix $\boldsymbol{\Gamma}^{-1}$ can be inverted, in a symbolic form, from Eq.(47) for $\boldsymbol{\Gamma}$. Pertinent formulae are given in Appendix B. Also vector $\tilde{\mathbf{q}}(\omega)$ in Eq.(50b) can be computed in a closed form, for any polynomial load, based on the symbolic inverse matrix $\boldsymbol{\Gamma}^{-1}$ and closed-form expressions for $\tilde{\mathbf{u}}_f$ and $\tilde{\mathbf{f}}_f$ in Eqs.(46). Obviously, point loads can be considered, provided that pertinent load-dependent terms

$\tilde{\mathbf{u}}_P = \left[\tilde{U}_P(0,\xi) \;\; \tilde{V}_P(0,\xi) \;\; \tilde{\Theta}_P(0,\xi) \;\; \tilde{U}_P(L,\xi) \;\; \tilde{V}_P(L,\xi) \;\; \tilde{\Theta}_P(L,\xi)\right]^T$, $\tilde{\mathbf{f}}_P = \left[-\tilde{N}_P(0,\xi) \;\; -\tilde{S}_P(0,\xi) \;\; \tilde{M}_P(0,\xi) \;\; \tilde{N}_P(L,\xi) \;\; \tilde{S}_P(L,\xi) \;\; -\tilde{M}_P(L,\xi)\right]^T$ are included in Eqs.(46), where ξ is the position of the point load (see Eqs.(18)-(21), Eqs.(36)-(39)).

Finally, notice that there is a formal correspondence between Eq.(49) and the standard equilibrium equation of a two-node beam element in the FE method. However, unlike in the FE method, $\mathbf{D}(\omega)$ and $\tilde{\mathbf{q}}(\omega)$ are the exact DSM and the exact LV.

5. FREQUENCY RESPONSE OF PLANE FRAMES WITH DAMPERS

The DSM and LV built in Section 4 for a single beam can serve as a basis for a frequency response analysis of plane frames with an arbitrary number of KV dampers, as shown in Figure 2. This task can be accomplished building the global DSM and LV by a standard FE-like assembling procedure.

Writing Eq.(49) for the generic frame member (e) between two beam-to-column nodes in the form $\mathbf{f}_{loc}^{(e)} = \mathbf{D}^{(e)}(\omega)\mathbf{u}_{loc}^{(e)} + \tilde{\mathbf{q}}_{loc}^{(e)}(\omega)$, where subscript "*loc*" means that all quantities are referred to the local coordinate system, enforcing equilibrium at the beam-to-column nodes and the external kinematic B.C. of the frame leads to the following global equilibrium equations:

$$\mathbf{D}_{GL}(\omega)\mathbf{U} = \mathbf{F} \tag{51}$$

$$\mathbf{D}_{GL}(\omega) = \sum_{e=1}^{N_e}\left(\mathbf{T}^{(e)}\mathbf{L}^{(e)}\right)^T \mathbf{D}^{(e)}(\omega)\mathbf{T}^{(e)}\mathbf{L}^{(e)} \tag{52a}$$

$$\mathbf{F} = -\sum_{e=1}^{N_e}\left(\mathbf{T}^{(e)}\mathbf{L}^{(e)}\right)^T \tilde{\mathbf{q}}_{loc}^{(e)} + \mathbf{F}^{(0)} \tag{52b}$$

In Eqs.(52), $\mathbf{T}^{(e)}$ and $\mathbf{L}^{(e)}$ are the standard coordinate transformation matrix and connectivity matrix for each frame member (e): i.e., $\mathbf{T}^{(e)}$ relates the local reference system to the global reference system, $\mathbf{u}_{loc}^{(e)} = \mathbf{T}^{(e)}\mathbf{u}^{(e)}$:

$$\mathbf{T} = \begin{bmatrix} \mathbf{T}_\vartheta & \mathbf{0} \\ \mathbf{0} & \mathbf{T}_\vartheta \end{bmatrix}; \qquad \mathbf{T}_\vartheta = \begin{bmatrix} \cos\vartheta & \sin\vartheta & 0 \\ -\sin\vartheta & \cos\vartheta & 0 \\ 0 & 0 & 1 \end{bmatrix} \tag{53a,b}$$

where ϑ is the angle between the local reference system and the global one (ϑ positive clockwise), while $\mathbf{L}^{(e)}$ relates $\mathbf{u}^{(e)}$ to the global vector of displacements $\mathbf{U}=\left[U_1 \quad U_2 \quad U_3....\right]^T$, i.e. $\mathbf{u}^{(e)}=\mathbf{L}^{(e)}\mathbf{U}$. In Eq.(52a), $\mathbf{D}_{GL}(\omega)$ is the exact global DSM [16], and in Eq.(52b) $\mathbf{F}$ is the exact global LV, including the contribution of loads acting along the frame members and the vector $\mathbf{F}^{(0)}$ of external nodal forces, if they exist. Notice that $\mathbf{F}^{(0)}$ may include also the reaction forces of external TDs/TMDs applied at nodes. In this case, the i^{th} component of vector $\mathbf{F}$ will include an additional term $F_i=-k_{eq_i}(\omega)U_i$, with $k_{eq_i}(\omega)$ frequency-dependent stiffness of the nodal damper, given either by Eq.(4a) or Eq.(4b), depending on whether the damper is a grounded TD or an attached TMD.

At this stage, the exact FRM of the frame can be derived by matrix inversion [16-18]:

$$\mathbf{U}=\mathbf{H}(\omega)\mathbf{F}, \qquad \text{for} \quad \mathbf{H}(\omega)=\left(\mathbf{D}_{GL}(\omega)\right)^{-1} \tag{54}$$

Upon computing $\mathbf{U}$ from Eq.(54), the exact FRFs of all response variables can be built in any frame member using Eqs.(41)-(42), where vector $\mathbf{c}$ pertaining to the frame member is computed as $\mathbf{c}=\left(\mathbf{\Gamma}^{(e)}\right)^{-1}\left(\mathbf{u}_{loc}^{(e)}-\left(\tilde{\mathbf{u}}_f^{(e)}\right)_{loc}\right)$, see Eq.(46a), for $\mathbf{u}_{loc}^{(e)}=\mathbf{T}^{(e)}\mathbf{L}^{(e)}\mathbf{U}$. Exact FRFs in frame members loaded by point loads can be obtained using Eqs.(18)-(21) and Eqs.(36)-(39), with vector $\mathbf{c}=\left(\mathbf{\Gamma}^{(e)}\right)^{-1}\left(\mathbf{u}_{loc}^{(e)}-\left(\tilde{\mathbf{u}}_P^{(e)}\right)_{loc}\right)$. It is worth noticing that the exact FRFs inherently fulfil all required conditions at the dampers locations, (i.e. shear force and rotation discontinuities, axial force and displacement discontinuities, as well as continuity of the other response variables), as these conditions are fulfilled by the DSM and LV of each frame element (see remarks in Section 3.3).

5.1. Remarks on the proposed solutions for plane frames with dampers

The size of the FRM and LV (see Eqs.(51)-(52)) depends only on the total number of beam-to-column nodes, regardless of number and position of dampers and loads in each frame member. The FRM and LV can readily be updated for any changing parameter of the dampers (location, stiffness, damping) and loads, as well as positions of loads relative to the dampers, by simply updating the local DSM and LV of the frame members in Eqs.(49).

The exact FRFs of all response variables, built based on the derived FRM and LV, can serve as benchmark for the corresponding FRFs built by a standard FE method with two-node beam elements. Further advantages are that, in a standard FE method, one node shall be considered at the application point of any damper or point load, and re-meshing may be required as the positions of dampers and loads change, while the size of the derived FRM and LV depends only on the total number of beam-to-column nodes.

The exact DSM in Eq.(51) may be used for free vibration analysis. Representing the sought eigenvalues as λ=iω in all terms on the l.h.s. of Eq.(51), the characteristic equation will be built as

$$\det\left(\mathbf{D}_{GL}\left(\lambda\right)\right)=0. \tag{55}$$

The eigenfunctions in any frame member will be built by Eqs.(41)-(42), where vector $\mathbf{c}$ pertaining to the frame member is given by $\mathbf{c}=\left(\mathbf{\Gamma}^{(e)}\right)^{-1}\mathbf{u}_{loc}^{(e)}$, i.e. by Eq.(46a) with load-dependent term $\left(\tilde{\mathbf{u}}_{f}^{(e)}\right)_{loc}=\mathbf{0}$. Obviously, $\mathbf{u}_{loc}^{(e)}=\mathbf{T}^{(e)}\mathbf{L}^{(e)}\mathbf{U}$ with $\mathbf{U}$ obtained as non-trivial solution of Eq.(51), where $\mathbf{F}=\mathbf{0}$ is set on the r.h.s., while the computed eigenvalues are replaced for λ on the l.h.s.

It has to be noticed, however, that difficulties arise in computing the eigenvalues λ with increasing size of matrix $\mathbf{D}_{GL}(\lambda)$, as pointed out by several authors [17-18]. Approximate solutions to overcome a similar problem have been proposed [13,59]. Notice that eigenvalues and associated modes could be extracted also using classical FRF-based modal identification methods [60-61], such as multi-degree-of-freedom (MDOF) methods targeting multiple modes at a time, based on single-input-single-output (SISO), single-input-multi-output (SIMO) or multi-input-multi-output (MIMO) data, computed from the derived exact FRM in Eq.(54). There exist MDOF methods that, in the most general MIMO case, would provide eigenvalues and modes upon solving a characteristic matrix polynomial equation, built from a set of equations where each involves the FRF values at a given frequency (see the comprehensive study on MDOF methods in ref.[62]). SDOF methods addressing a single mode at a time also exist, based on SISO or SIMO data, as the circle-fit method (for a review on this and other SDOF methods as inverse and Dobson's methods,

see ref. [60-61]). Any FRF-based method, however, relies on the assumption that the FRF can be reverted to specific analytical expressions, for instance a rational fraction form in some MDOF methods or, in the vicinity of resonances, the typical FRF of a SDOF system in SDOF methods, and accuracy may vary depending on the system under study [60-62]. Alternatively, for modal analysis of large size frames with KV dampers, it may be convenient to use a standard FE approach, which provides the eigenvalues as solutions of a standard linear eigenvalue problem, upon reducing the second-order differential equations to first-order ones in the state variables [13].

6. NUMERICAL APPLICATIONS

6.1. Example A

The beam in Figure 3 features two elastic translational supports, two TMDs and three RDs. Beam parameters are: $E=19.5\times10^{10}$ N m^{-2}, $I=5.41\times10^{-5}$ m^4, $m_0=49.54$ kg m^{-1}, $L=12$ m. For the RDs: $k_{\Delta\theta_j}=k_{\Delta\theta}=5.27\times10^6$ N m (=$6EI/L$), $c_{\Delta\theta_j}=c_{\Delta\theta}=10^3$ N m s for j=1,2,4; for the TMDs: $k_{M_j}^{(v)}=k_M^{(v)}=10^6$ N m^{-1}, $c_{M_j}^{(v)}=c_M^{(v)}=10^3$ N m^{-1}s, $M_j^{(v)}=M^{(v)}=2\times10^3$ kg for j=3,5; for the elastic translational supports: $k_{G_j}^{(v)}=k_G^{(v)}=10^5$ N m^{-1} for j=2,4 (i.e. $c_{G_j}^{(v)}=0$ in Eq.(4a)). The following frequency responses are sought: (a) DGFs for a transverse point load $1\cdot e^{i\omega t}$ at various $x=\xi$; (b) FRFs for a transverse triangular load $f(x)\cdot e^{i\omega t}$ over the interval [L/3, 2L/3], with $f(x)=(2L-3x)/L$.

The proposed method is implemented treating the left-end damper as an internal damper at $x=0^+=10^{-6}$ m, that is a total number of 5 damper locations is considered. For comparison, the solution is also built by the classical approach, i.e. representing the steady-state response in a trigonometric form with 4 integration constants over each segment between two consecutive dampers/point load locations, and enforcing matching conditions at the dampers/point load locations along with the B.C. For the segment under the triangular load, a particular integral can be obtained in a closed form [57]. It is important to point out that both methods provide the exact frequency response. However, by the proposed method DGFs and FRFs are available in a closed form using Eqs.(36)-(39) and Eqs.(42). In contrast, the classical solution involves 6×4 = 24

integration constants for the point load case, and 5×4 = 20 integration constants for the triangular load case, to be computed by inverting the coefficient matrix associated with the matching conditions + 4 B.C. Due to the large size, in this case matrix inversion is performed numerically, and the inverse matrix shall be re-computed for any forcing frequency of interest. Results will be presented in terms of real, imaginary parts and amplitude $\sqrt{\mathrm{Re}(\cdot)^2 + \mathrm{Im}(\cdot)^2}$.

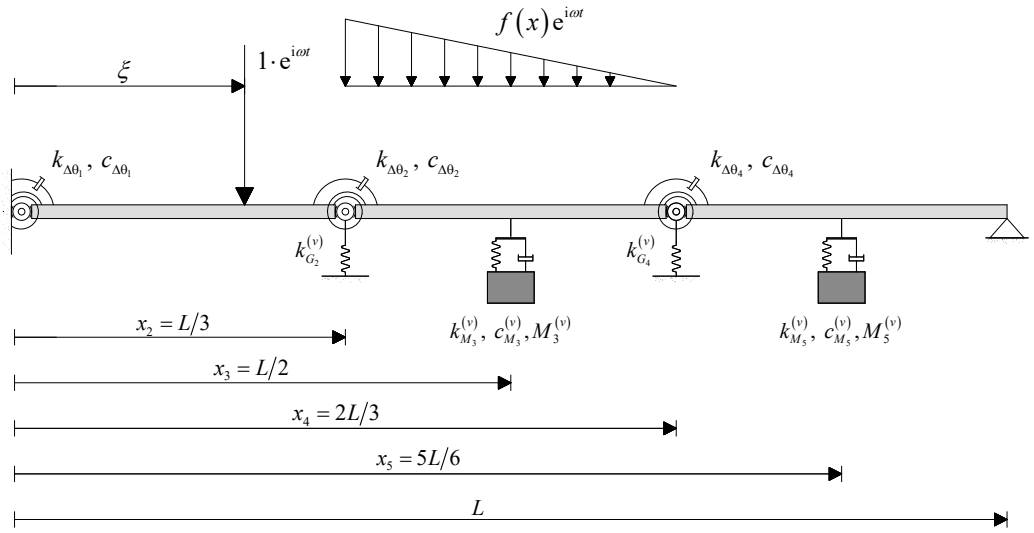

Figure 3. Beam with elastic translational supports, TMDs and RDs under two different loads: (a) unit point load; (b) triangular load.

Prior to discuss the frequency response, the eigenvalues of the first 7 modes are computed by the proposed method as roots of Eq.(45b), and by the classical approach, using Mathematica [57]. As shown in Table 1, the eigenvalues obtained by the two methods generally agree up to four decimal places. They occur in complex-conjugate pairs. It is noticed that the corresponding eigenfunctions, which can be computed as explained in Section 3.3, occur also in complex-conjugate pairs. Thus, the modal solution associated with each pair is given by the sum of two harmonic motions shifted by 90°, modulated by an exponentially-decaying function, as is typical in non-classically damped structural systems [63]. Time decay of the modulating exponential function and circular frequency of the component harmonic motions are given, respectively, by real part and absolute value of the imaginary part of the eigenvalue pair, while the beam configurations associated with the component harmonic motions are given by real and imaginary parts of the eigenfunction pair (see Eq. (21) in ref. [63]). Eigenfunctions are not shown for brevity.

Mode	Classical method	Proposed method
1	– 0.0200551 ± 11.670833 i	– 0.0200552 ± 11.670884 i
2	– 0.1674120 ± 20.216751 i	– 0.1674123 ± 20.216762 i
3	– 2.2983627 ± 79.851724 i	– 2.2983935 ± 79.851798 i
4	– 1.6086699 ± 125.63097 i	– 1.6086799 ± 125.63091 i
5	– 4.1011346 ± 309.52683 i	– 4.1011940 ± 309.52681 i
6	– 5.6167680 ± 459.64383 i	– 5.6167448 ± 459.64382 i
7	– 12.441175 ± 692.62783 i	– 12.441197 ± 692.62785 i

Table 1. Eigenvalues of the beam in Figure 3.

Figure 4 shows the exact DGFs of all response variables for a 5Hz point load $1e^{i\omega t}$ applied at $\xi=L/2$, as obtained by Eqs.(36)-(39) (continuous line) and by the classical approach (symbol "•"). The two solutions are in perfect agreement, in both real part and imaginary part. The proposed solution inherently satisfies all the required conditions at the dampers locations: the rotation is discontinuous at the RDs locations, the shear force is discontinuous at the locations of TMDs, translational supports and point load. Correspondingly, the deflection is not differentiable at the RDs locations and the bending moment is not differentiable at the locations of TMDs, translational supports and point load, in agreement with the beam governing equations in Appendix A.

Figure 5 shows the deflection DGF over the whole axis, for a 3Hz point load applied at ξ spanning [0,L]. As expected (see for instance ref. [25,65]), Figure 5a shows that the deflection DGF is symmetric, i.e. $V(x,\xi)=V(\xi,x)$. For a further insight, the deflection DGFs for a point load applied at $\xi=L/3$, $L/2$ and $2L/3$ are reported in Figure 5b (= cross sections of the deflection DGF in Figure 5a by a vertical plane at $\xi=L/3$, $L/2$ and $2L/3$), while the deflection DGFs computed at $x=L/3$, $L/2$ and $2L/3$ for a point load applied at ξ within [0, L] are reported in Figure 5c (= cross sections of the deflection DGF in Figure 5a by a vertical plane at $x=L/3$, $L/2$ and $2L/3$). Results in Figures 5b and 5c are coincident, due to the symmetry of the DGFs.

Finally, Figure 6 shows the deflection DGF amplitude at $x=L/3$, for a point load applied at $\xi=L/2$ with frequency spanning the interval 0-150 Hz, as obtained by Eq.(36) and by the classical approach. The two solutions are coincident.

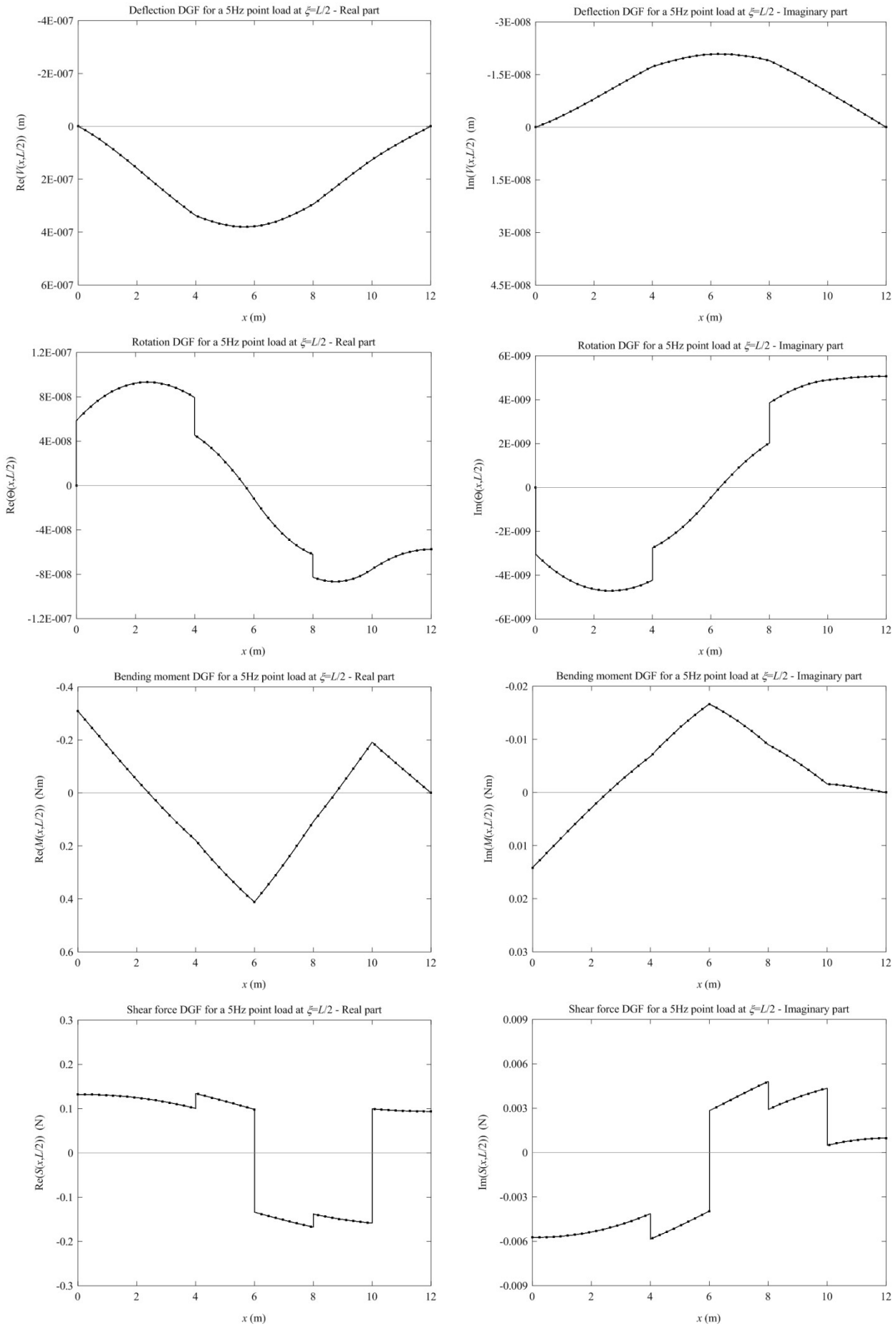

Figure 4. Beam in Figure 3: DGFs for a 5Hz point load applied at $\xi=L/2$; (continuous line: proposed exact solution; (•): classical exact solution).

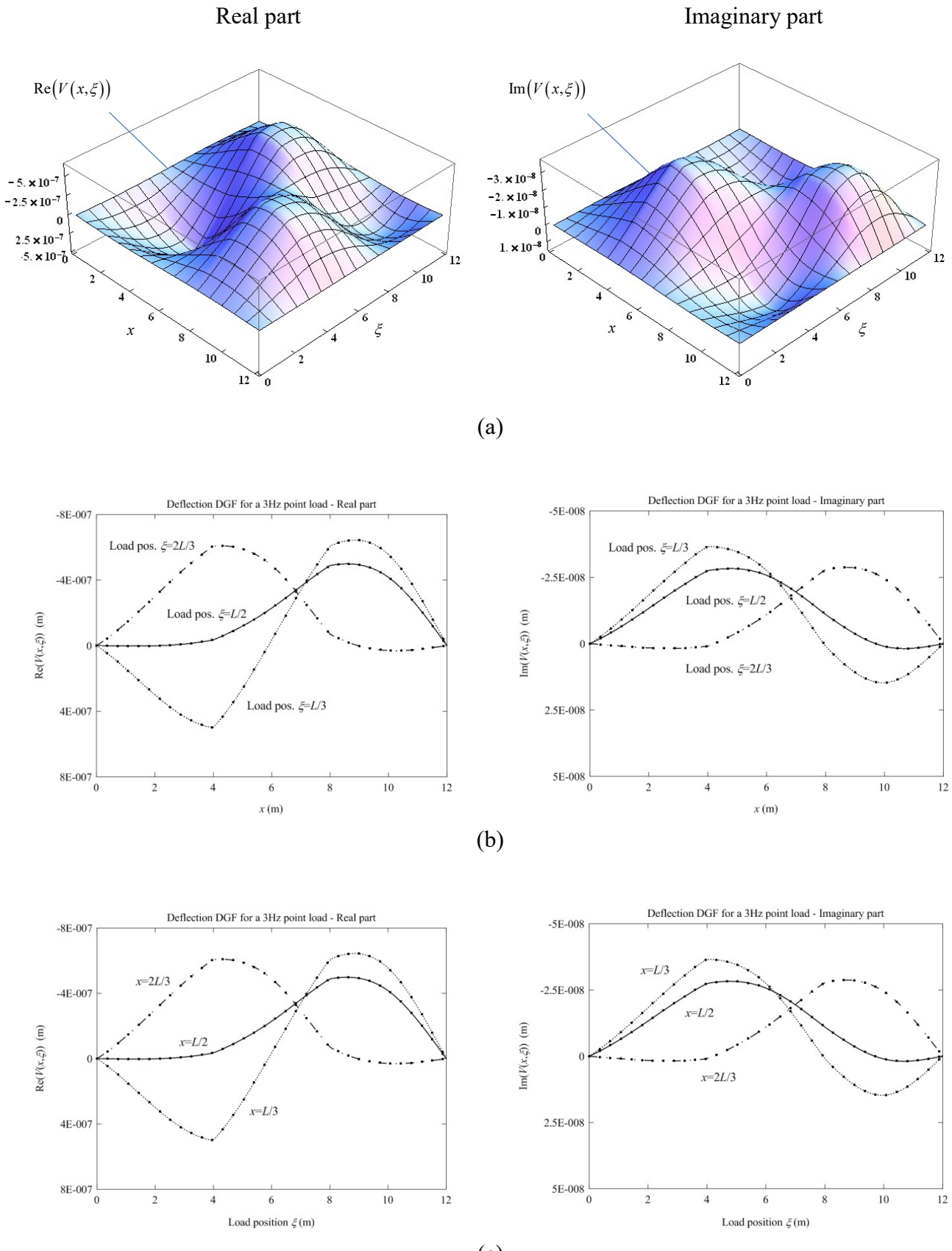

Figure 5. Beam in Figure 3: deflection DGF for a 3Hz point load, computed at x for various load positions ξ: (a) for all x and ξ, $x,\xi \in [0,L]$; (b) at all x for given load positions ξ (ξ=L/3, L/2, 2L/3); (c) at given x (x=L/3, L/2, 2L/3) for all load positions ξ; (continuous/dashed-dotted/dotted lines: proposed exact solution; (•): classical exact solution).

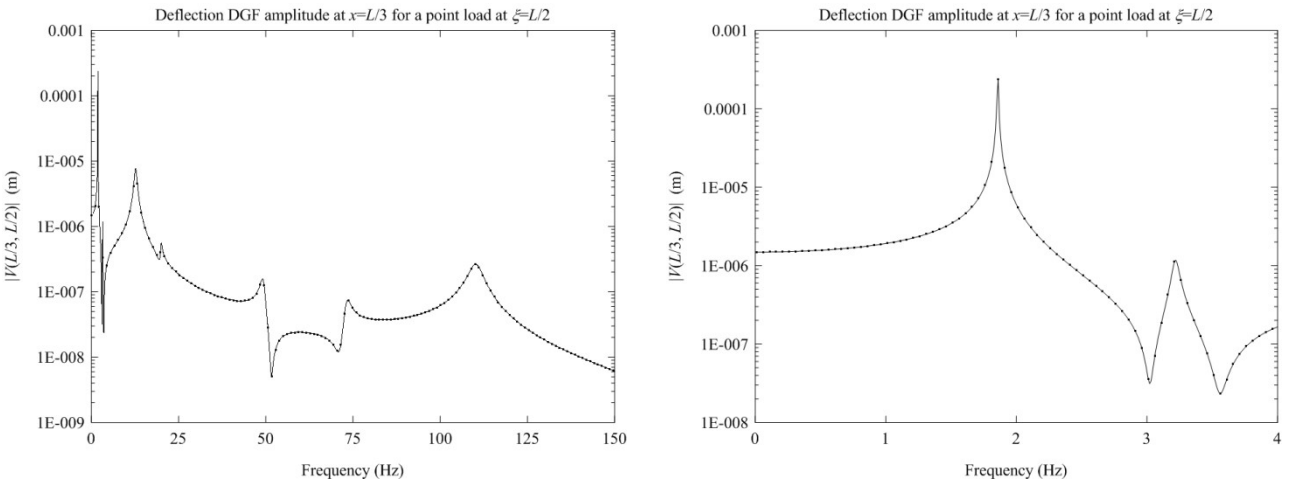

Figure 6. Beam in Figure 3: deflection DGF amplitude at $x=L/3$, for a 0-150 Hz point load applied at $\xi=L/2$, with a zoomed view on the right; (continuous line: proposed exact solution; (•): classical exact solution).

Next, Figure 7 shows the FRFs of rotation and shear force due to a 2Hz triangular load applied over [$L/3$, $2L/3$]. The FRFs are obtained by Eqs.(42), using Eq.(43) to express the load-dependent terms $\tilde{V}_f(x)$, $\tilde{\Theta}_f(x)$…. in a closed form. Again, a perfect agreement is encountered between the proposed exact solution and the classical exact solution.

Figure 8 shows the deflection FRF amplitude at $x=L/2$ due to the 2Hz triangular load, as computed by the proposed method, when damping and stiffness of certain dampers vary, while all other parameters hold the reference values taken in Figure 4 through Figure 7. In particular, damping and stiffness of the RDs vary in Figure 8a, while those of the TMDs vary in Figure 8b. In both cases, the deflection FRF progressively decreases as the damping parameter increases, with maxima at approximately $k_{\Delta\theta_j}=k_{\Delta\theta}=1.4\times10^7$ N m in Figure 8a and $k_{M_j}^{(v)}=k_M^{(v)}=2.2\times10^6$ N m^{-1} in Figure 8b, regardless of the damping parameter. It is also noticed that, by increasing the damping parameter $c_M^{(v)}$ in the TMDs, the deflection FRF reduces more rapidly than increasing the damping parameter $c_{\Delta\theta}$ in the RDs. For a further insight, Figure 9 shows the deflection FRF amplitude at $x=L/2$ for a forcing frequency within 0-4 Hz, considering $c_{\Delta\theta_j}=c_{\Delta\theta}=10^3$ N m s and various stiffness parameters $k_{\Delta\theta_j}=k_{\Delta\theta}$ in Figure 9a ($k_{\Delta\theta}=4.39\times10^5$ N m$=EI/2L$), $c_{M_j}^{(v)}=c_M^{(v)}=10^3$ N m^{-1}s and various stiffness parameters $k_{M_j}^{(v)}=k_M^{(v)}$ in Figure 9b. Consistently with results in Figure 8, the

deflection FRF at 2 Hz is larger for $k_{\Delta\theta} = 1.4\times10^{7}$ N m in Figure 9a, for $k_M^{(v)} = 2.2\times10^{6}$ N m^{-1} in Figure 9b.

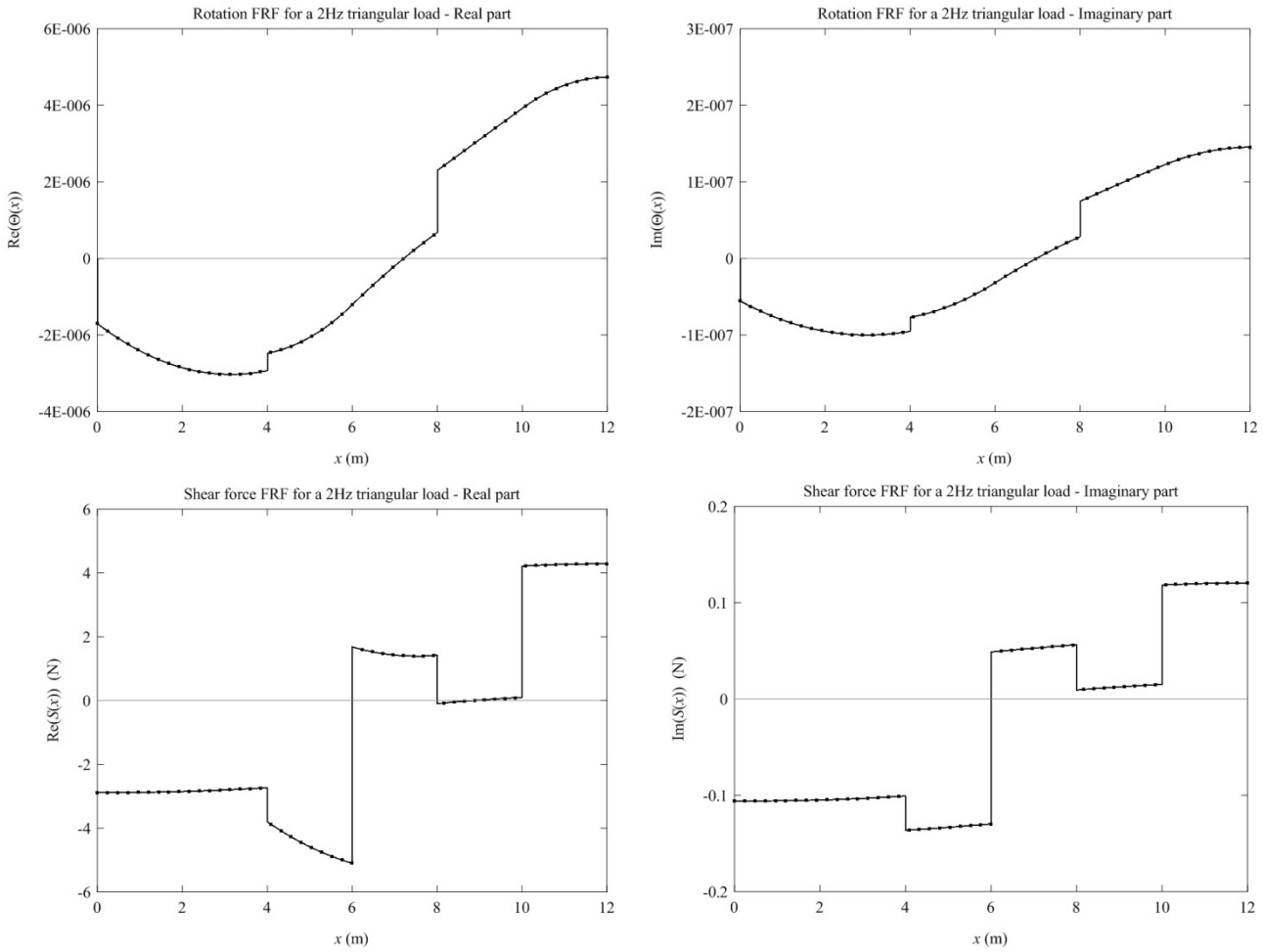

Figure 7. Beam in Figure 3: FRFs for a 2Hz triangular load over [L/3, 2L/3]; (continuous line: proposed exact solution; (•): classical exact solution).

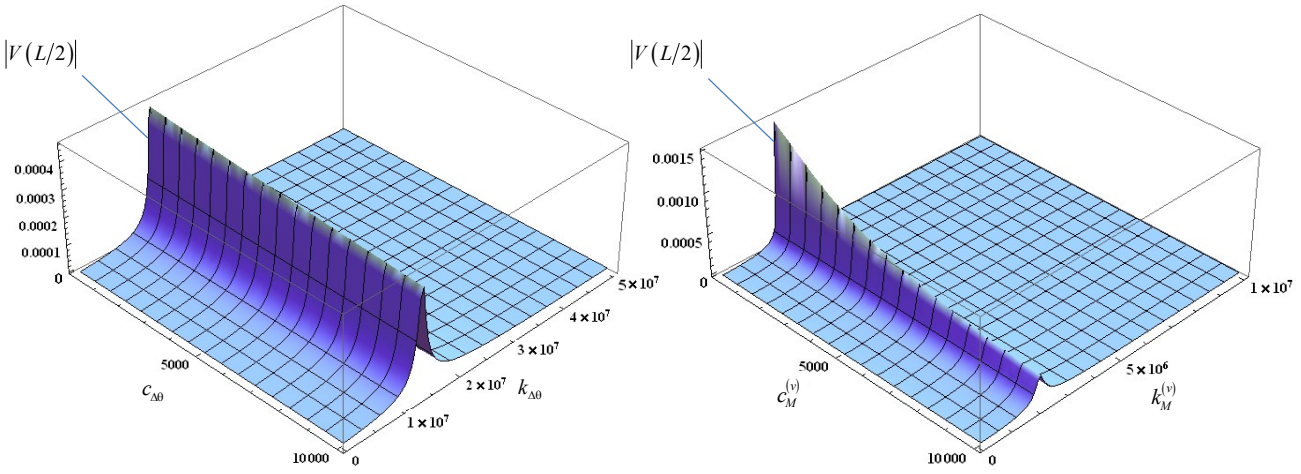

(a) (b)

Figure 8. Beam in Figure 3: deflection FRF amplitude at x=L/2 for a 2Hz triangular load over [L/3, 2L/3] and varying parameters; (a) for different $c_{\Delta\theta}$ and $k_{\Delta\theta}$ of the RDs; (b) for different $c_M^{(v)}$ and $k_M^{(v)}$ of the TMDs.

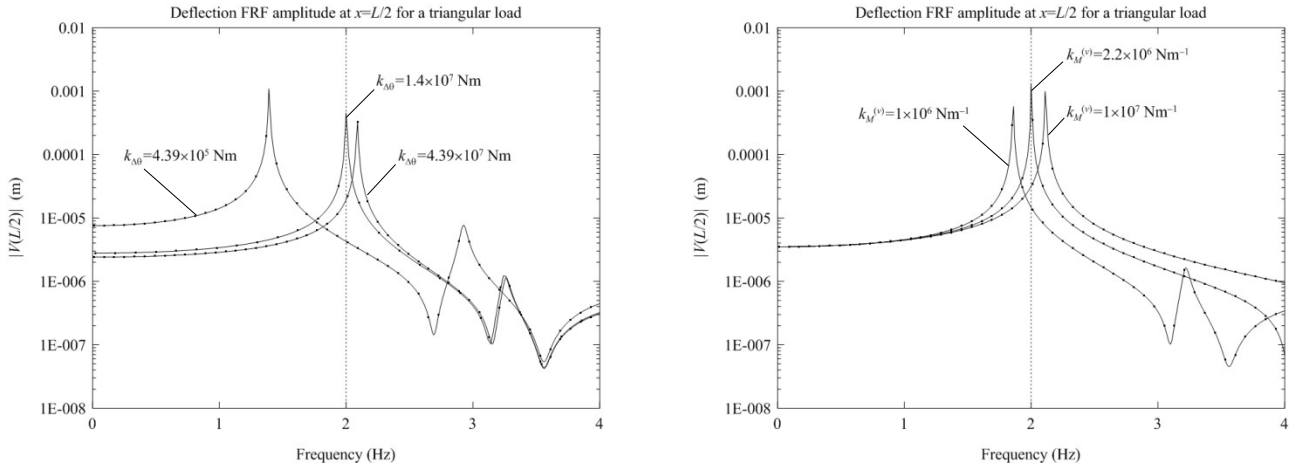

Figure 9. Beam in Figure 3: deflection FRF amplitude at $x=L/2$ for a 0-4 Hz triangular load over [$L/3$, $2L/3$]; (a) for $c_{\Delta\theta}=10^3$ N m s and various $k_{\Delta\theta}$ of the RDs; (b) for $c_M^{(v)}=10^3$ N m^{-1}s and various $k_M^{(v)}$ of the TMDs; (continuous line: proposed exact solution; (•): classical exact solution).

6.2. Example B

The beam in Figure 10 includes a fixed support, a viscous damper and a tip mass. For this beam, DGFs under a transverse point load have been built in ref. [25] by an approximate method using the eigenfunctions of the bare clamped-free beam, and by the classical exact approach (with 4×3 =12 equations).

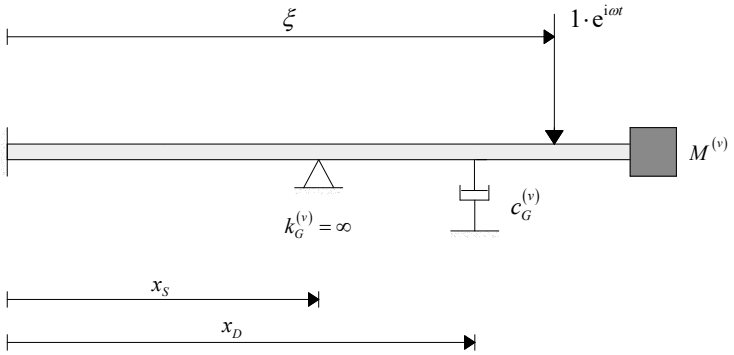

Figure 10. Beam with a fixed support, a viscous damper and a tip mass under a unit point load.

The following parameters are selected: E = 7.0×10^{10} N m^{-2}, I = 5.21×10^{-10} m^4, m_0 = 0.675 kg m^{-1}, L=1 m. For comparison with ref.[25] where results are dimensionless, damping parameter $c_G^{(v)}$ and forcing frequency ω are derived from the dimensionless parameters $\hat{c}_G^{(v)}=0.5$ and $\hat{\omega}=5$ used in ref. [25], i.e here $c_G^{(v)}=\hat{c}_G^{(v)}L^{-1}\left(m_0EI\right)^{1/2}=2.48$ N m^{-1}s

and $\omega = \hat{\omega}\left(EI/m_0L^4\right)^{1/2} = 36.75$ rad s^{-1} $(= 5.85$ Hz$)$ are selected. The proposed method is implemented modelling the fixed support as an elastic support with a relatively high stiffness value, namely $k_G^{(v)} = 10^7 \times EI/L^3$, and assuming the tip mass as located at $x=L^-=1-\varepsilon$, $\varepsilon=10^{-6}$ m.

	$\hat{x}_S$					
	0.25		0.50		0.75	
$\hat{x}$	Ref.[25]	Proposed method	Ref.[25]	Proposed method	Ref.[25]	Proposed method
0.1	0.000297	0.000297	0.000955	0.000960	0.001053	0.001054
0.2	0.000397	0.000395	0.002865	0.002878	0.003558	0.003558
0.3	0.000853	0.000858	0.004292	0.004312	0.006526	0.006529
0.4	0.003865	0.003877	0.003810	0.003828	0.008992	0.008993
0.5	0.008313	0.008342	0	0	0.009988	0.009993
0.6	0.013847	0.013909	0.008128	0.008174	0.008590	0.008592
0.7	0.020142	0.020256	0.019929	0.020051	0.003882	0.003878
0.8	0.026907	0.027099	0.034368	0.034593	0.004981	0.004982
0.9	0.033911	0.034200	0.050457	0.050817	0.017478	0.017489
1.0	0.040996	0.041394	0.067314	0.067825	0.031803	0.031829

Table 2. Beam in Figure 10: dimensionless deflection DGF amplitude for a point load at the tip, with dimensionless frequency $\hat{\omega} = 5$, $\hat{x}_D = 0.75$ and $M^{(v)}/m_0L = 1.0$.

	$\hat{x}_D$					
	0.25		0.50		0.75	
$\hat{x}$	Ref.[25]	Proposed method	Ref.[25]	Proposed method	Ref.[25]	Proposed method
0.1	0.000297	0.000297	0.000297	0.000297	0.000297	0.000297
0.2	0.000398	0.000396	0.000398	0.000396	0.000397	0.000395
0.3	0.000855	0.000858	0.000855	0.000858	0.000853	0.000858
0.4	0.003875	0.003878	0.003877	0.003878	0.003865	0.003877
0.5	0.008342	0.008343	0.008345	0.008343	0.008313	0.008342
0.6	0.013910	0.013912	0.013912	0.013912	0.013847	0.013909
0.7	0.020260	0.020261	0.020259	0.020261	0.020142	0.020256
0.8	0.027105	0.027105	0.027100	0.027105	0.026907	0.027099
0.9	0.034208	0.034208	0.034199	0.034208	0.033911	0.034200
1.0	0.041404	0.041401	0.041389	0.041402	0.040996	0.041394

Table 3. Beam in Figure 10: dimensionless deflection DGF amplitude for a point load at the tip, with dimensionless frequency $\hat{\omega} = 5$, $\hat{x}_S = 0.25$ and $M^{(v)}/m_0L = 1.0$.

	$\hat{\xi}$					
	0.5		0.75		1.00	
$\hat{x}$	Ref.[25]	Proposed method	Ref.[25]	Proposed method	Ref.[25]	Proposed method
0.1	0.000113	0.000113	0.000029	0.000029	0.000297	0.000297
0.2	0.000152	0.000150	0.000039	0.000039	0.000398	0.000396
0.3	0.000311	0.000313	0.000091	0.000090	0.000855	0.000858
0.4	0.001117	0.001118	0.000554	0.000554	0.003877	0.003878
0.5	0.001521	0.001523	0.001630	0.001628	0.008345	0.008343
0.6	0.000927	0.000929	0.003594	0.003592	0.013912	0.013912
0.7	0.000595	0.000593	0.006732	0.006732	0.020259	0.020261
0.8	0.002807	0.002804	0.011322	0.011320	0.027100	0.027105
0.9	0.005467	0.005464	0.017168	0.017168	0.034199	0.034208
1.0	0.008345	0.008343	0.023634	0.023638	0.041389	0.041402

Table 4. Beam in Figure 10: dimensionless deflection DGF amplitude for a point load at varying position $\hat{\xi}$, with dimensionless frequency $\hat{\omega} = 5$, $\hat{x}_S = 0.25$, $\hat{x}_D = 0.5$ and $M^{(v)}/m_0L = 1.0$.

	$M^{(v)}/m_0L$					
	0.5		1.50		2.50	
$\hat{x}$	Ref.[25]	Proposed method	Ref.[25]	Proposed method	Ref.[25]	Proposed method
0.1	0.000616	0.000615	0.000196	0.000196	0.000116	0.000116
0.2	0.000824	0.000820	0.000262	0.000261	0.000156	0.000155
0.3	0.001772	0.001778	0.000564	0.000565	0.000335	0.000336
0.4	0.008033	0.008037	0.002555	0.002555	0.001519	0.001519
0.5	0.017289	0.017292	0.005500	0.005498	0.003270	0.003269
0.6	0.028825	0.028834	0.009169	0.009167	0.005451	0.005450
0.7	0.041976	0.041994	0.013351	0.013352	0.007938	0.007938
0.8	0.056151	0.056179	0.017860	0.017862	0.010619	0.010619
0.9	0.070861	0.070901	0.022538	0.022542	0.013400	0.013402
1.0	0.085759	0.085811	0.027277	0.027283	0.016218	0.016220

Table 5. Beam in Figure 10: dimensionless deflection DGF amplitude for a point load at the tip, with dimensionless frequency $\hat{\omega}=5$, $\hat{x}_S=0.25$ and $\hat{x}_D=0.5$.

Table 2 through Table 5 report the dimensionless deflection DGF amplitude (dividing by FL^3/EI, with F=1) for various positions of fixed support ($\hat{x}_S=x_S/L$), viscous damper ($\hat{x}_D=x_D/L$), load ($\hat{\xi}=\xi/L$), tip-mass to beam-mass ratios $M^{(v)}/m_0L$, built by the proposed exact method and approximate method in ref. [25] (classical exact solutions reported in ref. [25] are identical to the proposed exact solutions, see ref. [25], and are omitted for brevity). Results agree well. As pointed in ref. [25], maxima values of deflection are generally attained at the tip, changing the damper position does not affect the deflection (Table 3), while tip deflections decrease for increasing tip-mass to beam-mass ratios (Table 5). For completeness, Figure 11 shows proposed and classical exact solutions, for the cases considered in Table 2 and Table 5. The two exact solutions coincide.

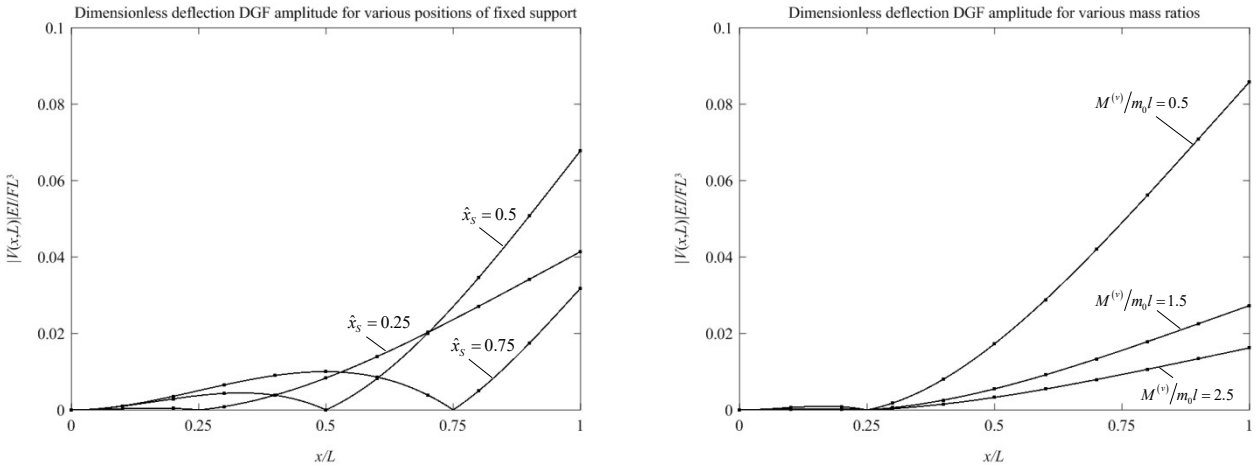

(a) (b)

Figure 11. Beam in Figure 10: deflection DGF amplitude for a point load at the tip, with dimensionless frequency $\hat{\omega}=5$; (a) varying fixed support position; (b) varying tip-mass to beam-mass ratio; (continuous line: proposed exact solution; (•): classical exact solution).

Next, for a further comparison with existing results, consider the beam in Figure 10 but without fixed support. For this beam, approximate eigenvalues have been built in ref. [64] using the eigenfunctions of the bare clamped-free beam, considering E, I, m_0, L selected above, and various damper positions x_D, damping parameters $c_G^{(v)}$, and tip-mass to beam-mass ratios $M^{(v)}/m_0 L$. Here, Table 6 compares the eigenvalues obtained in ref. [64] for $x_D = 0.2$ m, $c_G^{(v)} = 5.5$ N m^{-1}s, $M^{(v)}/m_0 L = 3.0$ (see Table 1 in ref. [64], left column) with those computed by the proposed exact method based on Eq.(45b), and classical exact approach, using Mathematica [57]. The eigenvalues built by proposed method and classical approach agree up to four decimal places. Also, the agreement with the eigenvalues built in ref. [64] is satisfactory, confirming that the eigenfunctions of the bare beam can provide accurate results [25, 64]. The eigenfunctions corresponding to the eigenvalues in Table 6 occur in complex-conjugate pairs (they can be computed as described in Section 3.3), and comments on the associated modal solutions are analogous to those on Table 1.

Mode	Ref. [64]	Classical method	Proposed method
1	– 0.0040272 ± 7.0761439 i	– 0.0040265 ± 7.0760199 i	– 0.0040265 ± 7.0760199 i
2	– 0.8645606 ± 115.55949 i	– 0.8643624 ± 115.53812 i	– 0.8643624 ± 115.53812 i
3	– 4.7401173 ± 369.87972 i	– 4.7274572 ± 369.63926 i	– 4.7274574 ± 369.63926 i
4	– 8.8695639 ± 769.52033 i	– 8.8637063 ± 768.46572 i	– 8.8637065 ± 768.46573 i
5	– 8.1726420 ± 1315.4709 i	– 8.1239558 ± 1312.3602 i	– 8.1239556 ± 1312.3602 i
6	– 2.9717554 ± 2008.9140 i	– 3.0503751 ± 2001.5821 i	– 3.0503748 ± 2001.5821 i
7	– 0.0007940 ± 2850.8149 i	– 0.0012171 ± 2835.8182 i	– 0.0012171 ± 2835.8182 i
8	– 3.0596072 ± 3843.1176 i	– 2.7547389 ± 3815.0261 i	– 2.7547386 ± 3815.0261 i
9	– 7.1857527 ± 4989.6100 i	– 7.3133397 ± 4939.2834 i	– 7.3133522 ± 4939.2834 i
10	– 8.2254317 ± 6300.5273 i	– 7.3296927 ± 6208.5998 i	– 7.3296734 ± 6208.5998 i

Table 6. Eigenvalues of the beam in Figure 10 without fixed support, damper position $x_D = 0.2$ m, damping parameter $c_G^{(v)} = 5.5$ N m^{-1}s, tip-mass to beam-mass ratio $M^{(v)}/m_0 L = 3.0$, as in ref. [64].

6.3. Example C

Consider the plane frame in Figure 12, where two RDs are applied at the ends of members 4-5, two TDs are applied along member 3, a TD is applied at node N3 and lumped masses are located at the mid span of members 4-5. Frame parameters are: $E = 19.5\times10^{10}$ N m^{-2}, $I = 5.41\times10^{-5}$ m^4, $A = 64.34\times10^{-4}$ m^2, $m_0 = 49.54$ kg m^{-1} (corresponding to a mass density = $7.7\cdot10^3$ kg m^{-3}), $L = 6$ m, $H = 3$ m. The TDs in member 3 are located at $x_1 = H/3$ and $x_2 = 2H/3$, with

$k_{G_j}^{(v)} = k_G^{(v)} = 5\times10^6$ N m^{-1}, $c_{G_j}^{(v)} = c_G^{(v)} = 1\times10^4$ N m^{-1}s, for j=1,2. In members 4-5, the RDs are located at $x_1 = 0^+ = \varepsilon$ and $x_3 = L^- = L - \varepsilon$, for $\varepsilon = 10^{-6}$ m, with $k_{\Delta\theta_j} = k_{\Delta\theta} = 1.05\times10^7$ N m (=6EI/L) and $c_{\Delta\theta_j} = c_{\Delta\theta} = 5\times10^3$ N m s, for j=1,3; also, the lumped mass is $M_2^{(v)} = 1\times10^3$ kg, with $k_{M_2}^{(v)} = \infty$; damper at node N3 is given the same parameters of dampers in member 3, i.e. $k_G^{(v)} = 5\times10^6$ N m^{-1} and $c_G^{(v)} = 1\times10^4$ N m^{-1}s. The lumped mass is considered in both bending and axial vibrations. A uniform transverse load, $1\cdot e^{i\omega t}$, acts on member 1.

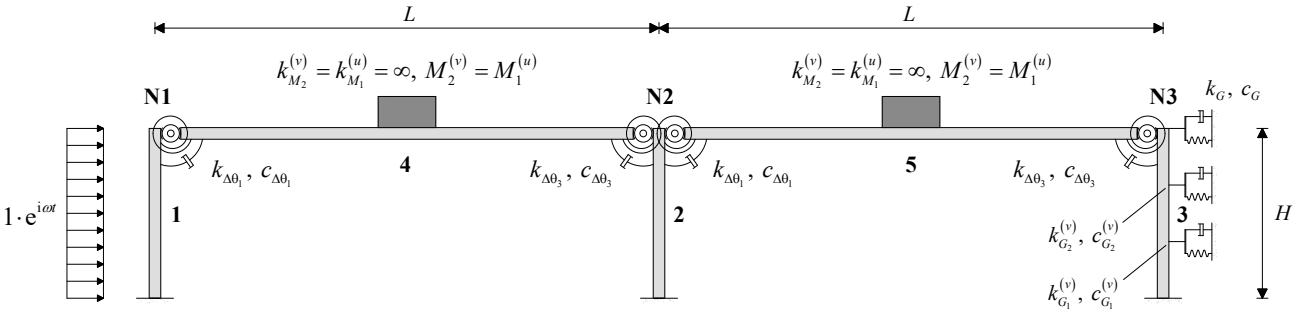

Figure 12. Plane frame with TDs, RDs and lumped masses under a transverse uniform load over member 1.

The proposed method is used to build the exact FRF of the response variables along the frame. Since a unique frame member can be taken between two beam-to-column nodes regardless of the presence of the TDs, RDs and lumped masses, the size of matrix $\mathbf{D}_{GL}(\omega)$ in Eq.(52a) is 9×9, corresponding to 3 degrees of freedom for each of the unrestrained nodes N1-N2-N3. Vector **F** in Eq.(52b) can be built upon building the exact LV of member 1 by Eq.(46b), where $\tilde{\mathbf{f}}_f$ is derived from the load-dependent terms in Eqs.(41)-(42). From the nodal displacements **U** in Eq.(54), the exact FRFs can be obtained in every frame member using Eqs.(41)-(42), with vector **c** pertaining to the frame member given as $\mathbf{c} = \left(\mathbf{\Gamma}^{(e)}\right)^{-1}\left(\mathbf{u}_{loc}^{(e)} - \left(\tilde{\mathbf{u}}_f^{(e)}\right)_{loc}\right)$. For comparison, the FRFs are also obtained by a classical FE method, with various two-node EB beam elements along the frame members.

Prior to discuss the frequency response, the eigenvalues of the first 6 modes are computed by the proposed method as roots of Eq.(55) and by the FE method with 6 and 30 elements along each frame member, using Mathematica [57]. As shown in Table 7, the two solutions agree very

satisfactorily, with higher accuracy as 30 elements are used. Notice that the eigenfunctions, which can be computed as explained in Section 5.1, occur also in complex-conjugate pairs. Comments on the associated modal solutions mirror those on Table 1 [63], and are not repeated for brevity.

Mode	FE method - 6 elements	FE method - 30 elements	Proposed method
1	– 0.1943286 ± 60.471774 i	– 0.1942934 ± 60.469847 i	– 0.1942933 ± 60.469297 i
2	– 0.2818721 ± 65.487715 i	– 0.2816758 ± 65.478913 i	– 0.2816440 ± 65.476398 i
3	– 2.3251913 ± 70.534882 i	– 2.3198923 ± 70.494422 i	– 2.3190771 ± 70.488197 i
4	– 4.4613978 ± 553.16064 i	– 4.4375381 ± 552.45443 i	– 4.4337247 ± 552.33254 i
5	– 4.1493087 ± 581.06553 i	– 4.1122161 ± 579.84834 i	– 4.1061937 ± 579.61649 i
6	– 4.3936082 ± 808.65483 i	– 4.3379125 ± 806.30717 i	– 4.3286780 ± 805.83441 i

Table 7. Eigenvalues of the frame in Figure 12.

Figure 13 through Figure 17 show the FRFs computed by the proposed method, as due to a 10Hz uniform load over member 1. All required conditions at the dampers/mass locations are satisfied: there are rotation discontinuities at nodes N1-N2-N3 due to the RDs, shear force discontinuities at the TDs and lumped masses locations, mirrored by slope discontinuities in the bending moment. Equilibrium is satisfied at all nodes (the nodal damper reaction is $-1.98 + i\ 0.27$ N).

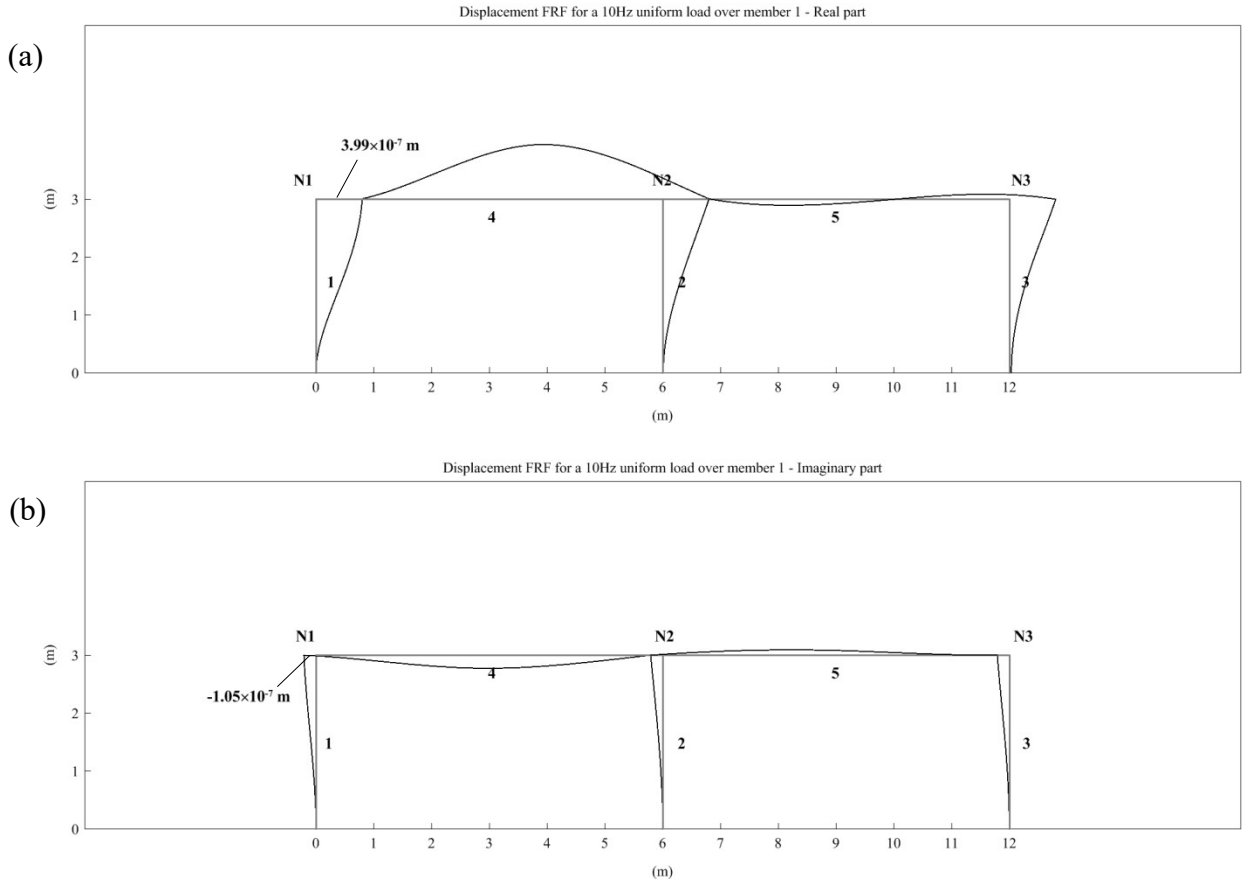

Figure 13. Displacement FRF for a 10Hz uniform load over member 1: (a) real part; (b) imaginary part.

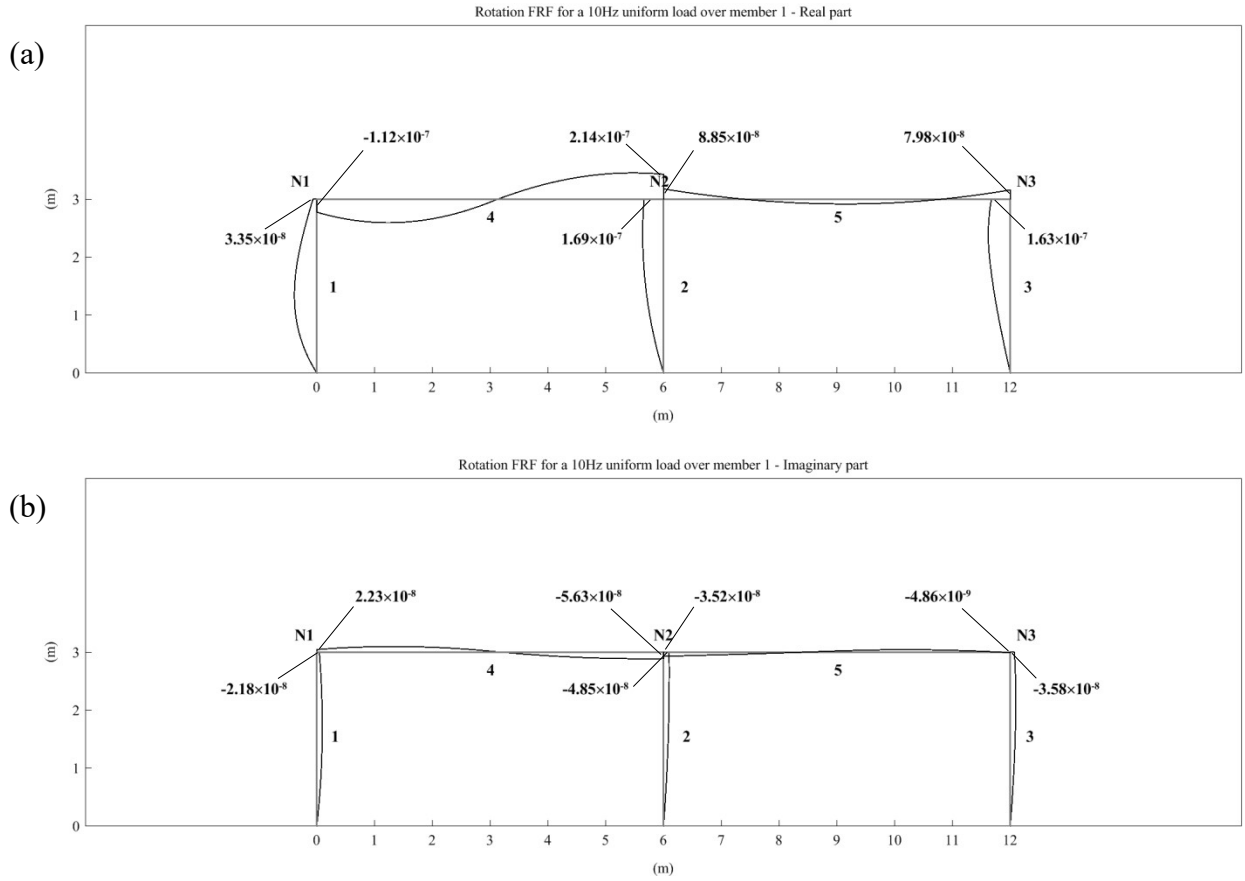

Figure 14. Rotation FRF for a 10Hz uniform load over member 1: (a) real part; (b) imaginary part.

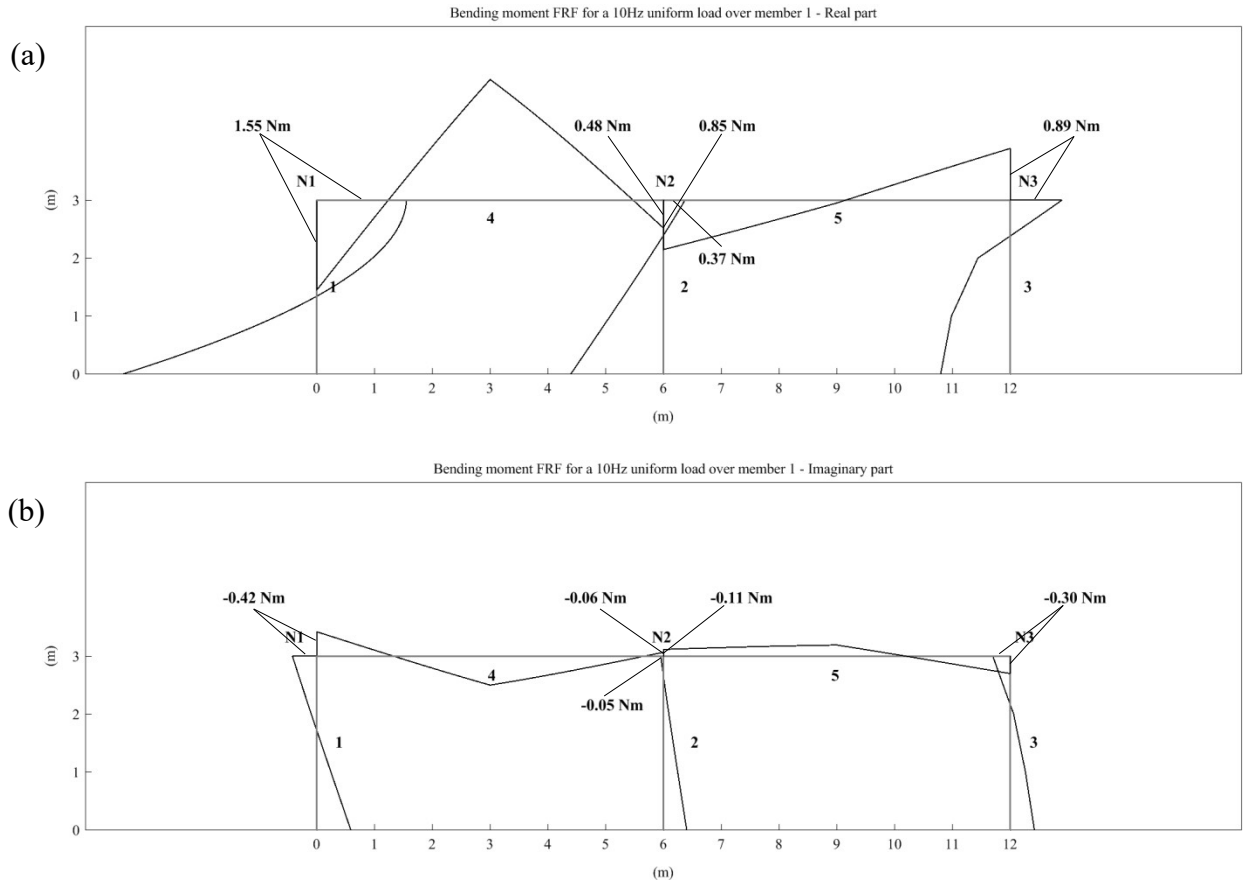

Figure 15. Bending moment FRF for a 10Hz uniform load over member 1; (a) real part; (b) imaginary part.

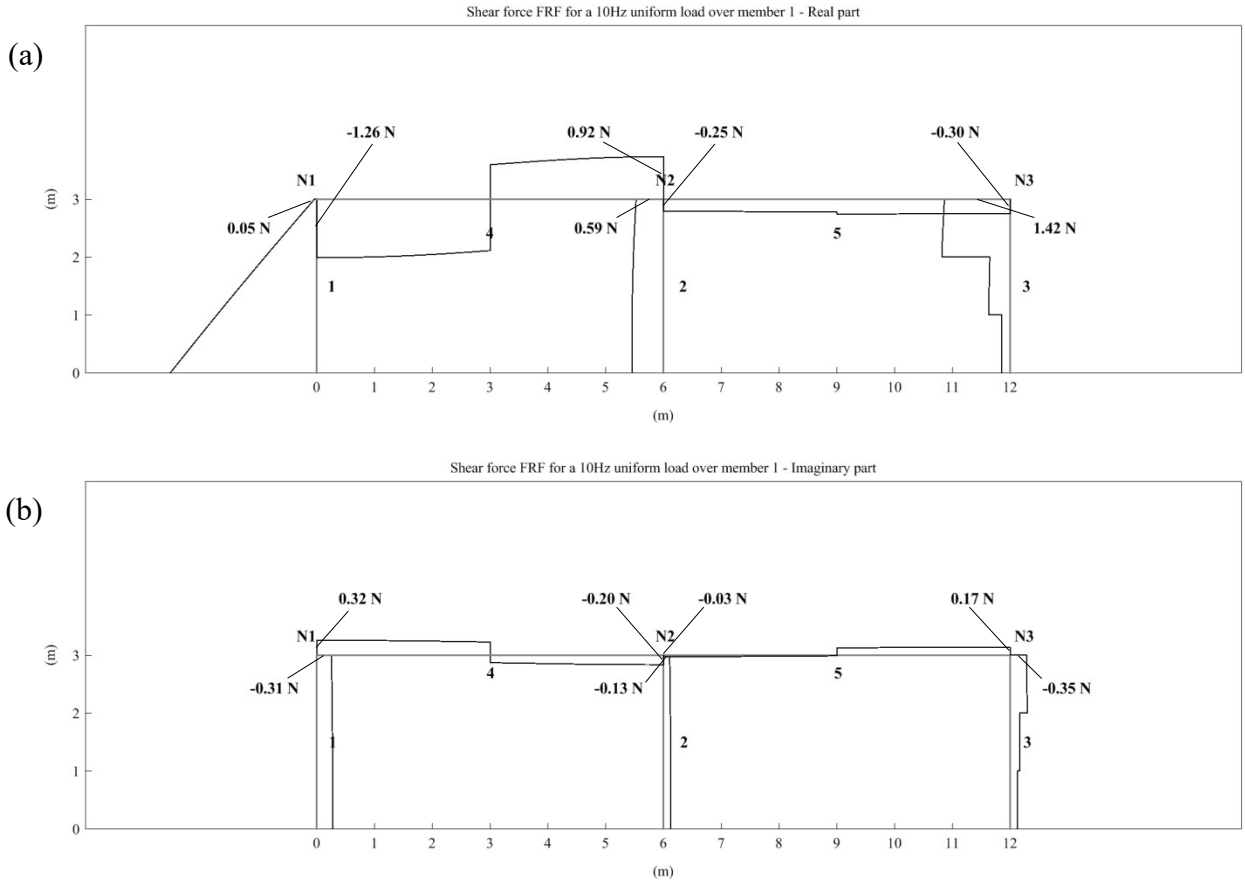

Figure 16. Shear force FRF for a 10Hz uniform load over member 1; (a) real part; (b) imaginary part.

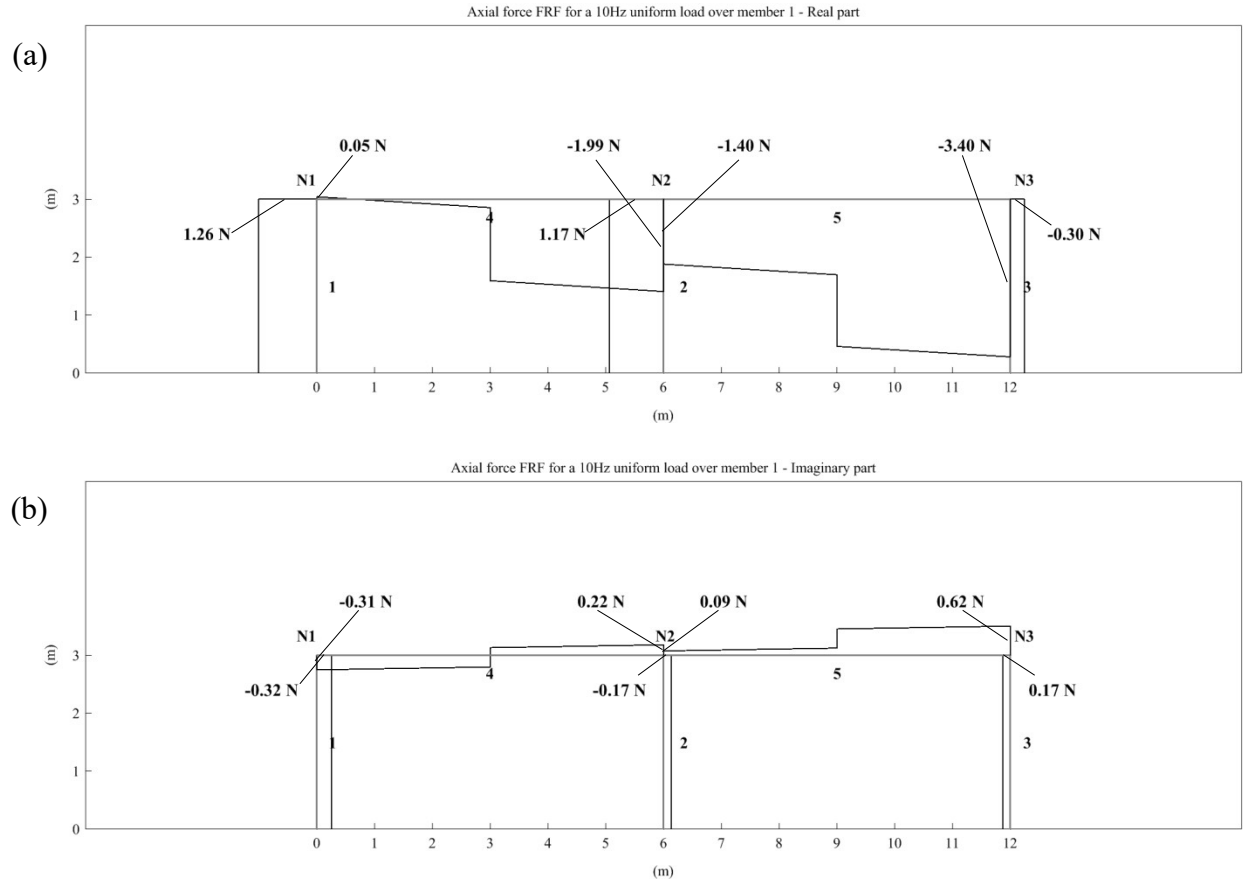

Figure 17. Axial force FRF for a 10Hz uniform load over member 1; (a) real part; (b) imaginary part.

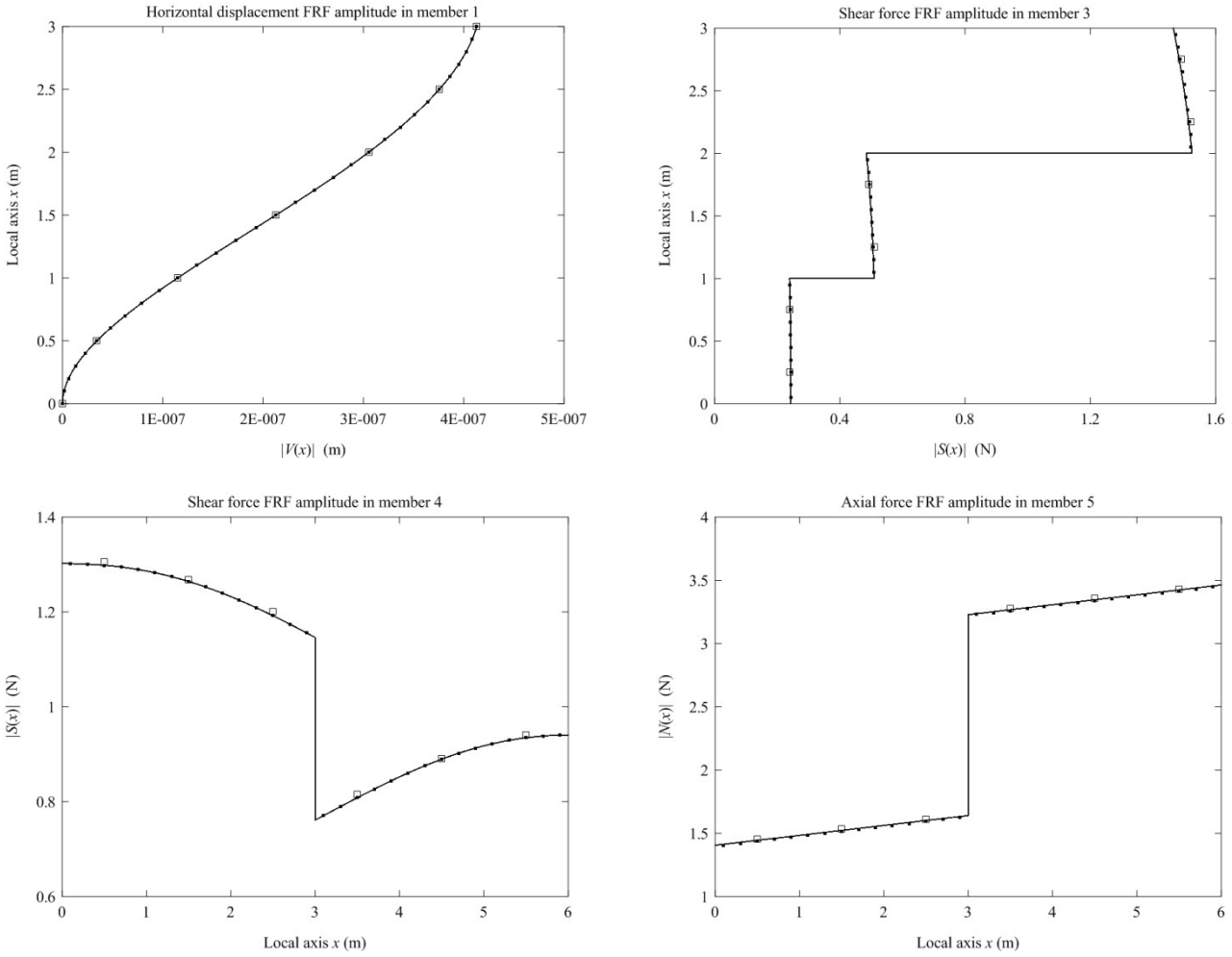

Figure 18. FRF amplitudes in various frame members, for a 10Hz uniform load over member 1; (continuous line: proposed exact solution; (□): FE solution with 6 elements; (●): FE solution with 30 elements).

In Figure 18, amplitudes of the exact FRFs, shown in Figure 13 through Figure 17, are compared with the corresponding FRFs obtained by the FE method, for different numbers of FEs along the frame members (6 elements = symbol "□"; 30 elements: symbol "●"). It can be noticed that, while an accurate description of the exact displacement solution can be obtained by 6 elements, shear-force and axial-force discontinuities are better captured by the refined mesh with 30 elements. Therefore, the exact FRFs obtained by the proposed method can serve as benchmark solutions for mesh refinement in the FE method. For completeness, Figure 19 shows the horizontal displacement FRF amplitude at node N1 (component U_1 of global vector **U** in Eq.(54)), as obtained by the proposed method and the FE method with 30 elements along each frame member, when the forcing frequency of the uniform load over member 1 spans the interval 0-150 Hz. The agreement between the two solutions is very satisfactory.

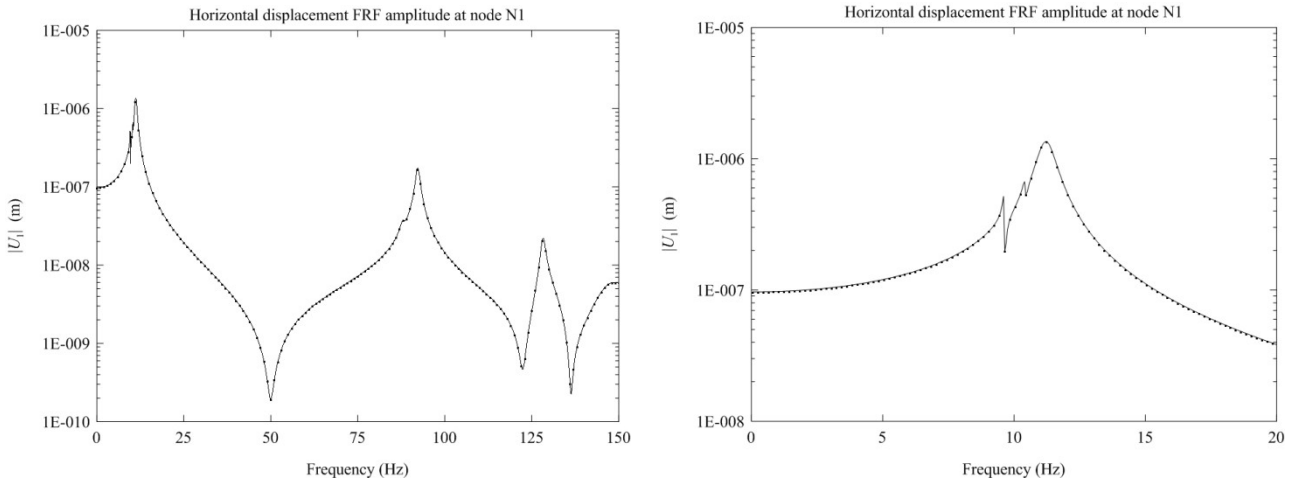

Figure 19. Horizontal displacement FRF amplitude at node N1, for a 0-150 Hz uniform load over member 1, with a zoomed view on the right; (continuous line: proposed exact solution; (•) FE solution with 30 elements along each frame member).

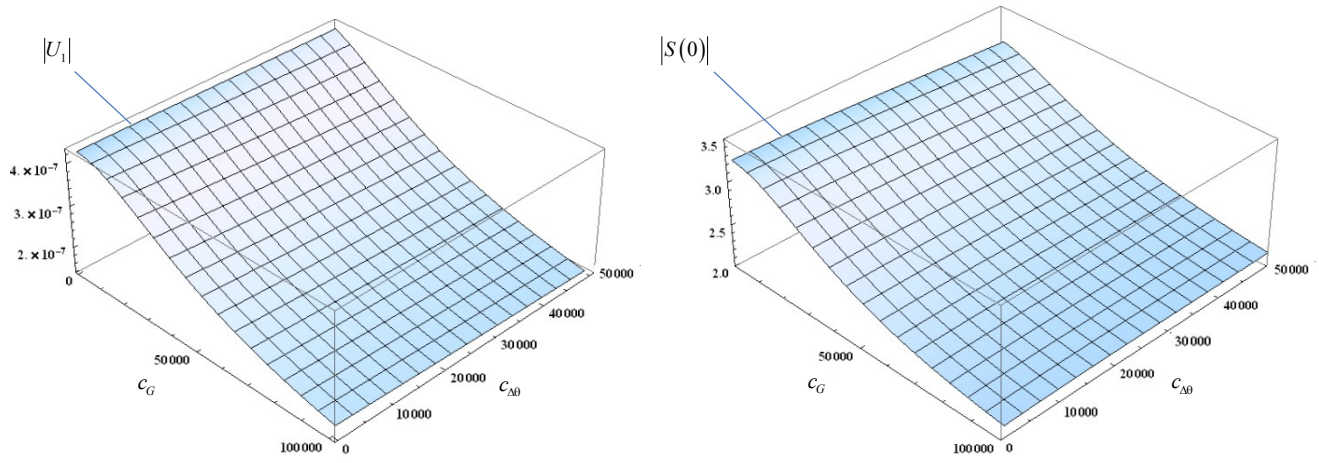

(a) (b)

Figure 20. FRF amplitudes for a 10Hz uniform load over member 1, for different $c_{\Delta\theta}$ of the RDs and c_G of the TDs; (a) horizontal displacement at node N1; (b) shear force at member 1 bottom.

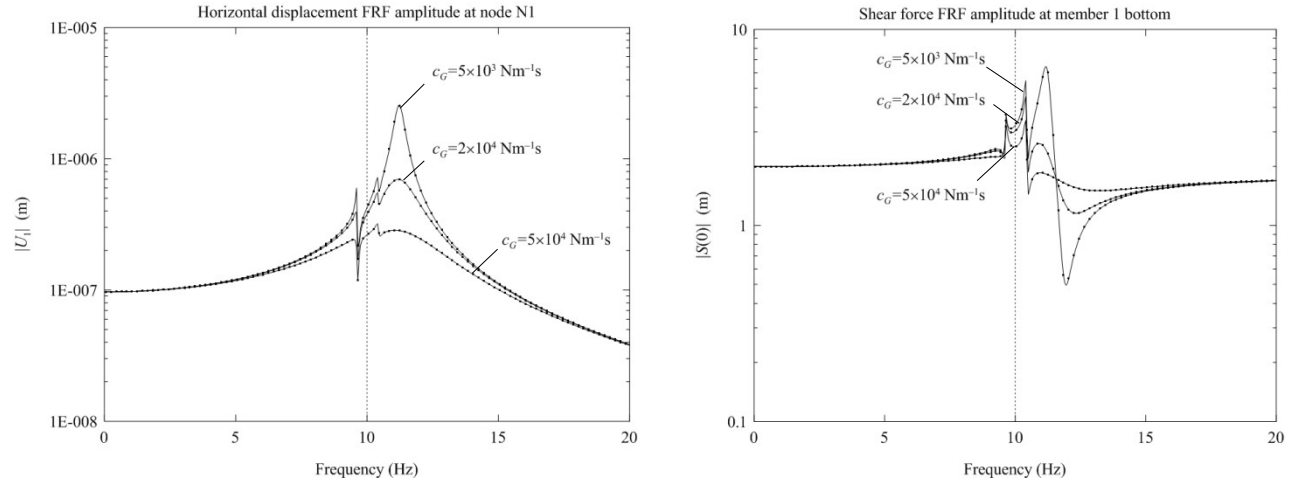

(a) (b)

Figure 21. FRF amplitudes for a 0-20 Hz uniform load over member 1, for $c_{\Delta\theta}$=5×10^3 N m s of the RDs and various c_G of the TDs; (a) horizontal displacement at node N1 (b) shear force at member 1 bottom; (continuous line: proposed exact solution; (•) FE solution with 30 elements along each frame member).

Finally, the proposed method is applied to compute exact FRFs as certain dampers parameters vary. For instance, Figure 20 shows the horizontal displacement FRF amplitude at node N1, and the shear force FRF amplitude at the bottom of member 1, as due to a 10Hz uniform load over member 1, for varying damping parameters $c_{\Delta\theta}$ of the RDs in members 4-5 and $c_G^{(v)}$ of the TDs in member 3/node N3 (all other parameters hold the reference values used in Figure 13 through Figure 19). The FRFs strongly reduce as the damping parameter $c_G^{(v)}$ of the TDs increases, but are not significantly affected by increasing the damping parameter $c_{\Delta\theta}$ of the RDs. For a further insight, Figure 21 shows the horizontal displacement FRF amplitude at node N1, and the shear force FRF amplitude at the bottom of member 1, for a forcing frequency within 0-20 Hz, a damping parameter $c_{\Delta\theta}=5\times10^3$ N m s of the RDs and various damping parameters $c_G^{(v)}$ of the TDs. Results in Figure 21 are consistent with those in Figure 20, as the FRFs at 10 Hz progressively decrease with increasing $c_G^{(v)}$. As in all previous cases, notice that the agreement with the 30 FE solution is very satisfactory.

7. CONCLUSIONS

This paper has presented exact solutions for frequency response analysis of EB beams and plane frames with an arbitrary number of KV TDs/TMDs and RDs for bending vibration, TDs/TMDs and ADs for axial vibration. Using suitable generalised integrals [56] and simple algebraic manipulations, the following results have been obtained:

(a) For a single beam, exact closed-form DGFs and FRFs under arbitrary polynomial load have been derived for all response variables, which can readily be computed for any forcing frequency, number and positions of dampers, positions of point/polynomial loads.

(b) For a plane frame, exact global DSM and LV have been built, with size depending only on the number of beam-to-column nodes, regardless of number and positions of dampers and point/polynomial loads, in each frame member. Thus, no re-meshing is required when number and positions of dampers or loads change. The exact FRM has been obtained by

inverting the global DSM and, from the nodal displacement solution, the exact FRFs in all frame members has been built in a closed form, for all response variables.

(c) For both single beams and plane frames, all proposed solutions are exact and inherently fulfil the required conditions at the locations of dampers/point loads.

These results cannot be obtained by a standard FE method where: (i) the accuracy of the solution depends on the mesh grid; (ii) mesh nodes have to be inserted where either a damper or a point load is applied; (iii) re-meshing is required whenever dampers or loads change position.

The proposed solutions can be implemented in any symbolic package. They could be used within commercial FE codes as exact benchmark solutions to check mesh refinement, and to allow an efficient evaluation of the frequency response for changing dampers parameters and loads without mesh updating.

Future work will focus on developing exact DSM and LV for space frames including an arbitrary number of viscoelastic dampers. Particular attention shall be devoted to treat torsional motion and associated damping. The axial vibration solutions presented here can be used to treat the uncoupled torsional vibration of beams of circular cross section, including any number of dampers along the beam axis, upon replacing axial force/displacement by torque/angle of twist (e.g., see ref. [66]), but a specific approach shall be devised for torsional vibration of beams with dampers in presence of more complex phenomena as coupled bending-torsion, warping. Notice that, for beams without dampers, exact DSMs already exist where torsional vibration is treated considering coupled bending-torsion, warping and also axial force effects (among others, see ref. [67-69]), but, to the best of author's knowledge, they are still to develop for beams with an arbitrary number of dampers.

APPENDIX A

This Appendix provides the exact analytical expressions of Eq.(21) and Eq.(39). They will be derived taking into account the following steady-state governing equations:

$$\frac{\bar{\mathrm{d}}N\left(x,\xi\right)}{\mathrm{d}x}+\sum_{j=1}^{N}R_j^{(u)}\delta\left(x-x_j\right)+P\delta\left(x-\xi\right)+m_0\omega^2U\left(x,\xi\right)=0 \tag{A.1}$$

$$\frac{\bar{\mathrm{d}}U(x,\xi)}{\mathrm{d}x}=\frac{N(x,\xi)}{EA}+\sum_{j=1}^{N}\Delta U_j\delta(x-x_j) \tag{A.2}$$

$$\frac{\bar{\mathrm{d}}S(x,\xi)}{\mathrm{d}x}+\sum_{j=1}^{N}R_j^{(v)}\delta(x-x_j)+P\delta(x-\xi)+m_0\omega^2V(x,\xi)=0\,;\quad \frac{\bar{\mathrm{d}}M(x,\xi)}{\mathrm{d}x}=S(x,\xi) \tag{A.3)-(A.4}$$

$$\frac{\bar{\mathrm{d}}\Theta(x,\xi)}{\mathrm{d}x}=-\frac{M(x,\xi)}{EI}+\sum_{j=1}^{N}\Delta\Theta_j\delta(x-x_j)\,;\qquad \frac{\bar{\mathrm{d}}V(x,\xi)}{\mathrm{d}x}=\Theta(x,\xi) \tag{A.5)-(A.6}$$

Generalized derivatives are introduced in Eqs.(A.3)-(A.4) since $S(x,\xi)$ and $M(x,\xi)$ are not differentiable in a classical sense: $S(x,\xi)$ has a jump discontinuity at $x=\xi$ due to the point load P, and at $x=x_j$ due to the reaction forces $R_j^{(v)}$ (Eq.(A.3)); consequently, the slopes of $M(x,\xi)$ to the left and right of abscissas $x=\xi$ and $x=x_j$ are different (Eq.(A.4)). Similar observations hold for Eq.(A.5) and Eq.(A.6), Eq.(A.1) and Eq.(A.2).

Axial force

Based on Eq.(A.2), the steady-state axial force can be obtained as follows:

$$\begin{aligned}N(x,\xi)&=EA\frac{\bar{\mathrm{d}}U(x,\xi)}{\mathrm{d}x}-EA\sum_{j=1}^{N}\Delta U_j\delta(x-x_j)=\mathbf{N}_{HM}(x)\mathbf{c}^{(u)}+\sum_{j=1}^{N}\mathbf{N}_{\Lambda}(x,x_j)\boldsymbol{\Lambda}_j^{(u)}+P\cdot N_P(x,\xi)\\&=\mathbf{N}(x)\mathbf{c}^{(u)}+\tilde{N}_P(x,\xi)\end{aligned} \tag{A.7}$$

In Eq.(A.7), $\mathbf{N}(x)$ and $\tilde{N}_P(x,\xi)$ are given as Eq.(19) for $\mathbf{U}(x)$ and Eq.(20) for $\tilde{U}_P(x,\xi)$, provided that $\mathbf{U}_{HM}(x)$, $\mathbf{U}_{\Lambda}(x,x_j)$ and $U_P(x,\xi)$ are replaced with $\mathbf{N}_{HM}(x)$, $\mathbf{N}_{\Lambda}(x,x_j)$, $N_P(x,\xi)$ given by

$$\mathbf{N}_{HM}(x)=\chi\left[\cos(\eta x)\quad \sin(\eta x)\right];\quad \mathbf{N}_{\Lambda}(x,x_j)=\left[N_R(x,x_j)\quad N_{\Delta\Theta}(x,x_j)\right] \tag{A.8a,b}$$

$$N_R(x,x_j)=-\cos\left(\eta(x-x_j)\right)H(x-x_j) \tag{A.9a}$$

$$N_{\Delta\Theta}(x,x_j)=-\chi\sin\left(\eta(x-x_j)\right)H(x-x_j) \tag{A.9b}$$

$$N_P(x,\xi)=-\cos\left(\eta(x-\xi)\right)H(x-\xi) \tag{A.10}$$

for $\eta = EA^{-1/2}m_0^{1/2}\omega$, $\rho = EA^{-1/2}m_0^{-1/2}\omega^{-1}$, $\chi = EA^{1/2}m_0^{1/2}\omega$. Notice that $N_R(x,x_j)$ has a jump discontinuity at $x = x_j$, $N_P(x,\xi)$ has a jump discontinuity at $x = \xi$, while all other terms are continuous.

Rotation

Using Eq.(A.6), the steady-state rotation is obtained in the following form:

$$\begin{aligned}\Theta(x,\xi) = \frac{\bar{\mathrm{d}}V(x,\xi)}{\mathrm{d}x} &= \boldsymbol{\Theta}_{HM}(x)\mathbf{c}^{(v)} + \sum_{j=1}^{N}\boldsymbol{\Theta}_{\Lambda}(x,x_j)\boldsymbol{\Lambda}_j^{(v)} + P\cdot\Theta_P(x,\xi) \\ &= \boldsymbol{\Theta}(x)\mathbf{c}^{(v)} + \tilde{\Theta}_P(x,\xi)\end{aligned} \tag{A.11}$$

It can readily be seen that $\boldsymbol{\Theta}(x)$ and $\tilde{\Theta}_P(x,\xi)$ in Eq.(A.11) are given as Eq.(37) for $\mathbf{V}(x)$ and Eq.(38) for $\tilde{V}_P(x,\xi)$, where $\mathbf{V}_{HM}(x)$, $\mathbf{V}_{\Lambda}(x,x_j)$ and $V_P(x,\xi)$ are replaced with $\boldsymbol{\Theta}_{HM}(x)$, $\boldsymbol{\Theta}_{\Lambda}(x,x_j)$ and $\Theta_P(x,\xi)$ given by

$$\boldsymbol{\Theta}_{HM}(x) = \beta\left[-\mathrm{e}^{-\beta x} \quad \mathrm{e}^{\beta x} \quad -\sin(\beta x) \quad \cos(\beta x)\right]; \qquad \boldsymbol{\Theta}_{\Lambda}(x,x_j) = \left[\Theta_R(x,x_j) \quad \Theta_{\Delta\Theta}(x,x_j)\right] \tag{A.12a,b}$$

$$\Theta_R(x,x_j) = \alpha\beta\left[-\cos\left(\beta(x-x_j)\right) + \cosh\left(\beta(x-x_j)\right)\right]H(x-x_j) \tag{A.13a}$$

$$\Theta_{\Delta\Theta}(x,x_j) = \gamma\beta\left[\cos\left(\beta(x-x_j)\right) + \cosh\left(\beta(x-x_j)\right)\right]H(x-x_j) \tag{A.13b}$$

$$\Theta_P(x,\xi) = \alpha\beta\left[-\cos\left(\beta(x-\xi)\right) + \cosh\left(\beta(x-\xi)\right)\right]H(x-\xi) \tag{A.14}$$

Notice that $\Theta_{\Delta\Theta}(x,x_j)$ has a jump discontinuity at $x = x_j$ while the other terms are continuous.

Bending moment

From Eq.(A.5), the steady-state bending moment is derived as

$$\begin{aligned}M(x,\xi) = -EI\frac{\bar{\mathrm{d}}^2V(x,\xi)}{\mathrm{d}x^2} + EI\sum_{j=1}^{N}\Delta\Theta_j\delta(x-x_j) &= \mathbf{M}_{HM}(x)\mathbf{c}^{(v)} + \sum_{j=1}^{N}\mathbf{M}_{\Lambda}(x,x_j)\boldsymbol{\Lambda}_j^{(v)} + P\cdot M_P(x,\xi) \\ &= \mathbf{M}(x)\mathbf{c}^{(v)} + \tilde{M}_P(x,\xi)\end{aligned} \tag{A.15}$$

As earlier noticed for the rotation (A.11), $\mathbf{M}(x)$ and $\tilde{M}_P(x,\xi)$ in Eq.(A.15) are given as Eq.(37) for $\mathbf{V}(x)$ and Eq.(38) for $\tilde{V}_P(x,\xi)$, where $\mathbf{V}_{HM}(x)$, $\mathbf{V}_\Lambda(x,x_j)$ and $V_P(x,\xi)$ are replaced with $\mathbf{M}_{HM}(x)$, $\mathbf{M}_\Lambda(x,x_j)$ and $M_P(x,\xi)$ given by

$$\mathbf{M}_{HM}(x)=\upsilon\left[-\mathrm{e}^{-\beta x} \quad -\mathrm{e}^{\beta x} \quad \cos(\beta x) \quad \sin(\beta x)\right]; \quad \mathbf{M}_\Lambda(x,x_j)=\left[M_R(x,x_j) \quad M_{\Delta\Theta}(x,x_j)\right] \tag{A.16a,b}$$

$$M_R(x,x_j)=\gamma\left[-\sin\left(\beta(x-x_j)\right)-\sinh\left(\beta(x-x_j)\right)\right]H(x-x_j) \tag{A.17a}$$

$$M_{\Delta\Theta}(x,x_j)=\lambda\left[\sin\left(\beta(x-x_j)\right)-\sinh\left(\beta(x-x_j)\right)\right]H(x-x_j) \tag{A.17b}$$

$$M_P(x,\xi)=\gamma\left[-\sin\left(\beta(x-\xi)\right)-\sinh\left(\beta(x-\xi)\right)\right]H(x-\xi) \tag{A.18}$$

being $\upsilon=EI^{1/2}m_0^{1/2}\omega$, $\gamma=2^{-1}EI^{1/4}m_0^{-1/4}\omega^{-1/2}$, $\lambda=2^{-1}EI^{3/4}m_0^{1/4}\omega^{1/2}$. All terms are continuous.

Shear force

The steady-state shear force can be derived from Eq.(A.4) as follows:

$$\begin{aligned} S(x,\xi)&=\frac{\bar{\mathrm{d}}M(x,\xi)}{\mathrm{d}x}=-EI\frac{\bar{\mathrm{d}}^3V(x,\xi)}{\mathrm{d}x^3}+EI\sum_{j=1}^{N}\Delta\Theta_j\delta^{(1)}(x-x_j)=\mathbf{S}_{HM}(x)\mathbf{c}^{(\nu)}+\sum_{j=1}^{N}\mathbf{S}_\Lambda(x,x_j)\boldsymbol{\Lambda}_j^{(\nu)}+P\cdot S_P(x,\xi) \\ &=\mathbf{S}(x)\mathbf{c}^{(\nu)}+\tilde{S}_P(x,\xi) \end{aligned} \tag{A.19}$$

where, as in previous Eq.(A.11) and Eq.(A.15), $\mathbf{S}(x)$ and $\tilde{S}_P(x,\xi)$ are given as Eq.(37) for $\mathbf{V}(x)$ and Eq.(38) for $\tilde{V}_P(x,\xi)$, provided that $\mathbf{V}_{HM}(x)$, $\mathbf{V}_\Lambda(x,x_j)$ and $V_P(x,\xi)$ are replaced with $\mathbf{S}_{HM}(x)$, $\mathbf{S}_\Lambda(x,x_j)$ and $S_P(x,\xi)$ given by

$$\mathbf{S}_{HM}(x)=\sigma\left[\mathrm{e}^{-\beta x} \quad -\mathrm{e}^{\beta x} \quad -\sin(\beta x) \quad \cos(\beta x)\right]; \quad \mathbf{S}_\Lambda(x,x_j)=\left[S_R(x,x_j) \quad S_{\Delta\Theta}(x,x_j)\right] \tag{A.20a,b}$$

$$S_R(x,x_j)=-2^{-1}\left[\cos\left(\beta(x-x_j)\right)+\cosh\left(\beta(x-x_j)\right)\right]H(x-x_j) \tag{A.21a}$$

$$S_{\Delta\Theta}(x,x_j)=\zeta\left[\cos\left(\beta(x-x_j)\right)-\cosh\left(\beta(x-x_j)\right)\right]H(x-x_j) \tag{A.21b}$$

$$S_P(x,\xi)=-2^{-1}\left[\cos\left(\beta(x-\xi)\right)+\cosh\left(\beta(x-\xi)\right)\right]H(x-\xi) \tag{A.22}$$

for $\sigma = EI^{1/4}m^{3/4}\omega^{3/2}$ and $\zeta = 2^{-1}EI^{1/2}m^{1/2}\omega$. Notice that $S_R\left(x,x_j\right)$ has a jump discontinuity at $x = x_j$, $S_P\left(x,\xi\right)$ has a jump discontinuity at $x = \xi$, while all other terms are continuous.

APPENDIX B

This Appendix provides closed-form expressions for the symbolic inverse of the 2×2 matrix $\mathbf{B}^{(u)}$ in Eq.(22b) and the 4×4 matrix $\mathbf{B}^{(v)}$ in Eq.(40b), and the symbolic inverse of the 6×6 matrix $\mathbf{\Gamma}$ in Eq.(47), to be used in Eqs.(49)-(50). They can be obtained by Mathematica [57], and are reported here for completeness.

Inverse matrices of $\mathbf{B}^{(u)}$, $\mathbf{B}^{(v)}$

Denoting by $B_{ij}^{(u)}$ the elements of the 2×2 matrix $\mathbf{B}^{(u)}$, by $A_{ij}^{(u)}$ the elements of the inverse matrix $\mathbf{A}^{(u)} = \left(\mathbf{B}^{(u)}\right)^{-1}$, the following expressions hold for $A_{ij}^{(u)}$:

First row:

$$A_{11}^{(u)} = \left(D^{(u)}\right)^{-1} B_{22}^{(u)}; \qquad A_{12}^{(u)} = -\left(D^{(u)}\right)^{-1} B_{12}^{(u)} \tag{B.1a,b}$$

Second row:

$$A_{21}^{(u)} = -\left(D^{(u)}\right)^{-1} B_{21}^{(u)}; \qquad A_{22}^{(u)} = \left(D^{(u)}\right)^{-1} B_{11}^{(u)} \tag{B.2a,b}$$

where $D^{(u)}$ denotes the determinant of matrix $\mathbf{B}^{(u)}$ given as

$$D^{(u)} = B_{11}^{(u)} B_{22}^{(u)} - B_{12}^{(u)} B_{21}^{(u)} \tag{B.3}$$

Eqs.(B.1)-(B.2) can be used to build the inverse matrix $\left(\mathbf{B}^{(u)}\right)^{-1}$ in a symbolic form, thus deriving closed-form expressions for the integration constants $\mathbf{c}^{(u)}$ in Eq.(22b).

Next, denoting by $B_{ij}^{(v)}$ the elements of the 4×4 matrix $\mathbf{B}^{(v)}$, by $A_{ij}^{(v)}$ the elements of the inverse matrix $\mathbf{A}^{(v)} = \left(\mathbf{B}^{(v)}\right)^{-1}$, the following expressions hold for $A_{ij}^{(v)}$:

First row:

$$A_{11}^{(v)} = \left(D^{(v)}\right)^{-1}\left[B_{24}^{(v)}\left(B_{32}^{(v)}B_{43}^{(v)} - B_{33}^{(v)}B_{42}^{(v)}\right) + B_{23}^{(v)}\left(B_{34}^{(v)}B_{42}^{(v)} - B_{32}^{(v)}B_{44}^{(v)}\right) + B_{22}^{(v)}\left(B_{33}^{(v)}B_{44}^{(v)} - B_{34}^{(v)}B_{43}^{(v)}\right)\right] \quad \text{(B.4a)}$$

$$A_{12}^{(v)} = \left(D^{(v)}\right)^{-1}\left[B_{14}^{(v)}\left(B_{33}^{(v)}B_{42}^{(v)} - B_{32}^{(v)}B_{43}^{(v)}\right) + B_{13}^{(v)}\left(B_{32}^{(v)}B_{44}^{(v)} - B_{34}^{(v)}B_{42}^{(v)}\right) + B_{12}^{(v)}\left(B_{34}^{(v)}B_{43}^{(v)} - B_{33}^{(v)}B_{44}^{(v)}\right)\right] \quad \text{(B.4b)}$$

$$A_{13}^{(v)} = \left(D^{(v)}\right)^{-1}\left[B_{14}^{(v)}\left(B_{22}^{(v)}B_{43}^{(v)} - B_{23}^{(v)}B_{42}^{(v)}\right) + B_{13}^{(v)}\left(B_{24}^{(v)}B_{42}^{(v)} - B_{22}^{(v)}B_{44}^{(v)}\right) + B_{12}^{(v)}\left(B_{23}^{(v)}B_{44}^{(v)} - B_{24}^{(v)}B_{43}^{(v)}\right)\right] \quad \text{(B.4c)}$$

$$A_{14}^{(v)} = \left(D^{(v)}\right)^{-1}\left[B_{14}^{(v)}\left(B_{23}^{(v)}B_{32}^{(v)} - B_{22}^{(v)}B_{33}^{(v)}\right) + B_{13}^{(v)}\left(B_{22}^{(v)}B_{34}^{(v)} - B_{24}^{(v)}B_{32}^{(v)}\right) + B_{12}^{(v)}\left(B_{24}^{(v)}B_{33}^{(v)} - B_{23}^{(v)}B_{34}^{(v)}\right)\right] \quad \text{(B.4d)}$$

Second row:

$$A_{21}^{(v)} = \left(D^{(v)}\right)^{-1}\left[B_{24}^{(v)}\left(B_{33}^{(v)}B_{41}^{(v)} - B_{31}^{(v)}B_{43}^{(v)}\right) + B_{23}^{(v)}\left(B_{31}^{(v)}B_{44}^{(v)} - B_{34}^{(v)}B_{41}^{(v)}\right) + B_{21}^{(v)}\left(B_{34}^{(v)}B_{43}^{(v)} - B_{33}^{(v)}B_{44}^{(v)}\right)\right] \quad \text{(B.5a)}$$

$$A_{22}^{(v)} = \left(D^{(v)}\right)^{-1}\left[B_{14}^{(v)}\left(B_{31}^{(v)}B_{43}^{(v)} - B_{33}^{(v)}B_{41}^{(v)}\right) + B_{13}^{(v)}\left(B_{34}^{(v)}B_{41}^{(v)} - B_{31}^{(v)}B_{44}^{(v)}\right) + B_{11}^{(v)}\left(B_{33}^{(v)}B_{44}^{(v)} - B_{34}^{(v)}B_{43}^{(v)}\right)\right] \quad \text{(B.5b)}$$

$$A_{23}^{(v)} = \left(D^{(v)}\right)^{-1}\left[B_{14}^{(v)}\left(B_{23}^{(v)}B_{41}^{(v)} - B_{21}^{(v)}B_{43}^{(v)}\right) + B_{13}^{(v)}\left(B_{21}^{(v)}B_{44}^{(v)} - B_{24}^{(v)}B_{41}^{(v)}\right) + B_{11}^{(v)}\left(B_{24}^{(v)}B_{43}^{(v)} - B_{23}^{(v)}B_{44}^{(v)}\right)\right] \quad \text{(B.5c)}$$

$$A_{24}^{(v)} = \left(D^{(v)}\right)^{-1}\left[B_{14}^{(v)}\left(B_{21}^{(v)}B_{33}^{(v)} - B_{23}^{(v)}B_{31}^{(v)}\right) + B_{13}^{(v)}\left(B_{24}^{(v)}B_{31}^{(v)} - B_{21}^{(v)}B_{34}^{(v)}\right) + B_{11}^{(v)}\left(B_{23}^{(v)}B_{34}^{(v)} - B_{24}^{(v)}B_{33}^{(v)}\right)\right] \quad \text{(B.5d)}$$

Third row:

$$A_{31}^{(v)} = \left(D^{(v)}\right)^{-1}\left[B_{24}^{(v)}\left(B_{31}^{(v)}B_{42}^{(v)} - B_{32}^{(v)}B_{41}^{(v)}\right) + B_{22}^{(v)}\left(B_{34}^{(v)}B_{41}^{(v)} - B_{31}^{(v)}B_{44}^{(v)}\right) + B_{21}^{(v)}\left(B_{32}^{(v)}B_{44}^{(v)} - B_{34}^{(v)}B_{42}^{(v)}\right)\right] \quad \text{(B.6a)}$$

$$A_{32}^{(v)} = \left(D^{(v)}\right)^{-1}\left[B_{14}^{(v)}\left(B_{32}^{(v)}B_{41}^{(v)} - B_{31}^{(v)}B_{42}^{(v)}\right) + B_{12}^{(v)}\left(B_{31}^{(v)}B_{44}^{(v)} - B_{34}^{(v)}B_{41}^{(v)}\right) + B_{11}^{(v)}\left(B_{34}^{(v)}B_{42}^{(v)} - B_{32}^{(v)}B_{44}^{(v)}\right)\right] \quad \text{(B.6b)}$$

$$A_{33}^{(v)} = \left(D^{(v)}\right)^{-1}\left[B_{14}^{(v)}\left(B_{21}^{(v)}B_{42}^{(v)} - B_{22}^{(v)}B_{41}^{(v)}\right) + B_{12}^{(v)}\left(B_{24}^{(v)}B_{41}^{(v)} - B_{21}^{(v)}B_{44}^{(v)}\right) + B_{11}^{(v)}\left(B_{22}^{(v)}B_{44}^{(v)} - B_{24}^{(v)}B_{42}^{(v)}\right)\right] \quad \text{(B.6c)}$$

$$A_{34}^{(v)} = \left(D^{(v)}\right)^{-1}\left[B_{14}^{(v)}\left(B_{22}^{(v)}B_{31}^{(v)} - B_{21}^{(v)}B_{32}^{(v)}\right) + B_{12}^{(v)}\left(B_{21}^{(v)}B_{34}^{(v)} - B_{24}^{(v)}B_{31}^{(v)}\right) + B_{11}^{(v)}\left(B_{24}^{(v)}B_{32}^{(v)} - B_{22}^{(v)}B_{34}^{(v)}\right)\right] \quad \text{(B.6d)}$$

Fourth row:

$$A_{41}^{(v)} = \left(D^{(v)}\right)^{-1}\left[B_{23}^{(v)}\left(B_{32}^{(v)}B_{41}^{(v)} - B_{31}^{(v)}B_{42}^{(v)}\right) + B_{22}^{(v)}\left(B_{31}^{(v)}B_{43}^{(v)} - B_{33}^{(v)}B_{41}^{(v)}\right) + B_{21}^{(v)}\left(B_{33}^{(v)}B_{42}^{(v)} - B_{32}^{(v)}B_{43}^{(v)}\right)\right] \quad \text{(B.7a)}$$

$$A_{42}^{(v)} = \left(D^{(v)}\right)^{-1}\left[B_{13}^{(v)}\left(B_{31}^{(v)}B_{42}^{(v)} - B_{32}^{(v)}B_{41}^{(v)}\right) + B_{12}^{(v)}\left(B_{33}^{(v)}B_{41}^{(v)} - B_{31}^{(v)}B_{43}^{(v)}\right) + B_{11}^{(v)}\left(B_{32}^{(v)}B_{43}^{(v)} - B_{33}^{(v)}B_{42}^{(v)}\right)\right] \quad \text{(B.7b)}$$

$$A_{43}^{(v)} = \left(D^{(v)}\right)^{-1}\left[B_{13}^{(v)}\left(B_{22}^{(v)}B_{41}^{(v)} - B_{21}^{(v)}B_{42}^{(v)}\right) + B_{12}^{(v)}\left(B_{21}^{(v)}B_{43}^{(v)} - B_{23}^{(v)}B_{41}^{(v)}\right) + B_{11}^{(v)}\left(B_{23}^{(v)}B_{42}^{(v)} - B_{22}^{(v)}B_{43}^{(v)}\right)\right] \tag{B.7c}$$

$$A_{44}^{(v)} = \left(D^{(v)}\right)^{-1}\left[B_{13}^{(v)}\left(B_{21}^{(v)}B_{32}^{(v)} - B_{22}^{(v)}B_{31}^{(v)}\right) + B_{12}^{(v)}\left(B_{23}^{(v)}B_{31}^{(v)} - B_{21}^{(v)}B_{33}^{(v)}\right) + B_{11}^{(v)}\left(B_{22}^{(v)}B_{33}^{(v)} - B_{23}^{(v)}B_{32}^{(v)}\right)\right] \tag{B.7d}$$

In Eqs.(B.4) through Eqs.(B.7) symbol $D^{(v)}$ denotes the determinant of matrix $\mathbf{B}^{(v)}$ given as

$$D^{(v)} = \det \mathbf{B}^{(v)} = \sum_{i=1}^{24} d_i^{(v)} \tag{B.8}$$

$$\begin{array}{llll}
d_1^{(v)} = B_{14}^{(v)}B_{23}^{(v)}B_{32}^{(v)}B_{41}^{(v)} & d_2^{(v)} = -B_{13}^{(v)}B_{24}^{(v)}B_{32}^{(v)}B_{41}^{(v)} & d_3^{(v)} = -B_{14}^{(v)}B_{22}^{(v)}B_{33}^{(v)}B_{41}^{(v)} & d_4^{(v)} = B_{12}^{(v)}B_{24}^{(v)}B_{33}^{(v)}B_{41}^{(v)} \\
d_5^{(v)} = B_{13}^{(v)}B_{22}^{(v)}B_{34}^{(v)}B_{41}^{(v)} & d_6^{(v)} = -B_{12}^{(v)}B_{23}^{(v)}B_{34}^{(v)}B_{41}^{(v)} & d_7^{(v)} = -B_{14}^{(v)}B_{23}^{(v)}B_{31}^{(v)}B_{42}^{(v)} & d_8^{(v)} = B_{13}^{(v)}B_{24}^{(v)}B_{31}^{(v)}B_{42}^{(v)} \\
d_9^{(v)} = B_{14}^{(v)}B_{21}^{(v)}B_{33}^{(v)}B_{42}^{(v)} & d_{10}^{(v)} = -B_{11}^{(v)}B_{24}^{(v)}B_{33}^{(v)}B_{42}^{(v)} & d_{11}^{(v)} = -B_{13}^{(v)}B_{21}^{(v)}B_{34}^{(v)}B_{42}^{(v)} & d_{12}^{(v)} = B_{11}^{(v)}B_{23}^{(v)}B_{34}^{(v)}B_{42}^{(v)} \\
d_{13}^{(v)} = B_{14}^{(v)}B_{22}^{(v)}B_{31}^{(v)}B_{43}^{(v)} & d_{14}^{(v)} = -B_{12}^{(v)}B_{24}^{(v)}B_{31}^{(v)}B_{43}^{(v)} & d_{15}^{(v)} = -B_{14}^{(v)}B_{21}^{(v)}B_{32}^{(v)}B_{43}^{(v)} & d_{16}^{(v)} = B_{11}^{(v)}B_{24}^{(v)}B_{32}^{(v)}B_{43}^{(v)} \\
d_{17}^{(v)} = B_{12}^{(v)}B_{21}^{(v)}B_{34}^{(v)}B_{43}^{(v)} & d_{18}^{(v)} = -B_{11}^{(v)}B_{22}^{(v)}B_{34}^{(v)}B_{43}^{(v)} & d_{19}^{(v)} = -B_{13}^{(v)}B_{22}^{(v)}B_{31}^{(v)}B_{44}^{(v)} & d_{20}^{(v)} = B_{12}^{(v)}B_{23}^{(v)}B_{31}^{(v)}B_{44}^{(v)} \\
d_{21}^{(v)} = B_{13}^{(v)}B_{21}^{(v)}B_{32}^{(v)}B_{44}^{(v)} & d_{22}^{(v)} = -B_{11}^{(v)}B_{23}^{(v)}B_{32}^{(v)}B_{44}^{(v)} & d_{23}^{(v)} = -B_{12}^{(v)}B_{21}^{(v)}B_{33}^{(v)}B_{44}^{(v)} & d_{24}^{(v)} = B_{11}^{(v)}B_{22}^{(v)}B_{33}^{(v)}B_{44}^{(v)}
\end{array} \tag{B.9}$$

Eqs.(B.4)-(B.7) can be used to build the inverse matrix $\left(\mathbf{B}^{(v)}\right)^{-1}$ in a symbolic form, thus deriving closed-form expressions for the integration constants $\mathbf{c}^{(v)}$ in Eq.(40b).

As for the construction of the DGFs, notice that the elements of matrix $\mathbf{B}^{(v)}$ are given by the response variables (36) and (39), computed at the beam ends $x = 0$ and $x = L$. Because the unit-step functions involved in Eq.(36) and Eqs.(39) vanish when computed at $x = 0$, elements in matrix $\mathbf{B}^{(v)}$ associated with the B.C. at $x = 0$ are given by either $\mathbf{V}_{HM}(0)$ or $\mathbf{S}_{HM}(0)$, $\mathbf{\Theta}_{HM}(0)$ or $\mathbf{M}_{HM}(0)$ (see Eq.(36); Eq.(A.11), Eq.(A.15) and Eq.(A.19) in Appendix A). It is immediate to recognize that the analytical expressions of $\mathbf{V}_{HM}(0)$ or $\mathbf{S}_{HM}(0)$, $\mathbf{\Theta}_{HM}(0)$ or $\mathbf{M}_{HM}(0)$ involve only 0 or 1, with significant advantages in the implementation of Eqs.(B.4)-(B.7) for the inverse matrix $\left(\mathbf{B}^{(v)}\right)^{-1}$.

Inverse matrix of $\mathbf{\Gamma}$

Denoting by Γ_{ij} the elements of the 6×6 matrix $\mathbf{\Gamma}$ in Eq.(47), by A_{ij} the elements of the inverse matrix $\mathbf{A}=\left(\mathbf{\Gamma}\right)^{-1}$, the following symbolic forms hold for A_{ij}:

First row:

$$A_{11}=D^{-1}D_0\Gamma_{42};\quad A_{14}=-D^{-1}D_0\Gamma_{12};\quad A_{12}=A_{13}=A_{15}=A_{16}=0 \qquad \text{(B.10a-f)}$$

Second row:

$$A_{21}=-D^{-1}D_0\Gamma_{41};\quad A_{24}=D^{-1}D_0\Gamma_{11};\quad A_{22}=A_{23}=A_{25}=A_{26}=0 \qquad \text{(B.11a,f)}$$

Third row:

$$A_{31}=A_{34}=0 \qquad \text{(B.12a,b)}$$

$$A_{32}=-D^{-1}d_0\left[\Gamma_{36}\left(\Gamma_{55}\Gamma_{64}-\Gamma_{54}\Gamma_{65}\right)+\Gamma_{35}\left(-\Gamma_{56}\Gamma_{64}+\Gamma_{54}\Gamma_{66}\right)+\Gamma_{34}\left(\Gamma_{56}\Gamma_{65}-\Gamma_{55}\Gamma_{66}\right)\right] \qquad \text{(B.12c)}$$

$$A_{33}=D^{-1}d_0\left[\Gamma_{26}\left(\Gamma_{55}\Gamma_{64}-\Gamma_{54}\Gamma_{65}\right)+\Gamma_{25}\left(-\Gamma_{56}\Gamma_{64}+\Gamma_{54}\Gamma_{66}\right)+\Gamma_{24}\left(\Gamma_{56}\Gamma_{65}-\Gamma_{55}\Gamma_{66}\right)\right] \qquad \text{(B.12d)}$$

$$A_{35}=-D^{-1}d_0\left[\Gamma_{26}\left(\Gamma_{35}\Gamma_{64}-\Gamma_{34}\Gamma_{65}\right)+\Gamma_{25}\left(-\Gamma_{36}\Gamma_{64}+\Gamma_{34}\Gamma_{66}\right)+\Gamma_{24}\left(\Gamma_{36}\Gamma_{65}-\Gamma_{35}\Gamma_{66}\right)\right] \qquad \text{(B.12e)}$$

$$A_{36}=D^{-1}d_0\left[\Gamma_{26}\left(\Gamma_{35}\Gamma_{54}-\Gamma_{34}\Gamma_{55}\right)+\Gamma_{25}\left(-\Gamma_{36}\Gamma_{54}+\Gamma_{34}\Gamma_{56}\right)+\Gamma_{24}\left(\Gamma_{36}\Gamma_{55}-\Gamma_{35}\Gamma_{56}\right)\right] \qquad \text{(B.12f)}$$

Fourth row:

$$A_{41}=A_{44}=0 \qquad \text{(B.13a,b)}$$

$$A_{42}=D^{-1}d_0\left[\Gamma_{36}\left(\Gamma_{55}\Gamma_{63}-\Gamma_{53}\Gamma_{65}\right)+\Gamma_{35}\left(-\Gamma_{56}\Gamma_{63}+\Gamma_{53}\Gamma_{66}\right)+\Gamma_{33}\left(\Gamma_{56}\Gamma_{65}-\Gamma_{55}\Gamma_{66}\right)\right] \qquad \text{(B.13c)}$$

$$A_{43}=-D^{-1}d_0\left[\Gamma_{26}\left(\Gamma_{55}\Gamma_{63}-\Gamma_{53}\Gamma_{65}\right)+\Gamma_{25}\left(-\Gamma_{56}\Gamma_{63}+\Gamma_{53}\Gamma_{66}\right)+\Gamma_{23}\left(\Gamma_{56}\Gamma_{65}-\Gamma_{55}\Gamma_{66}\right)\right] \qquad \text{(B.13d)}$$

$$A_{45}=D^{-1}d_0\left[\Gamma_{26}\left(\Gamma_{35}\Gamma_{63}-\Gamma_{33}\Gamma_{65}\right)+\Gamma_{25}\left(-\Gamma_{36}\Gamma_{63}+\Gamma_{33}\Gamma_{66}\right)+\Gamma_{23}\left(\Gamma_{36}\Gamma_{65}-\Gamma_{35}\Gamma_{66}\right)\right] \qquad \text{(B.13e)}$$

$$A_{46}=-D^{-1}d_0\left[\Gamma_{26}\left(\Gamma_{35}\Gamma_{53}-\Gamma_{33}\Gamma_{55}\right)+\Gamma_{25}\left(-\Gamma_{36}\Gamma_{53}+\Gamma_{33}\Gamma_{56}\right)+\Gamma_{23}\left(\Gamma_{36}\Gamma_{55}-\Gamma_{35}\Gamma_{56}\right)\right] \qquad \text{(B.13f)}$$

Fifth row:

$$A_{51} = A_{54} = 0 \tag{B.14a,b}$$

$$A_{52} = -D^{-1} d_0 \left[\Gamma_{36} \left(\Gamma_{54}\Gamma_{63} - \Gamma_{53}\Gamma_{64} \right) + \Gamma_{34} \left(-\Gamma_{56}\Gamma_{63} + \Gamma_{53}\Gamma_{66} \right) + \Gamma_{33} \left(\Gamma_{56}\Gamma_{64} - \Gamma_{54}\Gamma_{66} \right) \right] \tag{B.14c}$$

$$A_{53} = D^{-1} d_0 \left[\Gamma_{26} \left(\Gamma_{54}\Gamma_{63} - \Gamma_{53}\Gamma_{64} \right) + \Gamma_{24} \left(-\Gamma_{56}\Gamma_{63} + \Gamma_{53}\Gamma_{66} \right) + \Gamma_{23} \left(\Gamma_{56}\Gamma_{64} - \Gamma_{54}\Gamma_{66} \right) \right] \tag{B.14d}$$

$$A_{55} = -D^{-1} d_0 \left[\Gamma_{26} \left(\Gamma_{34}\Gamma_{63} - \Gamma_{33}\Gamma_{64} \right) + \Gamma_{24} \left(-\Gamma_{36}\Gamma_{63} + \Gamma_{33}\Gamma_{66} \right) + \Gamma_{23} \left(\Gamma_{36}\Gamma_{64} - \Gamma_{34}\Gamma_{66} \right) \right] \tag{B.14e}$$

$$A_{56} = D^{-1} d_0 \left[\Gamma_{26} \left(\Gamma_{34}\Gamma_{53} - \Gamma_{33}\Gamma_{54} \right) + \Gamma_{24} \left(-\Gamma_{36}\Gamma_{53} + \Gamma_{33}\Gamma_{56} \right) + \Gamma_{23} \left(\Gamma_{36}\Gamma_{54} - \Gamma_{34}\Gamma_{56} \right) \right] \tag{B.14f}$$

Sixth row:

$$A_{61} = A_{64} = 0 \tag{B.15a,b}$$

$$A_{62} = D^{-1} d_0 \left[\Gamma_{35} \left(\Gamma_{54}\Gamma_{63} - \Gamma_{53}\Gamma_{64} \right) + \Gamma_{34} \left(-\Gamma_{55}\Gamma_{63} + \Gamma_{53}\Gamma_{65} \right) + \Gamma_{33} \left(\Gamma_{55}\Gamma_{64} - \Gamma_{54}\Gamma_{65} \right) \right] \tag{B.15c}$$

$$A_{63} = -D^{-1} d_0 \left[\Gamma_{25} \left(\Gamma_{54}\Gamma_{63} - \Gamma_{53}\Gamma_{64} \right) + \Gamma_{24} \left(-\Gamma_{55}\Gamma_{63} + \Gamma_{53}\Gamma_{65} \right) + \Gamma_{23} \left(\Gamma_{55}\Gamma_{64} - \Gamma_{54}\Gamma_{65} \right) \right] \tag{B.15d}$$

$$A_{65} = D^{-1} d_0 \left[\Gamma_{25} \left(\Gamma_{34}\Gamma_{63} - \Gamma_{33}\Gamma_{64} \right) + \Gamma_{24} \left(-\Gamma_{35}\Gamma_{63} + \Gamma_{33}\Gamma_{65} \right) + \Gamma_{23} \left(\Gamma_{35}\Gamma_{64} - \Gamma_{34}\Gamma_{65} \right) \right] \tag{B.15e}$$

$$A_{66} = -D^{-1} d_0 \left[\Gamma_{25} \left(\Gamma_{34}\Gamma_{53} - \Gamma_{33}\Gamma_{54} \right) + \Gamma_{24} \left(-\Gamma_{35}\Gamma_{53} + \Gamma_{33}\Gamma_{55} \right) + \Gamma_{23} \left(\Gamma_{35}\Gamma_{54} - \Gamma_{34}\Gamma_{55} \right) \right] \tag{B.15f}$$

In Eqs.(B.10)-(B.15), D is the determinant of the 6×6 matrix $\boldsymbol{\Gamma}$ in Eq.(47), i.e.

$$D = \det \boldsymbol{\Gamma} = d_0 D_0 ; \tag{B.16}$$

$$d_0 = \Gamma_{11}\Gamma_{42} - \Gamma_{12}\Gamma_{41} ; \qquad D_0 = \sum_{k=1}^{11} d_k \tag{B.17a,b}$$

$$d_1 = \Gamma_{24}\Gamma_{36}\Gamma_{55}\Gamma_{63} \quad d_2 = -\Gamma_{24}\Gamma_{35}\Gamma_{56}\Gamma_{63} \quad d_3 = -\Gamma_{23}\Gamma_{36}\Gamma_{55}\Gamma_{64} \quad d_4 = \Gamma_{23}\Gamma_{35}\Gamma_{56}\Gamma_{64}$$

$$d_5 = -\Gamma_{24}\Gamma_{36}\Gamma_{53}\Gamma_{65} \quad d_6 = \Gamma_{23}\Gamma_{36}\Gamma_{54}\Gamma_{65} \quad d_7 = \Gamma_{24}\Gamma_{33}\Gamma_{56}\Gamma_{65} \quad d_8 = -\Gamma_{23}\Gamma_{34}\Gamma_{56}\Gamma_{65}$$

$$d_9 = \Gamma_{26} \left[\Gamma_{55} \left(-\Gamma_{34}\Gamma_{63} + \Gamma_{33}\Gamma_{64} \right) + \Gamma_{35} \left(\Gamma_{54}\Gamma_{63} - \Gamma_{53}\Gamma_{64} \right) + \Gamma_{65} \left(\Gamma_{34}\Gamma_{53} - \Gamma_{33}\Gamma_{54} \right) \right] \tag{B.18}$$

$$d_{10} = \Gamma_{66} \left[\Gamma_{24} \left(\Gamma_{35}\Gamma_{53} - \Gamma_{33}\Gamma_{55} \right) + \Gamma_{23} \left(-\Gamma_{35}\Gamma_{54} + \Gamma_{34}\Gamma_{55} \right) \right]$$

$$d_{11} = \Gamma_{25} \left[\Gamma_{56} \left(\Gamma_{34}\Gamma_{63} - \Gamma_{33}\Gamma_{64} \right) + \Gamma_{36} \left(-\Gamma_{54}\Gamma_{63} + \Gamma_{53}\Gamma_{64} \right) + \Gamma_{66} \left(-\Gamma_{34}\Gamma_{53} + \Gamma_{33}\Gamma_{54} \right) \right]$$

APPENDIX C

This Appendix explains how the procedure to build the DGFs and FRFs, presented in Section 3.1.2 under the assumption that a *y*-direction TD/TMD and a RD occur simultaneously at every location x_j, can readily be modified when, at a given location x_j, either a *y*-direction TD/TMD or a RD occurs. In this case, modifications affect only $\mathbf{h}^{(\nu)}$, $\mathbf{E}^{(\nu)}$ and $\mathbf{p}^{(\nu)}$ in Eq.(32), as detailed next:

(a) if only a TD/TMD occurs at x_j (i.e., $\Delta\Theta_j = 0$):

$$h_{11}^{(\nu)},\ h_{12}^{(\nu)},\ h_{13}^{(\nu)} \text{ and } h_{14}^{(\nu)} \text{ are given as Eqs.(33a-d)} \tag{C.1a-h}$$

$$h_{21}^{(\nu)} = h_{22}^{(\nu)} = h_{23}^{(\nu)} = h_{24}^{(\nu)} = 0;$$

$$E_{11}^{(\nu)} = \begin{cases} \alpha\left(k_{Geq_j}^{(\nu)}(\omega) + k_{Meq_j}^{(\nu)}(\omega)\right)\left[\sin\left(\beta\left(x_j - x_k\right)\right) - \sinh\left(\beta\left(x_j - x_k\right)\right)\right] & \text{if a } y\text{-direction TD/TMD occurs at } x_k \\ 0 & \text{if no } y\text{-direction TD/TMD occurs at } x_k \end{cases} \tag{C.2a}$$

$$E_{12}^{(\nu)} = \begin{cases} 0 & \text{if no RD occurs at } x_k \\ -\gamma\left(k_{Geq_j}^{(\nu)}(\omega) + k_{Meq_j}^{(\nu)}(\omega)\right)\left[\sin\left(\beta\left(x_j - x_k\right)\right) + \sinh\left(\beta\left(x_j - x_k\right)\right)\right] & \text{if a RD occurs at } x_k \end{cases} \tag{C.2b}$$

$$E_{21}^{(\nu)} = E_{22}^{(\nu)} = 0 \quad \text{for any } k \tag{C.2c,d}$$

$$p_1^{(\nu)} \text{ is given as Eq.(35a)}; \quad p_2^{(\nu)} = 0 \tag{C.3a,b}$$

(b) if only a RD occurs at x_j (i.e., $R_j^{(\nu)} = 0$):

$$h_{11}^{(\nu)} = h_{12}^{(\nu)} = h_{13}^{(\nu)} = h_{14}^{(\nu)} = 0$$

$$h_{21}^{(\nu)},\ h_{22}^{(\nu)},\ h_{23}^{(\nu)} \text{ and } h_{24}^{(\nu)} \text{ are given as Eqs.(33e-h);} \tag{C.4a-h}$$

$$E_{11}^{(\nu)} = E_{12}^{(\nu)} = 0 \quad \text{for any } k \tag{C.5a,b}$$

$$E_{21}^{(\nu)} = \begin{cases} \gamma\left(k_{\Delta\theta eq_j}(\omega)\right)^{-1}\left[\sin\left(\beta\left(x_j - x_k\right)\right) + \sinh\left(\beta\left(x_j - x_k\right)\right)\right] & \text{if a } y\text{-direction TD/TMD occurs at } x_k \\ 0 & \text{if no } y\text{-direction TD/TMD occurs at } x_k \end{cases} \tag{C.5c}$$

$$E_{22}^{(v)} = \begin{cases} 0 & \text{if no RD occurs at } x_k \\ \lambda\left(k_{\Delta\theta eq_j}(\omega)\right)^{-1}\left[-\sin\left(\beta\left(x_j - x_k\right)\right) + \sinh\left(\beta\left(x_j - x_k\right)\right)\right] & \text{if a RD occurs at } x_k \end{cases} \quad \text{(C.5d)}$$

$$p_1^{(v)} = 0; \quad p_2^{(v)} \text{ is given as Eq.(35b)} \quad \text{(C.6a,b)}$$

REFERENCES

[1] G.W. Housner, L.A. Bergman, T.K. Caughey, A.G. Chassiakos, R.O. Claus, S.F. Masri, et al., Structural control: Past, present, and future. ASCE Journal of Engineering Mechanics 123 (1997) 897-971.

[2] G. Genta, Vibration of Structures and Machines: Practical Aspects, Springer, New York, 1995.

[3] J.P. Den Hartog, Mechanical Vibrations, McGraw-Hill, New York, 1956.

[4] A.K. Shukla, T.K. Datta, Optimal use of viscoelastic dampers in building frames for seismic force. Journal of Structural Engineering 125(4) (1999) 401-409.

[5] M.P. Sing, L.M. Moreschi, Optimal placement of dampers for passive response control. Earthquake Engineering and Structural Dynamics 31 (2002) 955-976.

[6] J.P. Ou, X. Long, Q.S. Li, Seismic response analysis of structures with velocity-dependent dampers. Journal of Constructional Steel Research 63 (2007) 628-638.

[7] M. Abé, T. Igusa, Tuned mass dampers for structures with closely spaced natural frequencies. Earthquake Engineering and Structural Dynamics 24 (1995) 247-261.

[8] A. Kareem, S. Kline, Performance of multiple mass dampers under random loading. Journal of Structural Engineering 121(2) (1995) 348-361.

[9] F. Sadek, B. Mohraz, A.W. Taylor, R.M. Chung, A method of estimating the parameters of tuned mass dampers for seismic applications. Earthquake Engineering and Structural Dynamics 26 (1997) 617-635.

[10] R. Lewandowski, J. Grzymisławska, Dynamic analysis of structures with multiple tuned mass dampers. Journal of Civil Engineering and Management 15(1) (2009) 77-86.

[11] Y.L. Xu, W.S. Zhang, Modal analysis and seismic response of steel frames with connection dampers. Engineering Structures 23 (2001) 385-396.

[12] Federal Emergency Management Agency (FEMA). NEHRP Guidelines and Commentary for the Seismic Rehabilitation of Buildings. Reports N. 273-274. Building Seismic Council, Washington, 1997.

[13] S. Kawashima, T. Fujimoto, Vibration analysis of frames with semi-rigid connections. Computers and Structures 19 (1984) 85-92.

[14] M. Sekulovic, R. Salatic, M. Nefovska, Dynamic analysis of steel frames with flexible connections. Computers and Structures 80 (2002) 935-955.

[15] M. Hanss, S. Oexl, L. Gaul, Identification of a bolted-joint model with fuzzy parameters loaded normal to the contact interface. Mechanics Research Communications 29 (2-3) (2002) 177-187.

[16] J.R. Banerjee, Dynamic stiffness formulation for structural elements: A general approach. Computers and Structures 63(1) (1997) 101-103.

[17] L. Li, Y. Hu, X. Wang, Eliminating the modal truncation problem encountered in frequency responses of viscoelastic systems. Journal of Sound and Vibration 333 (2014) 1182-1192.

[18] L. Li, Y. Hu, X. Wang, L. Lü, A hybrid expansion method for frequency response functions of non-proportionally damped systems. Mechanical Systems and Signal Processing 42 (2014) 31-41.

[19] S. Sorrentino, S. Marchesiello, B.A.D. Piombo, A new analytical technique for vibration analysis of non-proportionally damped beams. Journal of Sound and Vibration 265 (2003) 765-782.

[20] S. Sorrentino, A. Fasana, S. Marchesiello, Frequency domain analysis of continuous systems with viscous generalized damping. Shock and Vibration 11 (2004) 243-259.

[21] S. Sorrentino, A. Fasana, S. Marchesiello, Analysis of non-homogeneous Timoshenko beams with generalized damping distributions. Journal of Sound and Vibration 304 (2007) 779-792.

[22] S.W. Hong, J.W. Kim, Modal analysis of multi-span Timoshenko beams connected or supported by resilient joints with damping. Journal of Sound and Vibration 227(4) (1999) 787-806.

[23] H.B. Tang, C.J. Wu, X.Q. Huang, Vibration analysis for a coupled beam-sdof system by using the recurrence equation method. Journal of Sound and Vibration 311 (2008) 912-923.

[24] J.S. Wu, D.W. Chen, Dynamic analysis of a uniform cantilever beam carrying a number of elastically mounted point masses with dampers. Journal of Sound and Vibration 229(3) (2000) 549-578.

[25] M. Gürgöze, H. Erol, On the frequency response function of a damped cantilever simply supported in-span and carrying a tip mass. Journal of Sound and Vibration 255(3) (2002) 489-500.

[26] M. Gürgöze, H. Erol, Dynamic response of a viscously damped cantilever with a viscous end condition. Journal of Sound and Vibration 298 (2006) 132-153.

[27] G. Failla, On the dynamics of viscoelastic discontinuous beams. Mechanics Research Communications 60 (2014) 52-63.

[28] G. Oliveto, A. Santini, E. Tripodi, Complex modal analysis of a flexural vibrating beam with viscous end conditions. Journal of Sound and Vibration 200(3) (1997) 327-345.

[29] H.Y. Lin, Dynamic analysis of a multi-span uniform beam carrying a number of various concentrated elements. Journal of Sound and Vibration 309 (2008) 262-275.

[30] D.V. Bambill, C.A. Rossit, Forced vibrations of a beam elastically restrained against rotation and carrying a spring–mass system. Ocean Engineering 29 (2002) 605-626.

[31] M. Abu-Hilal, Forced vibration of Euler–Bernoulli beams by means of dynamic Green functions. Journal of Sound and Vibration 267 (2003) 191-207.

[32] K. Alsaif, M.A. Foda, Vibration suppression of a beam structure by intermediate masses and springs. Journal of Sound and Vibration 256(4) (2002) 629-645.

[33] M.A. Foda, B.A. Albassam, Vibration confinement in a general beam structure during harmonic excitations. Journal of Sound and Vibration 295 (2006) 491-517.

[34] N.T. Khiem, T.V. Lien, The dynamic stiffness matrix method in forced vibration analysis of multiple-cracked beam. Journal of Sound and Vibration 254(3) (2002) 541-555.

[35] M. Gürgöze, H. Erol, Determination of the frequency response function of a cantilevered beam simply supported in-span. Journal of Sound and Vibration 247(2) (2001) 372-378.

[36] A.J. Hull, A closed form solution of a longitudinal bar with a viscous boundary condition. Journal of Sound and Vibration 169(1) (1994) 19-28.

[37] N. Alati, G. Failla, A. Santini, Complex modal analysis of rods with viscous damping devices. Journal of Sound and Vibration 333 (2014) 2130-2163.

[38] Y.Q. Guo, W.Q. Chen, Dynamic analysis of space structures with multiple tuned mass dampers. Engineering Structures 29 (2007) 3390-3403.

[39] S. Caddemi, I. Caliò, Exact closed-form solution for the vibration modes of the Euler-Bernoulli beam with multiple open cracks. Journal of Sound and Vibration 327 (2009) 473-489.

[40] S. Caddemi, I. Caliò, The exact explicit dynamic stiffness matrix of multi-cracked Euler–Bernoulli beam and applications to damaged frame structures. Journal of Sound and Vibration 332 (2013) 3049-3063.

[41] S. Caddemi, I. Caliò, F. Cannizzaro, D. Rapicavoli, A novel beam finite element with singularities for the dynamic analysis of discontinuous frames. Archive of Applied Mechanics 83(10) (2013) 1451-1468.

[42] M. Donà, A. Palmeri, M. Lombardo, A. Cicirello, An efficient two-node finite element formulation of multi-damaged beams including shear deformation and rotatory inertia. Computers and Structures 147 (2015) 96-106.

[43] A. Yavari, S. Sarkani, E.T. Moyer, On applications of generalized functions to beam bending problems. International Journal of Solids and Structures 37 (2000) 5675-5705.

[44] A. Yavari, S. Sarkani, On applications of generalized functions to the analysis of Euler-Bernoulli beam-columns with jump discontinuities. International Journal of Mechanical Sciences 43 (2001) 1543-1562.

[45] A. Yavari, S. Sarkani, J.N. Reddy, Generalized solutions of beams with jump discontinuities on elastic foundations. Archive of Applied Mechanics 71 (9) (2001) 625-639.

[46] G. Falsone, The use of generalised functions in the discontinuous beam bending differential equation. International Journal of Engineering Education 18(3) (2002) 337-343.

[47] B. Biondi, S. Caddemi, Euler-Bernoulli beams with multiple singularities in the flexural stiffness. European Journal of Mechanics A/Solids 26(5) (2007) 789-809.

[48] S. Caddemi, I. Caliò, F. Cannizzaro, Closed-form solutions for stepped Timoshenko beams with internal singularities and along-axis external supports. Archive of Applied Mechanics 83(4) (2013) 559-577.

[49] S. Caddemi, I. Caliò, F. Cannizzaro, The influence of multiple cracks on tensile and compressive buckling of shear deformable beams. International Journal of Solids Structures 50 (20-21) (2013) 3166-3183.

[50] S. Caddemi, A. Morassi, Multi-cracked Euler-Bernoulli beams: Mathematical modeling and exact solutions. International Journal of Solids and Structures 50(6) (2013) 944-956.

[51] S. Caddemi, I. Caliò, Exact reconstruction of multiple concentrated damages on beams. Acta Mechanica 225(11) (2014) 3137-3156.

[52] G. Failla, A. Santini, On Euler-Bernoulli discontinuous beam solutions via uniform-beam Green's functions. International Journal of Solids and Structures 44 (2007) 7666-7687.

[53] G. Failla, A. Santini, A solution method for Euler–Bernoulli vibrating discontinuous beams. Mechanics Research Communications 35 (2008) 517-529.

[54] G. Failla, Closed-form solutions for Euler-Bernoulli arbitrary discontinuous beams. Archive of Applied Mechanics 81 (2011) 605-628.

[55] A. Palmeri, A. Cicirello, Physically-based Dirac's delta functions in the static analysis of multi-cracked Euler-Bernoulli and Timoshenko beams. International Journal of Solids and Structures 48(14-15) (2011) 2184-2195.

[56] J. Wang, P. Qiao, Vibration of beams with arbitrary discontinuities and boundary conditions. Journal of Sound and Vibration 308 (2007) 12-27.

[57] Mathematica Version 7.0, Wolfram Research Inc., Champaign, 2008.

[58] L. Sun, A closed-form solution of a Bernoulli-Euler beam on a viscoelastic foundation under harmonic line loads. Journal of Sound and Vibration 242(4) (2001) 619-627.

[59] S. Adhikari, An iterative approach for nonproportionally damped systems. Mechanics Research Communications 38 (2011) 226-230.

[60] D.J. Ewins, Modal Testing: Theory, Practice and Application, Research Studies Press, Baldock, 2000.

[61] N.M.M. Maia, J.M.M. Silva, Theoretical and Experimental Modal Analysis, Research Studies Press, Baldock, 1997.

[62] R.J. Allemang, D.L. Brown, A unified matrix polynomial approach to modal identification. Journal of Sound and Vibration 211(3) (1998) 301-322.

[63] A.S. Veletsos, C.E. Ventura, Modal analysis of non-classically damped linear systems. Earthquake Engineering and Structural Dynamics 14 (1986) 217-243.

[64] M. Gürgöze, On the sensitivities of the eigenvalues of a viscously damped cantilever carrying a tip mass. Journal of Sound and Vibration 216(2) (1998) 215-225.

[65] A. Brandt, Noise and Vibration analysis: Signal Analysis and Experimental Procedures, John Wiley and Sons, Chichester, 2011.

[66] J.L. Humar, Dynamics of Structures, Swets & Zeitlinger B.V., Lisse, 2002.

[67] J.R. Banerjee, Coupled bending–torsional dynamic stiffness matrix for beam elements. International Journal for Numerical Methods in Engineering 28(6) (1989) 1283-1298.

[68] J.R. Banerjee, S. Guo, W.P. Howson, Exact dynamic stiffness matrix of a bending-torsion coupled beam including warping. Computers and Structures 59(4) (1996) 613-621.

[69] J.R. Banerjee, S.A. Fisher, Coupled bending–torsional dynamic stiffness matrix for axially loaded beam elements, International Journal for Numerical Methods in Engineering 33(4) (1992) 739-751.

FIGURES CAPTIONS

Figure 1. Beam with arbitrary number of KV dampers: (a) axial problem; (b) bending problem.

Figure 2. A plane frame with arbitrary number of KV dampers.

Figure 3. Beam with elastic translational supports, TMDs and RDs under two different loads: (a) unit point load; (b) triangular load.

Figure 4. Beam in Figure 3: DGFs for a 5Hz point load applied at $\xi=L/2$; (continuous line: proposed exact solution; (•): classical exact solution).

Figure 5. Beam in Figure 3: deflection DGF for a 3Hz point load, computed at x for various load positions ξ: (a) for all x and ξ, $x,\xi\in[0,L]$; (b) at all x for given load positions ξ ($\xi=L/3$, $L/2$, $2L/3$); (c) at given x ($x=L/3$, $L/2$, $2L/3$) for all load positions ξ; (continuous/dashed-dotted/dotted lines: proposed exact solution; (•): classical exact solution).

Figure 6. Beam in Figure 3: deflection DGF amplitude at x=L/3, for a 0-150 Hz point load applied at $\xi=L/2$, with a zoomed view on the right; (continuous line: proposed exact solution; (•): classical exact solution).

Figure 7. Beam in Figure 3: FRFs for a 2Hz triangular load over [$L/3$, $2L/3$]; (continuous line: proposed exact solution; (•): classical exact solution).

Figure 8. Beam in Figure 3: deflection FRF amplitude at $x=L/2$ for a 2Hz triangular load over [$L/3$, $2L/3$] and varying parameters; (a) for different $c_{\Delta\theta}$ and $k_{\Delta\theta}$ of the RDs; (b) for different $c_M^{(v)}$ and $k_M^{(v)}$ of the TMDs.

Figure 9. Beam in Figure 3: deflection FRF amplitude at $x=L/2$ for a 0-4 Hz triangular load over [$L/3$, $2L/3$]; (a) for $c_{\Delta\theta}=10^3$ N m s and various $k_{\Delta\theta}$ of the RDs; (b) for $c_M^{(v)}=10^3$ N m^{-1}s and various $k_M^{(v)}$ of the TMDs; (continuous line: proposed exact solution; (•): classical exact solution).

Figure 10. Beam with a fixed support, a viscous damper and a tip mass under a unit point load.

Figure 11. Beam in Figure 10: deflection DGF amplitude for a point load at the tip, with dimensionless frequency $\hat{\omega}=5$; (a) varying fixed support position; (b) varying tip-mass to beam-mass ratio; (continuous line: proposed exact solution; (•): classical exact solution).

Figure 12. Plane frame with TDs, RDs and lumped masses under a transverse uniform load over member 1.

Figure 13. Displacement FRF for a 10Hz uniform load over member 1: (a) real part; (b) imaginary part.

Figure 14. Rotation FRF for a 10Hz uniform load over member 1: (a) real part; (b) imaginary part.

Figure 15. Bending moment FRF for a 10Hz uniform load over member 1; (a) real part; (b) imaginary part.

Figure 16. Shear force FRF for a 10Hz uniform load over member 1; (a) real part; (b) imaginary part.

Figure 17. Axial force FRF for a 10Hz uniform load over member 1; (a) real part; (b) imaginary part.

Figure 18. FRF amplitudes in various frame members, for a 10Hz uniform load over member 1; (continuous line: proposed exact solution; (□): FE solution with 6 elements; (•): FE solution with 30 elements).

Figure 19. Horizontal displacement FRF amplitude at node N1, for a 0-150 Hz uniform load over member 1, with a zoomed view on the right; (continuous line: proposed exact solution; (•) FE solution with 30 elements along each frame member).

Figure 20. FRF amplitudes for a 10Hz uniform load over member 1, for different $c_{\Delta\theta}$ of the RDs and c_G of the TDs; (a) horizontal displacement at node N1; (b) shear force at member 1 bottom.

Figure 21. FRF amplitudes for a 0-20 Hz uniform load over member 1, for $c_{\Delta\theta}=5\times10^3$ N m s of the RDs and various c_G of the TDs; (a) horizontal displacement at node N1 (b) shear force at member 1 bottom; (continuous line: proposed exact solution; (•) FE solution with 30 elements along each frame member).

TABLES CAPTIONS

Table 1. Eigenvalues of the beam in Figure 3.

Table 2. Beam in Figure 10: dimensionless deflection DGF amplitude for a point load at the tip, with dimensionless frequency $\hat{\omega} = 5$, $\hat{x}_D = 0.75$ and $M^{(v)}/m_0 L = 1.0$.

Table 3. Beam in Figure 10: dimensionless deflection DGF amplitude for a point load at the tip, with dimensionless frequency $\hat{\omega} = 5$, $\hat{x}_S = 0.25$ and $M^{(v)}/m_0 L = 1.0$.

Table 4. Beam in Figure 10: dimensionless deflection DGF amplitude for a point load at varying position $\hat{\xi}$, with dimensionless frequency $\hat{\omega} = 5$, $\hat{x}_S = 0.25$, $\hat{x}_D = 0.5$ and $M^{(v)}/m_0 L = 1.0$.

Table 5. Beam in Figure 10: dimensionless deflection DGF amplitude for a point load at the tip, with dimensionless frequency $\hat{\omega} = 5$, $\hat{x}_S = 0.25$ and $\hat{x}_D = 0.5$.

Table 6. Eigenvalues of the beam in Figure 10 without fixed support, damper position $x_D = 0.2$ m, damping parameter $c_G^{(v)} = 5.5$ N m^{-1}s, tip-mass to beam-mass ratio $M^{(v)}/m_0 L = 3.0$, as in ref. [64].

Table 7. Eigenvalues of the frame in Figure 12.